Palacký University Olomouc

Faculty of Science

Department of Physical Chemistry

Reactivity of fluorographenes obtained from structurally different fluorographites

Master's thesis

Author:	Bc. Vítězslav Hrubý
Supervisor:	Mgr. Aristeidis Bakandritsos, Ph.D.
Study program:	N 1407 Chemistry
Field of study:	Material chemistry
Form of study:	Full-time study
Year:	2021

I hereby declare that this master's thesis has been composed solely by myself and that any part of this thesis has not been submitted in any previous application for a degree. It is a result of my own work, except where stated otherwise by acknowledgment or by reference to information source quoted in the list of references.

In Olomouc . . . .

. . . .

Bc. Vítězslav Hrubý

Acknowledgments

Bibliografická identifikace

Jméno a příjmení autora:	Bc. Vítězslav Hrubý
Název práce:	Reaktivita fluorografenů získaných ze strukturně odlišných grafitfluoridů
Typ práce:	Diplomová magisterská
Pracoviště:	Katedra fyzikální chemie a CATRIN - RCPTM
Vedoucí práce:	Mgr. Aristeidis Bakandritsos, Ph.D.
Rok obhajoby práce:	2021

Abstrakt: Fluorografen připravený z exfoliovaného grafitfluoridu je úspěšně používaný jako vstupní materiál pro vývoj početné rodiny grafenových derivátů s významným aplikačním potenciálem. Díky tomu má významný vliv na výzkum v oblasti dvoudimenzionálních materiálů. Tato práce zkoumá jiný aspekt chemie fluorografenu, a to vzhledem k pozorováním odlišné reaktivity fluorografenů/grafitfluoridů připravených z různých forem uhlíku. Byla provedena podrobná charakterizace grafitfluoridů od různých komerčních dodavatelů pro určení jejich složení, struktury a optoelektronických vlastností. Jejich reaktivita byla studována pomocí reakcí s azidem sodným a oktylaminem a produkty těchto reakcí byly analyzovány a porovnány pro identifikaci nejvíce reaktivních grafitfluoridů a příčin pro jejich vysokou reaktivitu. Jako společné znaky reaktivních grafitfluoridů se ukázal být vyšší obsah fluoru vstupních grafitfluoridů kvůli přítomnosti CF_2 skupin spojených s přítomností defektů/vakancí, což bylo mimo jiné pozorováno rentgenovou fotoelektronovou spektroskopií a nukleární magnetickou rezonancí. Tyto materiály mohou být snadno rozpoznány pomocí spektroskopie difúzní reflektance, neboť jejich optický pás měl šířku přibližně 5,8 eV.

Klíčová slova: grafitfluorid, fluorografen, grafenové deriváty, dusíkem dopovaný grafen, rentgenová fotoelektronová spektroskopie, nukleární magnetická rezonance, termická analýza, zakázaný pás, spektroskopie difúzní reflektance, elektronová paramagnetická rezonance, rentgenová difrakce, infračervená spektroskopie, Ramanova spektroskopie

Počet stran:	82
Počet příloh:	0
Jazyk:	Angličtina

Bibliographical identification

Author:	Bc. Vítězslav Hrubý
Title:	Reactivity of fluorographenes obtained from structurally different fluorographites
Type of thesis:	Master's
Department:	Department of Physical Chemistry and CATRIN - RCPTM
Supervisor:	Mgr. Aristeidis Bakandritsos, Ph.D.
Defense year:	2021

Abstract: Fluorographene prepared from the exfoliation of graphite fluoride has been successfully used as a starting material for the development of a wide family of graphene derivatives with broad application potential. It has thus made a significant impact on the science of two-dimensional materials. The present work explores a different facet of fluorographene's chemistry, motivated by observations on the distinct reactivity of fluorographenes/graphite fluorides originating from the fluorination of different types of carbons. Elaborate characterization of graphite fluorides from various commercial suppliers was performed for determining their composition, structure, and optoelectronic properties. Their reactivity was studied via their reaction with sodium azide and octylamine and the products were analyzed and compared in order to identify the most reactive graphite fluorides and the reasons behind the reactivity. The very high fluorine content in the starting graphite fluorides and the presence of CF_2 groups connected to the presence of defects/vacancies were shared traits among the most reactive graphite fluorides, as verified by X-ray photoelectron spectroscopy and nuclear magnetic resonance. These materials may be easily identified by using UV-VIS diffuse reflectance spectroscopy since these had optical gap with the width of ~5.8 eV.

Keywords: Graphite fluoride, fluorographene, graphene derivatives, nitrogen-doped graphene, X-ray photoelectron spectroscopy, nuclear magnetic resonance, thermal analysis, bandgap, diffuse reflectance spectroscopy, electron paramagnetic resonance, X-ray diffraction, infrared spectroscopy, Raman spectroscopy

Number of pages:	82
Number of appendices:	0
Language:	English

Table of contents

1 Introduction

Graphite is the most stable allotrope of carbon, where its atoms being in sp^2 hybridization create layers of honeycomb lattice stacked on each other in hexagonal symmetry and held together via van der Waals forces.[1] This naturally occurring material is thanks to delocalized unhybridized 2p electrons conductive and therefore readily used as an electrode.[1] A single layer of graphite is called graphene, which was first successfully isolated by Geim and Novoselov in 2004 by mechanical exfoliation of highly oriented pyrolytic graphite since the individual layers of graphite are weakly bound.[2] Its properties regarding its mechanical strength and mainly its high electric conductivity due to ballistic transport of charge carriers caused by its zero-bandgap electronic structure stimulated extensive research of this material.[1,3] Some other properties, particularly the difficulty of its production in practical quantities, the high tendency of restacking, hydrophobicity, and chemical inertness were found limiting for applications in other fields as (electro)catalysis, (bio)sensing, and optoelectronics. For altering this material to suit the needs of various potential applications, its derivatization was proposed as an effective pathway to achieve these goals.[4]

Since graphene is a single layer of graphite, the chemical alteration of graphene sheets within graphite started to be explored long before graphene isolation. This is thanks to the fact, that graphite interlayers are prone to the insertion of other chemical species. The materials resulting from such insertion are referred to as graphite intercalation compounds or GICs. Inserted species can be either positively charged, e.g. highly electropositive metal atoms, making graphene layers within the GIC negatively charged, or vice versa, e.g. intercalation of negatively charged ions into the graphite.[5] The first GIC was reported in 1841 by intercalating potassium atoms into the interlayers of graphite.[5] Materials like this were later found to have well-defined stoichiometry and superconductive properties, either from the insertion of potassium or calcium ions.[6]

Intercalation of highly oxidative species may lead to oxidation of the graphene films within the graphite. In 1859, the graphite was found to change its properties when subjected to treatment with fuming nitric and potassium chlorate producing graphite oxide.[7] This yellow-colored material was later found, owing to the presence of oxygen-bearing functionalities, prone to hydrolysis and easily exfoliating in water due to its interactions with the functionalities of the material and disintegrating into single layers of graphene oxide long before the discovery of graphene,[8] although the name graphene oxide was started to be used after the discovery of graphene.[9] Many other methods of graphite oxide preparation were proposed since

then[10] affording materials slightly varying in their compositions and properties.[11] The oxygen-bearing functionalities of these materials could also be removed by reduction, such as by using hydrazine, to produce reduced graphene oxide.[9] These materials, despite their problematic structure that was hard to define due to the presence of various oxygen-bearing moieties and highly disordered regions,[12] have been heavily used as precursors for the synthesis of graphene derivatives via reactions of the oxygen-containing functionalities since then.[4]

In 1934, the fluorine reacting with graphite was found to produce a gray solid of composition $CF_{0.92}$ stable under normal conditions.[13] This was due to the formation of graphite fluoride, a material with fluorine atoms covalently bonded to carbon atoms. More investigation of the fluorination of graphite led also to the preparation of unstable fluorine intercalated graphite GICs and other fluorinated graphites of various stoichiometries.[14] None of the prepared materials was strictly stoichiometric, but two crystal forms of covalent graphite fluoride compounds were observed and described – poly(carbon monofluoride) composed of sheets of the composition of $(CF)_n$ and poly(dicarbon monofluoride) with the representative formula of $(C_2F)_n$.[14] These materials were exploited as a solid lubricant,[15] cathode materials for Li-ion batteries,[16] and water and oil repellent agent due to very low surface energy.[17] Poly(carbon monofluoride) $(CF)_n$ was in 2010 found to exfoliate when dispersed in solvents with high surface tension (or mechanically) forming single sheets called fluorographene,[18] one of two stoichiometric graphene derivatives with the latter being graphane, fully hydrogenated graphene.[19] Fluorographene was also immediately recognized as an excellent precursor for the synthesis of graphene and its derivatives.[20–22] Till this day, many important graphene derivatives, such as cyanographene, graphene acid,[23] alkyl-, aryl-,[24] and alkynyl-[25] graphenes or even nitrogen-doped graphene[26,27] were found to be formed when fluorographene produced by exfoliation of graphite fluoride was used for their synthesis as a starting material.

1.1 Graphite fluorides

The class of material briefly introduced in the paragraph above, graphite fluorides, are the focus of this work. As mentioned, the term graphite fluoride comprises a wide variety of non-stoichiometric covalent compounds of fluorinated graphite with two being stoichiometric as well as rare fluorine GICs. Due to their connection to GICs, these materials keep their layered structure of graphite.[14]

1.1.1 Synthesis of graphite fluorides

The definitive composition and structure of graphite fluoride strictly depend on the fluorination procedure as well as on the type and structure of starting pristine graphitic material. After the

material was first synthesized in 1934, the synthesis of this material was revisited few times, however, the material and preferable conditions of its synthesis for best results were not studied in high detail until 1960 since the material seemed not to have any apparent applications at first. The preparation methods differ greatly if the synthesis of a fully fluorinated or partially fluorinated product is desired. The factors highly affecting the outcome of the fluorination are the purity of the fluorination atmosphere, the temperature of the process, and the graphitic material used for the synthesis as a starting material.[14]

For the fluorination, only a high purity fluorine gas needs to be used[14] or in the mixtures with gas-diluents, such as CF_4, Ar or N_2.[28] Pressure of fluorine in the reaction chamber does not inflict the outcome of the reaction very much and is kept usually at atmospheric pressure. The fluorine needs to be passed through the reaction chamber to allow fluorine molecules to diffuse into the material and to keep the synthesized graphite fluoride in the presence of fluorine, otherwise, an explosive decomposition of graphite fluoride may occur. The hydrogen fluoride (HF) content within the reaction mixture needs to be minimalized for a successful fluorination process leading towards covalent fluorographites.[14] First, the presence of HF in fluorine atmosphere instead of production of covalent graphite fluoride may produce partially fluorinated graphene resembling fluorine-GIC already at room temperature since HF acts as a catalyst for the production of this material.[29] As a side note, several other catalysts have been reported to facilitate the formation of fluorine GICs, such as AsF_5, IF_5, OsF_6.[30] If the temperature of fluorination of these fluorine-GICs is elevated, graphite fluoride is formed containing HF as an impurity. HF, however, facilitates the thermal decomposition of the prepared graphite fluoride making it less thermally stable.[31] The initiation of the decomposition may also occur spontaneously during the fluorination process causing an explosion.[32] Therefore, when the covalent graphite fluoride is meant to be produced, the HF amounts within the reaction vessel need to be kept very low and strictly controlled, preferably below 0.01 vol. %. To purify fluorine gas from contaminant HF flowing into the reaction chamber, it should be passed through NaF pellets heated at 100 °C that bind the HF while producing $NaHF_2$ in the process.[14] However, the HF can be used for activation of the carbon source material before the fluorination, if the HF can be successfully purged by an inert gas from the system before the temperature is elevated.[32] This effect may be enhanced when the mixture also contains BF_3 or IF_5 catalysts producing partially mixtures of partially fluorinated graphites with fluorine-GICs even at room temperature.[33]

As a result of the fluorination of graphite, non-stoichiometric graphite fluorides are produced, which are complex mixtures of two different compounds, poly(carbon

monofluoride) $(CF)_n$ and poly(dicarbon monofluoride) $(C_2F)_n$ of different crystallite sizes and their partially fluorinated derivatives. Generally, it can be said that the higher the fluorination temperature and the lower the crystallinity of the graphitic source material, the higher the fluorine contents of the product, therefore higher the content of $(CF)_n$. The stoichiometries of these crystal structures are not always strictly C_1F_1 or $C_1F_{0.5}$, but rather between $CF_{0.5}$ and $CF_{1.3}$ due to the presence of CF_2 and CF_3 groups at the edges of the crystallites or due to present defects containing excess fluorine in the crystal lattice.[14]

If the temperature of fluorination is in the range between 600 and 640 °C, practically only $(CF)_n$ is produced. For best result, the fluorine gas is introduced into the reaction chamber after the graphite temperature reaches desired temperature by heating in an argon atmosphere to prevent the formation of $(C_2F)_n$ or other possible byproducts. The production of $(CF)_n$ proceeds more easily when a graphitic source material of lower crystallinity is used as a starting material. Such materials can be petroleum coke or carbon black.[14] This is however for the expense of smaller particle size of the product. Graphitic materials of higher crystallinity and larger particles, such as natural graphite or highly oriented pyrolytic graphite (HOPG) can be also converted to $(CF)_n$, however, the synthesized material will contain portions of unreacted graphite due to the lower ability of the fluorine gas to diffuse in the interlayers of larger particles.[34]

If $(C_2F)_n$ compound is desired, its formation is maximized in the temperature range of 350-370 °C.[14] For the graphitic source for the synthesis of $(C_2F)_n$ graphite source materials are preferred, such as natural graphite or highly oriented pyrolytic graphite.[14,34] The products are however often non-stoichiometric materials consisting of particles with regions differing in degree of fluorination. If the particle would have for example disk-shaped, it would contain a thin layer of $(CF)_n$ on the surface followed by $(C_2F)_n$ phase under it. Once the $(C_2F)_n$ phase is formed in the whole particle, further fluorination at higher temperatures causes the $(CF)_n$ phase to start forming from the center of the disk particle growing in the direction towards the surface of the particle.[14]

If the fluorination is conducted between 370 and 600 °C, the reaction results in non-stoichiometric graphite fluoride with compositions $(CF_x)_n$, where $0.5 < x < 1$ composed of a mixture of its two crystal forms and their partially fluorinated derivatives. There is no specific boundary between the formation temperature of each compound. It also highly depends on the graphitic source material used for the reaction as a starting material since some graphitic materials of very low crystallinity may produce $(CF)_n$ even at low temperatures (for petroleum

coke or carbon black it is between 300 and 400 °C). For a final note, since petroleum coke is a graphitizable carbon source, it also highly depends if the petroleum coke is heat-treated prior to the fluorination. While fluorination of the untreated petroleum coke produces graphite fluoride of white color due to low crystallite sizes of petroleum coke after it is heated above 1630 °C, the graphite crystallites of petroleum coke grow in size significantly and the fluorination degree is lower. The more the petroleum coke is thermally treated before the fluorination, the lower fluorine content in the resulting graphite fluoride by fluorination of the relevant material.[14]

The fluorination process takes place in the reactors built from metals or alloys suitable for handling fluorine gas, such as copper, stainless steel, and nickel or its alloys with certain parts made from polytetrafluoroethylene of polytrifluorochloroethylene. Prior the fluorination, the entire system of the reactor needs to be passivated with elemental fluorine. There are three types of reactors used for the fluorination of graphite and carbon materials. In a static reactor, the graphite is fluorinated without any movement just using the fluorine pass through the reaction chamber with the heated graphite. However, this method produces samples inhomogeneously fluorinated due to fluorine gas retardation while diffusing into the voids between the particles of graphite. Moreover, if graphite fluoride is created and further heated while not surrounded by elemental fluorine, it may decompose explosively. This may be overcome by a rotary reactor, where graphite is placed into the reaction tube, heated, and then rotated while fluorine gas is passed through the tube. The reactor allowing the production of larger amounts of homogeneous materials is a vertical vibrating reactor mixing the system by rapidly vibrating the reaction chamber during the fluorination process.[14]

1.1.2 Properties of graphite fluorides

Crystal structures of stoichiometric graphite fluorides. As mentioned, graphite fluoride may contain, among various amorphous fluorocarbons, two different covalent stoichiometric compounds, poly(carbon monofluoride) $(CF)_n$ and poly(dicarbon monofluoride) $(C_2F)_n$, whose most stable layered structures are depicted in Figure 1.[35] C-C bond lengths of $(CF)_n$ and $(C_2F)_n$ were determined to be essentially the same (1.57 and 1.58 Å, respectively) as well as C-F bonds (both 1.36 Å).[36]
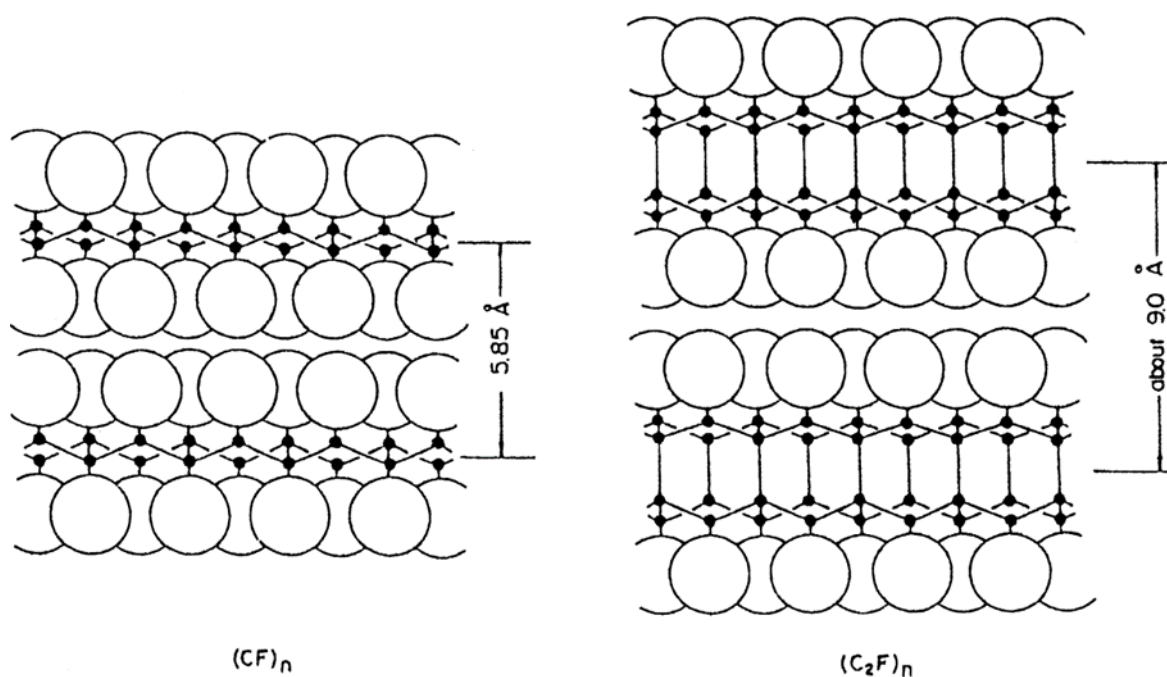
Figure 1: Structures of two stoichiometric graphite fluoride materials, poly(carbon monofluoride) $(CF)_n$ and poly(dicarbon monofluoride) $(C_2F)_n$, in their most stable forms with experimentally determined interlayer spacings values. Reproduced from reference.[17]

Poly(carbon monofluoride) $(CF)_n$ (Figure 1, left) is most stable in chair conformation (Figure 2a) that forms layers of an infinite array of trans-linked cyclohexane chairs with fluorine atoms bonded covalently to the carbon atoms and alternating on both sides of basal plane. These layers are held together by van der Waals forces in symmetry of hexagonal crystal lattice.[37] However, the $(CF)_n$ sheets may also be in metastable boat conformation forming layers of an infinite array of cis-trans-linked cyclohexane boats as depicted in Figure 2b.[38] Such structure has a symmetry of orthorhombic crystal lattice. Theoretically determined values of the unit cell constants of both structures are inscribed in Figure 2. The energy difference between the chair and boat conformations is 0.145 eV per CF unit with a 2.72 eV energy barrier.[37] There are more possible metastable forms of $(CF)_n$ conformations structurally similar to the boat conformation, such as zig-zag, warped, or armchair conformations.[39] These structures, since they cannot be studied directly by X-ray diffraction due to the inability to produce their single crystals, have been observed indirectly by employing solid-state NMR measurements combined with theoretical simulations.[39] $(CF)_n$ sheets interlayer spacing was predicted for both structures, according to the DFT calculation, to 5.67 Å,[37] however, X-ray diffraction observations of real samples found interlayer spacing for chair and boat conformation to be 5.85 Å[35] and 6.16 Å,[38] respectively, but was recorded to be as high as 7.76 Å for graphite fluoride prepared from petroleum coke.[14]
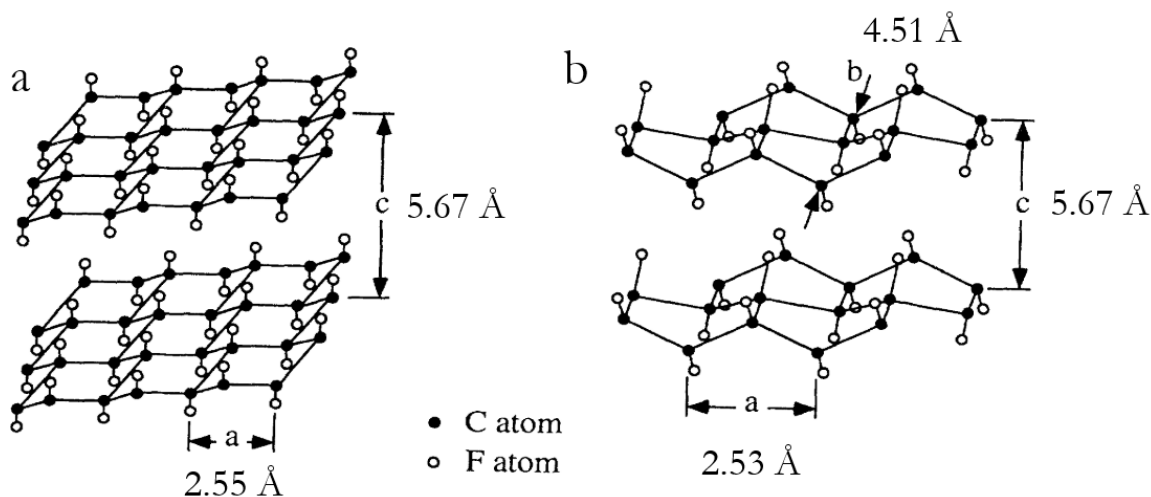
Figure 2: Structures of different conformations of poly(carbon monofluoride) $(CF)_n$ fluorographene layers: (a) stable chair conformation with theoretical values of hexagonal unit cell constants a and c, (b) metastable boat conformation with theoretical values of orthorhombic unit cell constants a, b and c. Reproduced from reference.[37]

In the case of poly(dicarbon monofluoride) $(C_2F)_n$ (Figure 1, right), the fluorine atoms are inserted into every other graphite layer. The structure of this material again consists of trans-linked cyclohexane chairs, where three carbon atoms are bonded to fluorine atoms and the other three are connected to three carbon atoms of an adjacent layer via interlayer covalent sp^3 diamond-like C-C bonds perpendicular to the basal planes of the two connected graphite layers stacked in hexagonal symmetry.[35,36,40] Theoretically, two types of $(C_2F)_n$ structures may exist, AB-type and AA'-type, both depicted in Figure 3.[36,40] Neutron diffraction measurements suggested that real samples contain AB-type $(C_2F)_n$ rather than AA'-type.[36] The interlayer spacing for this structure was determined to be around 8.72 Å.[36]
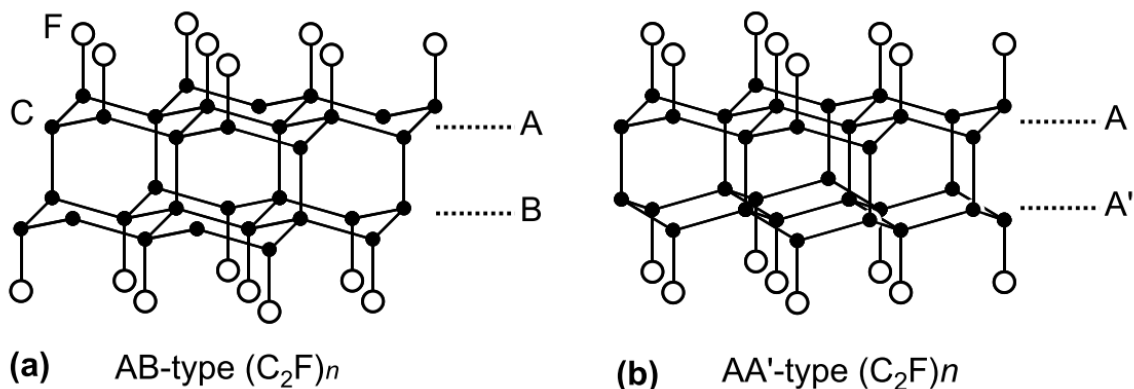
Figure 3: Two possible structures of $(C_2F)_n$: AB-type (a) and AA'-type (b). Reproduced from reference.[36]

Partially fluorinated graphites. In the case of partially fluorinated graphite, such a system is more of a character of fluorine-GIC. In this, the carbon atoms mostly retain their sp^2 character and, in such areas, the C-F bond is next to the conjugated C=C double bonds. This causes hyperconjugation of C-F binding orbitals with π-antibonding orbitals resulting in delocalization of electron density of C-F bonds causing lower bond order than that of the covalent C-F bonds in the perfluorinated $(CF)_n$ or $(C_2F)_n$ sites. Such bond is also slightly elongated (1.40 Å) in comparison with the covalent C-F bond (1.36 Å). This bond is mostly referred to as a semi-ionic bond.[30]

Paramagnetism of graphite fluorides. Graphite fluoride has also been recognized as paramagnetic due to the presence of defects introduced by the fluorination. The unpaired electrons of graphite fluorides have g-values close to 2, very close to that of free electron (g = 2.0023), which is typical for localized structural defects.[34,41] Such defects are described as dangling bonds at carbon atoms[34] and may be generally of two different types. The first type is found in $(CF)_n$ sheets, due to observed hyperfine interaction of spins with ^{19}F nuclei, introducing high structural disorder observed as a broadening of the signal from electron paramagnetic resonance (EPR) spectroscopy reflecting various configurations of these defects.[41] The nature of these defects is further discussed in the paragraph about the properties of fluorographene below. The other type of defect is manifested by a sharp line of EPR signal signifying isolation of the spin from ^{19}F nuclei due to different environments of the defect. Since it is observed only in $(C_2F)_n$ spectra, it stems from the interrupted C-C bonds within the interlayer of the $(C_2F)_n$ structure.[41]

Spectroscopic fingerprints of graphite fluorides. Differences between $(CF)_n$ and $(C_2F)_n$ structures may be tracked by spectroscopic measurements. An indication of the presence of each phase can be determined by using X-ray powder diffractometry, where the (001) plane reflection should appear at lower 2θ angles for $(C_2F)_n$ and at higher angles for $(CF)_n$. However, the peaks are usually very broad due to irregularities in stacking and many defects of real samples. The Raman spectra of both structures should be silent with no features with only fluorescence as a background when a visible radiation laser is used.[42] If graphite fluoride contains D and G bands, it signifies non-fluorinated sp^2 regions on the material. These bands are found at 1360 and 1580 cm^{-1}, respectively, corresponding to phonons linked with aromatic ring vibrations that are part of an array of conjugated sp^2 domains near defects (D, edges, vacancies, or sp^3 carbon) or in pristine regions (G), respectively. If a laser with the energy of its radiation greater than the bandgap of the graphite fluoride is used for the Raman spectroscopy analysis, two bands are observable at 1270 cm^{-1} and 1345 cm^{-1} for $(CF)_n$ further proving its crystallinity.[43]

FTIR spectra of both $(CF)_n$ and $(C_2F)_n$ structures are more distinct with $(CF)_n$ exhibiting one broad feature at 1200 cm^{-1} with a shoulder around 1310 cm^{-1} representing covalent C-F and CF$_2$ bond vibrations, respectively. The $(C_2F)_n$ has additional corresponding features at 940 cm^{-1} and 1350 cm^{-1}. The semi-ionic bond can be observed around 1100 cm^{-1}.[33,44,45] In the X-ray photoelectron spectroscopy focused on the core C 1s spectra, the main feature at 290.2 eV corresponds to the C-F covalent bond and the feature at 292.4 eV corresponds to CF$_2$ groups of edges and defects. If the structure is partially fluorinated containing semi-ionic C-F bonds, these configurations may be observed at 287.3 eV.[45] Additionally, the peak at 288.5 eV should correspond to $(C_2F)_n$ specific vibration.[14]

Optical and electronic properties of graphite fluorides. Both $(CF)_n$ and $(C_2F)_n$ are very good electrical insulators with conductivity $<10^{-15}$ S·cm^{-1}. However, partially fluorinated graphite materials with C/F ratios different than 1 or 2 have much higher conductivities (10^{-7} S·cm^{-1}) due to a partially maintained network of conjugated double bonds.[30] $(CF)_n$ is considered as a direct-transition, wide-gap semiconductor.[46] Regarding the bandgap energy of the $(CF)_n$ material, it was theoretically first estimated to amount up to 8.4 eV.[47] After that, the electronic structure of $(CF)_n$ has been extensively studied due to the higher popularity of fluorographene and its insulating properties when compared to graphene.[48] When comparing fluorographene and graphite fluoride, the electronic structure of the $(CF)_n$ doesn't change much with the number of layers present.[49] Therefore, the values determined experimentally for graphite fluoride may also characterize the electric properties of single-layer fluorographene prepared from it.[49] If hole-electron interactions are taken into the account during the interaction with electromagnetic radiation, the optical gap drops to 5.2 eV with the exciton binding energy determined to 1.85 eV.[49] Experimental observations of the bandgap estimated value of 3 eV from emission measurements of graphite fluorides[50] or 3.8 eV according to X-ray absorption spectroscopy and photoluminescence measurements of fluorographene.[51] In the case of partially fluorinated graphene, the electronic structure highly depends on the structural motifs (pattern of fluorination).[52]

1.1.3 Reactivity of graphite fluorides

Graphite fluorides are stable in normal and oxidative environments than in reductive ones. However, they thermally decompose at higher temperatures without the presence of fluorine and are reactive towards various species often leading to their reduction. The materials were also found more reactive upon UV radiation.[50]

Thermal decomposition. Generally, graphite fluorides thermally decompose at temperatures above 500 °C. Regarding $(CF)_n$, this process starts at a lower temperature for materials of lower crystallinity, e.g. 400 °C for fluorinated petroleum coke and 600 °C for $(CF)_n$ synthesized from natural graphite. In the latter case, however, the decomposition is more rapid. For both cases, weight loss at 700 °C (5 °C/min) is around 70 %. Interesting about the decomposition is, that the composition of the gaseous products released during the process can be expressed as C_xF_{2x} and that the residual carbon has a graphite-like structure. The mechanism, therefore, proceeds through the disintegration of every second layer of the material rupturing its C-C bonds and bonding fluorine atoms bonded to the two neighboring layers as shown in Figure 4. As for the $(C_2F)_n$ structure, it is thermally stable up to 600 °C and also decomposing into graphite under an inert atmosphere with a weight loss of 55 % releasing CF_4 species in the process. Its mechanism is however unclear.[50]
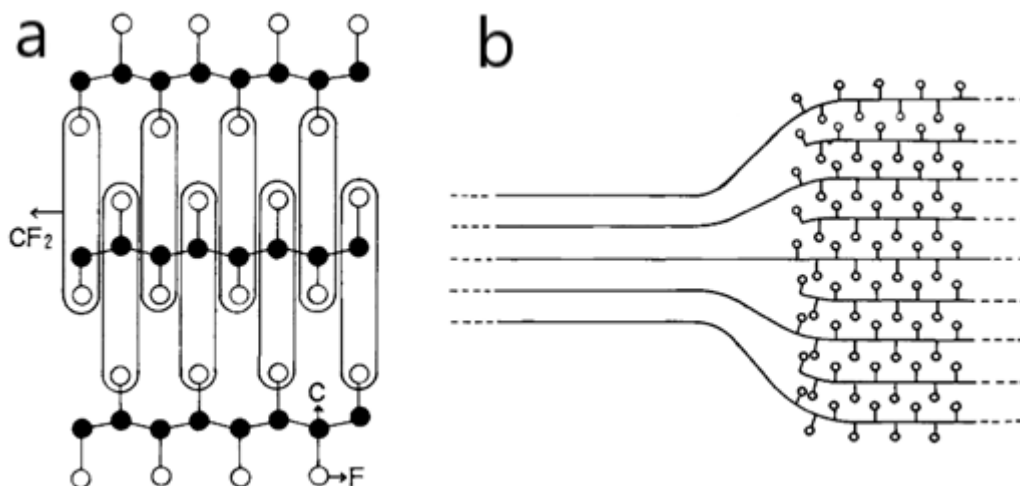
Figure 4: Mechanism of thermal decomposition of $(CF)_n$ graphite fluoride, releasing CF_2 species (a) and producing graphite in the process (b). Adapted from reference.[50]

Reduction. When the graphite fluoride is heated above 400 °C with alkali iodides, bromides, or chlorides, it is reduced into graphite, producing metal fluorides and elemental halogens. The reduction in hydrogen atmosphere proceeds also above 400 °C producing hydrogen fluoride in the process. Graphite fluoride is reduced even in chlorine atmosphere producing graphite-like carbon and interhalogen compounds such as ClF and ClF_3. These processes apply to both $(CF)_n$ and $(C_2F)_n$.[50]

Photochemical decomposition. A remarkable reaction of $(CF)_n$ graphite fluoride is its defluorination upon irradiation by UV radiation when dispersed in an appropriate solvent, observed by a color change of the dispersion from opaque white to black. The graphite fluoride

is therefore photoactive. Graphite fluoride during this process loses fluorine atoms creating hydrogen fluoride and oxidizing the solvent. For example, if isopropanol is used as a solvent, acetone is produced as a byproduct. The extent of the defluorination is however small. A reason for this might be the fact that the reaction does occur only at the surface of the particle.[50]

Liquid-phase reactions. This paragraph shows that $(CF)_n$ graphite fluoride was known to produce covalent graphene derivatives even before the fluorographene was isolated in 2010.[18,48] Briefly, when subjected to liquid primary, secondary and tertiary amines, graphite fluoride defluorinates even at room temperature.[53] Reaction of graphite fluoride with the alkyl-lithium compound was reported to produce graphene functionalized with alkyl chains and such material was readily dispersible in organic solvents forming stable colloids showing the possibility of nucleophilic substitution of the fluorine by different moiety.[54] This process was also observed when the material was treated in molten NaOH-KOH eutectic, it produced photoluminescent graphene particles well-soluble in water due to the presence of hydroxyl groups.[55] After the discovery of fluorographene,[18] many more of the reactions producing graphene derivatives were discovered and studied.[56] Their mechanisms are therefore discussed in the next section focused mainly on the fluorographene chemistry.

1.2 Fluorographene

Fluorographene is a stoichiometric graphene derivative that can be regarded as fluorinated graphene or as a single layer of hexagonal $(CF)_n$ graphite fluoride.[56] Since most of the characteristics of fluorographene are intrinsic to graphite fluoride, this section will be more focused on its reactivity.

1.2.1 Preparation of fluorographene

There are generally two approaches for fluorographene preparation. First is a top-down approach of graphite fluoride exfoliation into several or single-layered sheets of fluorographene using several different procedures. Latter is a bottom-up approach of direct graphene fluorination using various fluorination agents.[56]

Exfoliation of graphite fluoride. Although mechanical exfoliation of graphite fluoride by micromechanical cleavage using scotch-tape can result in monolayer fluorographene of high quality,[48] such approach is hardly scalable and, therefore, not suitable for chemical application by using the resulting fluorographene as a starting material form synthesis of graphene derivatives. Nevertheless, there were approaches testing ball milling for exfoliation of graphite fluoride with help of melamine that resulted in few-layered nanosheets of partially fluorinated graphene.[57] Similar outcome was recorded by using thermal exfoliation approach, that was

found effective above temperatures above 600 °C causing profound defluorination of emerging fluorographene nanosheets.[58]

For the production of fluorographene on a larger scale, a liquid-phase chemical exfoliation is a viable option, although it does not produce materials of as high quality as thorough mechanical exfoliation.[19] The most common and simplest method employs specific organic solvents whose molecules may, due to similarities in surface energies of the material and solvent,[59] intercalate within the interlayers of graphite fluoride thus weakening its structure due to interruption of van der Waal's forces between the layers.[19] Such weakened systems can be then disintegrated into colloids containing monolayer or few-layered fluorographene sheets.[19] Described mechanism is depicted in Figure 5. The pioneer solvent used for this purpose was sulfolane.[18] Recently, DMF,[22,23,26,56,60] NMP,[61] oDCB[1,22] have been used the most. The effectivity of low-molecular amides like NMP and DMF for exfoliation of both fluorographene and graphene was further proved with force-field simulations.[59] Fluorine contents of thus prepared fluorographene depend on the used graphite fluoride and solvent, since some solvents may react with the fluorographene during the process.[21]

a)   b)   c)

DMF   sonication
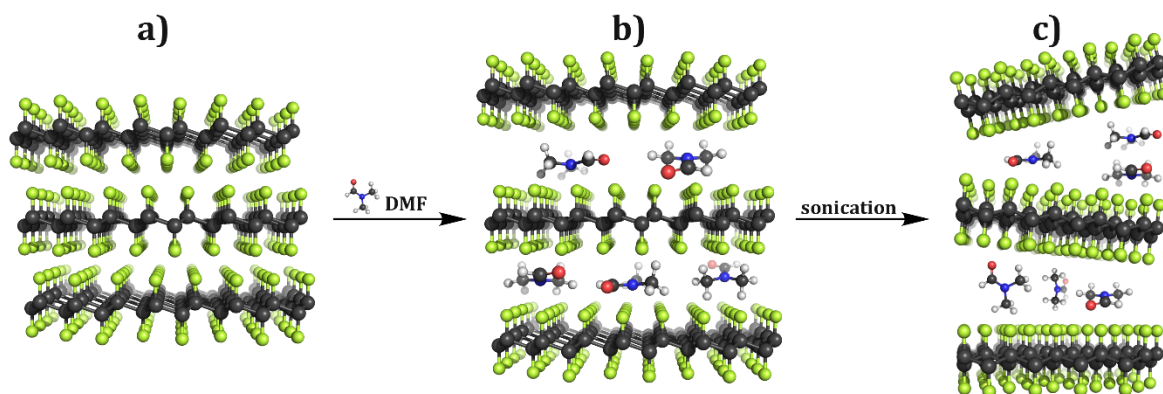
Figure 5: Depiction of preparation of fluorographene by chemical exfoliation of graphite fluoride. The graphite fluoride (a) is dispersed in the solvent that may intercalate within its interlayers (b) weakening the structure that can be disintegrated into individual fluorographene sheets by mere sonication (c).

Fluorination of graphene. Despite how advantageous GF exfoliation is in terms of simplicity and (cost)effectiveness since it produces fluorographene in a form of colloids containing particles of small lateral dimensions., it is not suitable for most physical experiments and applications that require larger sheets with precise stoichiometries.[19] For this, fluorination of graphene is an option. Since fluorination using fluorine gas occurs only at higher temperatures thus introducing many defects into the graphene structure, the use of different fluorination agents or a whole different approach needs to be considered. XeF$_2$ was found to be effective at

temperatures as low as 30 °C[62] producing fluorographene sheets of high quality.[48,51,62] Optionally, treatment of graphene using plasma containing various fluorine-containing species, such as elemental fluorine,[63] CF_4,[64] CHF_3,[65] or SF_6,[66] can be done. As starting materials, CVD-grown graphene sheets[64] or graphene made by mechanical cleavage of graphite[48,66] are applicable for the synthesis of fluorographene sheets of high quality. Fluorination can be also applied to graphene oxide thus producing fluorinated graphene oxide by the above-mentioned procedures, or by HF treatment.[56] Finally, an interesting approach for graphene fluorination with an option of patterned fluorination is a photoinduced decomposition of fluoropolymers on graphene. By placing CVD-grown graphene onto a substrate coated with CYTOP polymer and successive laser irradiation of this system leads towards one-sided fluorographene on spots where the sample was irradiated.[67]

1.2.2   Properties of fluorographene

Practically, fluorographene is a single layer of hexagonal $(CF)_n$ graphite fluoride, therefore it also consists of an array of trans-linked sp^3 fluorinated cyclohexane chairs in its most stable form. Such structure is terminated by CF_2 moieties forming its edges, which may also contain $(CF_2)_n$-CF_3 chains bonded to it. Although the thickness of a single-layer of hexagonal $(CF)_n$ graphite fluoride sheet should theoretically be 3.3 Å, the thickness of single layer fluorographene was experimentally determined in a range of 6.7-8.7 Å.[56] Because most of the properties of fluorographene were already described in the graphite fluorides section, only the properties linked with its reactivity are described.

Fluorographene is, as its bulk counterpart, paramagnetic due to the presence of structural defects containing unpaired electrons.[68] First it was thought, that mere point defects, dangling bonds on carbon atoms where fluorine atoms are missing, are present in its structure (Figure 6a). These may appear naturally with growing fluorine regions on graphene where the unpaired electrons can be stabilized by mutual mixing of their orbitals with adjacent σ* orbitals of C-F bonds. This phenomenon was observed in saturated perfluorocarbons.[21] However, just recently it was found that the defects found in the fluorographene lattice are in fact vacancies, where a whole part of the structure, C and F atoms included, are missing. According to ab-initio calculations, the most stable vacancies were found to be monovacancies and divacancies shown in Figure 6bc. These vacancies contain unpaired electrons and CF_2 moieties thus explaining paramagnetism of the material and higher fluorine contents of some graphite fluorides or fluorographenes with F/C > 1.[26] As the research continued, the presence of unpaired electrons within the fluorographene and graphite fluoride were found as a cause of their reactivity.[21,22] The mechanisms of these processes are described in the next part.
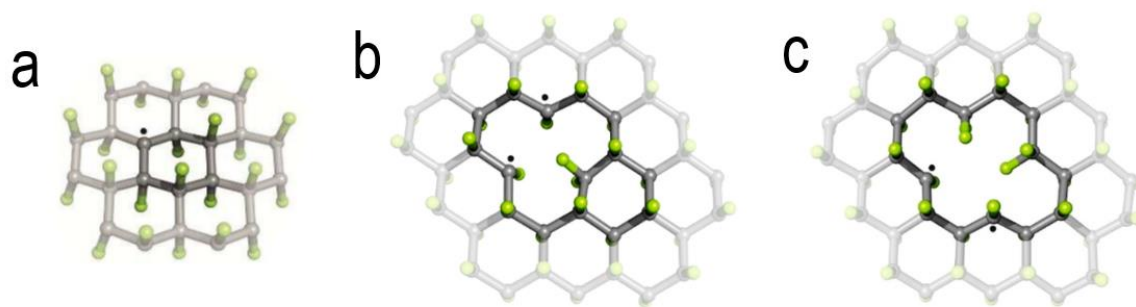
Figure 6: Most stable defects in the fluorographene structure containing unpaired electrons. Fluorine vacancy (a), monovacancy in the fluorographene sheet (b), and divacancy (c). Adapted from references.[21,26]

1.2.3 Reactivity of fluorographene

The presence of unpaired electrons in graphite fluoride and fluorographene causes these materials to undergo various reactions already feasible under ambient conditions. The reason for this is the very high electron affinity of the site containing the unpaired electron, which may amount up to 117 kcal/mol. This is due to the electron-withdrawing effect of neighboring fluorine atoms.[21] This makes fluorographene (and graphite fluoride) electrophilic, therefore prone to reduction, nucleophilic substitution, and other reactions in environments containing nucleophilic species, processes important for syntheses of vide variety of graphene derivatives.[22] A description of so-far explored reactions and their mechanisms follows. Since this field has been heavily studied recently, more reactions can be expected to be discovered.

Reductive defluorination. Similar to graphite fluoride, fluorographene can be reduced as well to form partially fluorinated graphene or graphene by using mild or stronger reducing agents, respectively. The partial defluorination of fluorographene can already occur by dispersing the paramagnetic fluorographene in a solvent such DMF, NMP,[61] or dimethylacetamide (DMAc),[69] which are used as intercalation agents for the preparation of fluorographene by chemical exfoliation of graphite fluoride.[18,19,56] Such solvents also have mild reducing activity causing the fluorographene to lose fluorine atoms thus developing sp^2 regions that can be observed by a color change of the fluorographene dispersion after some time.[69] The reaction runs through a radical mechanism and was described for DMF in detail.[21] In the first step, the DMF molecule hydrogenates the radical center of fluorographene forming DMF radicals that then attack another radical center forming a C=C bond in the fluorographene and *N,N*-dimethylcarbamoyl fluoride. Vicinity of the emerged double bond is prone to another attack by DMF radical thus recreating radical on the fluorographene that can create another C=C bond. This cascade gradually creates sp^2 domains of π-conjugated systems. The whole mechanism is drawn in Figure 7. Such defluorination process ceases after the creation of larger

domains since electron affinities of radicals drop with the increasing size of the π-conjugated site.[21] Such phenomenon, although with NMP, was also observed experimentally, when, after one day of the reaction, the rate of defluorination decreased significantly.[69] This phenomenon is very important for tuning the outcome of nucleophilic substitution reactions. The use of the defluorinating solvent caused the formation of graphene derivatives with very low residual fluorine contents. If a non-defluorinating solvent is used, such as oDCB, the products contain higher amounts of fluorine.[22]
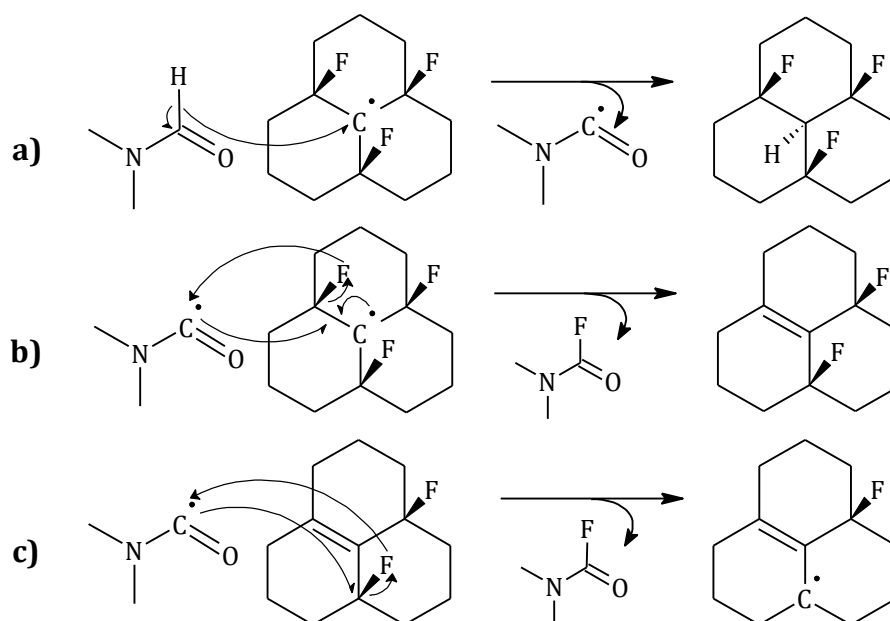
Figure 7: Mechanism of fluorographene defluorination by the defluorinating solvent (DMF). First, the radical site on the fluorographene is protonated by DMF creating DMF radical (a), which attacks another radical site forming *N,N*-dimethylcarbamoyl fluoride, and a new sp^2 region on the fluorographene (b). The radical on the fluorographene may be recreated by a consecutive attack by another DMF radical (c). Redrawn based on results of reference.[21]

Regarding the other defluorination reactions that were also mentioned in the graphite fluoride section, thermal decomposition of graphite fluoride (as well as fluorographene) leads to the evolution of low-molecular-weight C_xF_y species thus gradually creating graphite-like or amorphous carbon.[14,50] If the process is well-controlled, it may lead towards exfoliation of the graphite fluoride creating partially fluorinated graphene.[58] This process is much more effective, if a gaseous reducing agent is present, e.g. hydrogen[50] or hydrazine vapors.[62] Finally, the fluorographene prepared from graphite fluoride can be converted to graphene by treating the fluorographene in dispersion with alkali metal iodides.[18] This leads to nucleophilic substitution of iodine to fluorographene at the radical site and since the iodographene is metastable,[19] this product disproportionates into elemental iodine and graphene.[18]

Nucleophilic substitution. Although the fluorographene has been known to behave as an electrophile undergoing nucleophilic substitution,[70] its mechanism was unknown until recently. First attempts suggested S_N1 mechanism,[70] although the dissociation energy of the C-F bond was predicted to be very high thus favoring the S_N2 mechanism.[20] However, this process would be sterically challenging since the nucleophile would have to be in the proximity of the other three fluorine atoms on the fluorographene, and the energy barrier of consecutive Walden inversion would be too high.[22]

After the radicals naturally present in the fluorographene were included in the models, a different, radical mechanism was proposed. Nucleophiles, instead of attacking the C-F bond, attack the carbon atoms with unpaired electrons due to their electrophilic character. The unpaired electron is thus displaced to the neighboring carbon atom on the fluorographene causing heterolytic cleavage of the C-F bond releasing fluoride ion and recreating the radical site (Figure 8). The recreated radical site can further react with a nucleophile or can participate in the defluorination of the fluorographene, if the reaction is performed in a solvent, such as DMF or NMP. This way a plethora of graphene derivatives can be synthesized by using various nucleophiles and the outcome of the reaction can be tuned by varying solvents and/or reaction times since the nucleophilic substitution and defluorination run competitively.[22]
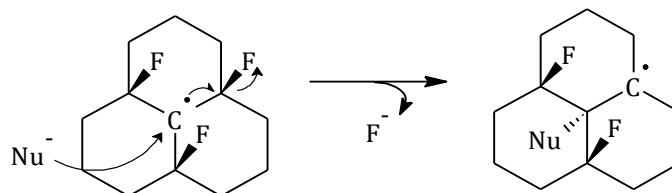
Figure 8: Mechanism of nucleophilic substitution on the fluorographene. Redrawn according to the reference.[22]

The nucleophiles may range for instance from inorganic salts, e.g. alkali metal cyanides causing attachment of nitrile groups[23], to alkylation and arylation of graphene by using relevant Grignard reagents as nucleophiles.[24] Their attachment is straightforward. There are, however, exceptions, where a catalyst is needed for grafting of the desired moiety onto the fluorographene.

Sonogashira coupling. For attachment of alkynyl groups by using the alkynyl metal compounds, an environment conditioning Sonogashira coupling needs to be used for the reaction, mainly the use of a palladium catalyst. In this process, the palladium catalyst binds to the radical site of fluorographene making neighboring C-F bonds susceptible to heterolytic

cleavage of fluorine and simultaneously binding the alkynyl in its stead. The reaction mechanism of this process is depicted in Figure 9.[25]
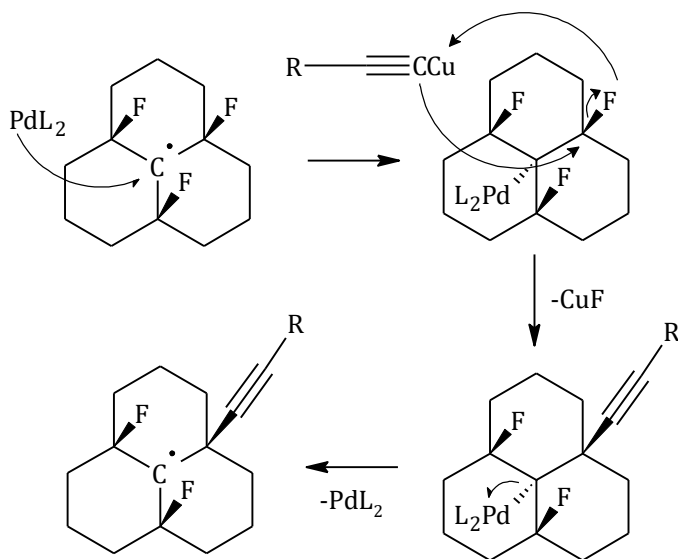
Figure 9: Mechanism of Sonogashira coupling on fluorographene. First, the Pd catalyst binds onto the radical site of the fluorographene making adjacent C-F bond susceptible to heterolytic cleavage allowing attack of the alkynyl residue that, as a result, binds to that particular site. At the end of the process, the Pd catalyst is released recreating fluorographene radical. Redrawn according to reference.[25]

Suzuki-Miyaura reaction. In this reaction, C-C bonds are created between the fluorographene and residue of an organic boronic acid derivative grafting it on the emerging graphene surface. The reaction also requires the presence of the palladium catalyst and runs very similarly to the Sonogashira coupling. However, the leaving fluorine anions may bond to the ligand of the Pd catalyst causing the formation of Pd nanoparticles during the process, which may be undesirable.[71]

Cycloaddition. Partially fluorinated graphene may act as a dienophile undergoing Diels-Alder cycloaddition. This is thanks to the electron-withdrawing effect of fluorine atoms that lower the energy of lowest unoccupied orbitals (LUMO) of π-conjugated domains of graphene that may therefore react with diene in s-cis-conformation by the overlap of the energies of highest occupied orbitals of the diene with LUMO of graphene. Thanks to this, it can occur even under ambient conditions. During the process, two σ-bonds are formed from two π-electrons of former dienophile (graphene) and four π-electrons of former diene connecting the graphene with the former diene structure as depicted in Figure 10.[72]

23

Figure 10: Mechanism of Diels-Alder reaction on partially fluorinated graphene.

Although such a process may also run using graphene oxide, the use of partially fluorinated graphene is important for a possibility of heterobifunct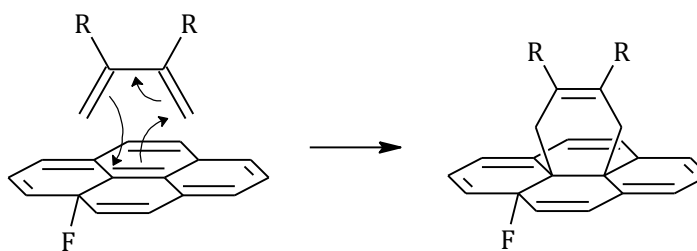ionalization of graphene by first reacting fully fluorinated graphene with a certain nucleophile in non-defluorinating solvent thus creating graphene derivative with a higher number of residual fluorine. Consecutive Diels-Alder reaction of this material with diene would lead to bonding another structure onto the graphene surface thus creating graphene derivative containing two different chemical moieties. Due to the high energy of dienes in s-cis conformation, such structure may be formed in-situ by light-induced isomerization.[72]

Nitrogen doping. The reaction of amide ions with fluorographene was first thought to produce graphene with amino groups grafted onto its surface.[73] However, a thorough study regarding the characterization of the product of this reaction showed no signs of amino groups in the material.[26] Instead, the material exhibited traits of nitrogen-doped graphene. The theoretical study supported by analysis of reaction byproducts regarding disentangling of the reaction mechanism showed, that a disruption of the fluorographene backbone needed for the insertion of a nitrogen atom into the emerging graphene skeleton following the nucleophilic substitution of the amino group is energetically impossible. It was therefore this study, that suggested, that fluorographene prepared by exfoliation of graphite fluoride contains many vacancies because of extensive fluorination. Since the reactivity of the fluorographene is caused by unpaired electrons present in the material, the most stable vacancies with unpaired electrons residing within them were found to be a single vacancy and double vacancy depicted in Figure 6bc and Figure 11ab showing the mechanism of insertion of nitrogen into them. The amino group first attacks the radical in the vacancy and bonds there through nucleophilic substitution. This step is energetically favorable for the double vacancy and slightly energetically demanding for a single vacancy due to steric reasons. Then, healing of the vacancy follows by cleavage of hydrogen atoms from an amino group induced by another amide ions producing ammonia, which is highly energetically favorable. Thus, three different nitrogen configurations

within the graphene backbone may be created: pyrrolic, pyridinic, and graphitic nitrogen (Figure 11).[26]
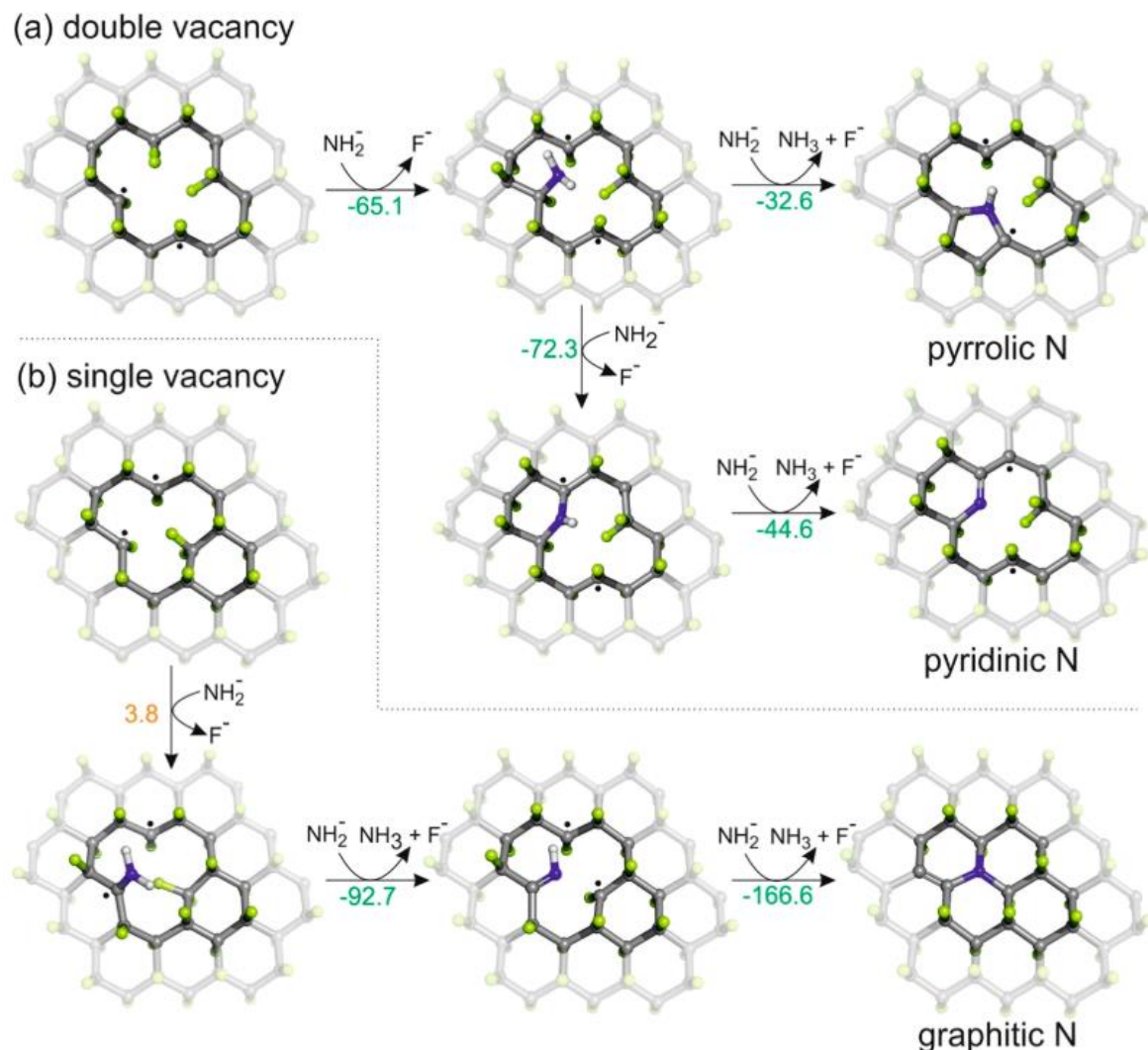
Figure 11: Mechanism of nitrogen doping of fluorographene running on its vacancies. The nucleophilic substitution at the site of a stable double vacancy (a) leads towards the formation of either pyrrolic or pyridinic nitrogen configuration in the emerging graphene. The same process on the single vacancy (b) leads to the formation of graphitic nitrogen configuration. Numbers below the arrows indicate the reaction energies between the two depicted states in kcal/mol. Adapted from reference.[26]

The process of nitrogen doping of fluorographene was also described by the reaction of ammonia with fluorographene, either gaseous[74] or in liquid phase reaction generated in situ as in the study of Zoppelaro *et al*. In this work, hydroxylamine was used, decomposing under the reaction conditions, creating ammonia that reacts with the fluorographene and produces graphene doped mainly with pyridinic nitrogen.[75]

The nitrogen-doped graphene was also found to be formed via the reaction of fluorographene with sodium azide in the environment of solvent.[27,76] The mechanism is believed to run similar to the attack of amide ion on the radical within the vacancy. First, the nucleophilic substitution of azide ions takes place which was observed from FTIR spectra[76] after which healing of vacancies occurs by cleavage of nitrogen molecule from the bonded azide group. The procedure of production of nitrogen-doped graphene via reaction of graphite fluoride with sodium azide in DMF is the subject of PCT application titled "Nitrogen-doped graphene and use thereof" with application number PCT/CZ2021/050016 which claims priority of the patent application EP20173178.3. The nitrogen doping was also found to occur when fluorographene was let to react with sodium nitrate.[27]

The degree of nitrogen doping is higher the higher is the temperature of the treatment and is also specific to the treatment. For example, when sodium amide was used for this purpose, the rate of the reaction running in DMF was decreased by an order of magnitude, when the temperature was decreased from 130 °C to 70 °C. The highest recorded N-doping degree for this reaction was when done in acetonitrile at 70 °C with resulting nitrogen content of 17 at. %.[26] The doping via reaction with ammonia resulted in 9.8 at. % of N when done in DMF at 130 °C using decomposition of hydroxylamine,[75] and in 19.9 at. % of N when done in the gas phase at 400 °C.[74] When sodium azide approach is used, in DMF at 130 °C it achieves 13 at. % of N[76] compared to 30.7 at. % of N by using the same treatment done in tetraethylene glycol dimethyl ether at 200 °C.[27] The results of several works show, that if fluorographene is used as a starting material, the synthesis of nitrogen-doped graphene is readily tunable by varying reaction conditions.

2 Aim of the thesis

Fluorographene has been used as a precursor for the synthesis of a wide variety of covalent graphene derivatives.[56] Its reactivity with many nucleophiles, proceeding simultaneously with defluorination,[22] has afforded graphene analogs with different chemical moieties covalently grafted onto graphene's skeleton. For example, the first organic magnet ever described, with tunable magnetic properties by varying its functionalization degree, was based on hydroxofluorographene synthesized by fluorographene reacting with tetraethylammonium hydroxide.[77] Cyanographene is another graphene derivative containing nitrile groups from fluorographene reacting with alkali cyanides.[23] Such derivative readily binds metal atoms[78] making it a suitable substrate for effective cooperative single-atom catalysts.[79] Cyanographene was also found to immobilize silver nanoparticles (AgNPs) thus making a potent non-toxic antibacterial agent effective towards AgNP- and antibiotic-resistant bacteria.[80] Via acidic hydrolysis, cyanographene can be converted into graphene acid, containing carboxyl groups,[23] that may act as a durable supercapacitor electrode material,[81] and can be readily further functionalized,[23] e.g. by binding enzymes via peptide bond thus making nanobiocatalyst.[82] This approach may in the future produce a new class of biosensors and may lead towards the production of biofuel cells. In the field of energy storage, many of such covalently functionalized graphenes proved themselves as effective supercapacitor electrode materials,[83] and, graphene interlinked with sulfur-chains has the potential to significantly improve Li-ion batteries performance.[84]

From these examples, it becomes apparent that the chemistry of fluorographene and the respective derivatives have particularly high applicability in key scientific and technological areas such as catalysis, energy storage, and biomedicine. To obtain such derivatives florographene prepared mostly with exfoliation of graphite fluoride is used. However, as described in the introduction, graphite fluoride, rather than being a single compound with clearly defined structure and composition, is often a complicated mixture of various fluorocarbon compounds of various stoichiometries with total composition and structure highly depending on the fluorination procedure and carbon source. Since some graphite fluoride properties, e.g. thermal stability, differ significantly depending on the carbon source used for the fluorination,[50] we hypothesized that such differences might be also reflected on the chemical reactivity of fluorographene prepared thereof. It would be therefore desirable to test if different graphite fluorides exhibit different reactivity. Indeed, preliminary results verified this hypothesis, therefore, it is a matter of paramount importance to address the reasons behind these.

On this basis, the present thesis aims to understand and relate the structural properties of graphite fluorides with their chemical reactivity, to identify the graphite fluorides which are most preferable for the synthesis of graphene derivatives (to identify preferable carbon source whose fluorination produces reactive fluorographite) and to find a method that could be used for simple and quick distinguishing of the reactive materials. For this, several graphite fluoride materials purchased from commercial suppliers were characterized by employing a large gamut of instrumental techniques, and their reactivity was tested primarily by analyzing the reaction products of them reacting with sodium azide (producing nitrogen-doped graphene) and with octylamine, affording alkylated graphene derivatives. Knowledge obtained by this study will be very useful for future research in the development of novel graphene derivatives, and for possible future industrial practice focused on the production of graphene derivatives from graphite fluoride on a large scale.

3 Experimental part

3.1 Materials

3.1.1 Graphite fluorides

During the whole study, 8 different graphite fluorides (GFs) were tested. All these materials are listed in Table 1 with characterization information provided by the supplier. GF from Merck Sigma Aldrich was in this study referred to as a benchmark regarding its reactivity (Graphite fluoride, polymer, >61 wt. % F - codename GFS) since it was used in most of the previous studies as the starting material thus its reactivity is known and consistent with every batch.

Three other different GFs were purchased from an American supplier. Those materials differed in graphitic source material and therefore in final characteristics of derived graphite fluorides. The first material codenamed GFA1 had declared to have an average particle size ranging from 1 to 10 um with a fluorine content of 56-61 wt. % and for its synthesis, charcoal was used. The second material codenamed GFA2 had declared an average particle size of 10-20 µm and fluorine content between 60 and 65 wt. % synthesized from artificial graphite. The last material codenamed GFA5 was made from natural graphite, therefore it had much bigger particles containing flakes of the declared size of 200-500 um and with fluorine content of 56-61 wt. %.

Other graphite fluorides were purchased from various Chinese suppliers. The first was codenamed GFC1 with 50-56 wt. % of fluorine. The second material codenamed GFC3 had declared fluorine content of 61-64 wt. %. The last two materials differed in the purpose of use – one was lubricant type with declared fluorine to carbon (F/C) ratio of 1.23 synthesized by fluorination of petroleum coke (codenamed GFC2L) and the latter described as battery type was synthesized by fluorinating carbon fibers (codenamed GFC2B) and had declared F/C ratio of 1.23.

Table 1: List of graphite fluorides studied in this work with their characteristics provided by suppliers.

GF codename	Source material	declared average size	declared fluorine content
GFS	*confidential*	-	>61 wt. %
GFA1	charcoal	1-10 um	56-61 wt. %
GFA2	artificial graphite	10-20 um	60-65 wt. %
GFA5	natural graphite	200-500 um	56-61 wt. %
GFC1	*unknown*	-	50-56 wt. %
GFC3	*unknown*	-	61-64 wt. %
GFC2L	petroleum coke	-	F/C = 1.23
GFC2B	carbon fiber	-	F/C = 1.07

3.1.2 Other chemicals and materials

For characterization of graphite fluorides and synthesis and consecutive treatment of graphene derivatives derived from the listed graphite fluorides, the following chemicals were used. Sodium azide (NaN_3, reagent grade) was purchased from Sigma Aldrich, n-octylamine (n-OA, 99+%) was purchased from Acros Organics, acetone (p.a.) was purchased from VWR Chemicals, ethanol (EtOH, 99.8 %) was purchased from BC Chemservis, N,N-dimethylformamide (DMF, for peptide synthesis) was purchased from Merck LiChrosolv, 1,2-dichlorobenzene (oDCB, 99%, pure) was purchased from Acros Organics, dichloromethane (DCM, 98%) was purchased from Sigma Aldrich.

3.2 Testing of reactivity of the graphite fluorides

All the graphite fluorides were tested by using them as starting materials for the synthesis of graphene derivatives. As the main reaction for this purpose, a synthesis of nitrogen-doped graphene was chosen. The procedure for this is subject of PCT application titled "Nitrogen-doped graphene and use thereof" with application number PCT/CZ2021/050016 claiming the priority of the patent application EP 20173178.3. The second reaction used for further support of the first testing results was the synthesis of octylamine-grafted graphene reported in references.[85]

3.2.1 Synthesis of GN3 materials

All GN3 materials syntheses were started by making a dispersion of relevant graphite fluoride in DMF (60 mL of DMF for 1 g of material), which was stirred for 2 days in a 100mL glass round-bottom flask. On the third day, the dispersion was sonicated for 4 hours (Sonorex Digitec) and then stirred overnight till the next day. Then, sodium azide (NaN_3) was added to the dispersion (2 g of NaN_3 for 1 g of GF) after which the mixture was heated at 130 °C on an oil bath while stirring for another 3 days with reflux and under ambient atmosphere. After the mixture was cooled down to room temperature, it was transferred into a 50mL centrifuge polypropylene tube with conical bottom. The solid product was separated from the liquid by centrifugation (Sigma 4-16K centrifuge, 13 000 rpm, 5 minutes) and washed 3x with DMF, 3x with acetone, 3x with EtOH, once with hot deionized water, 3x with acidified water (100 µL of 3% HCl per 30 mL of dispersion), and then with deionized water till the conductivity of the material-containing dispersion was below 100 μScm^{-1} (WTW Cond 3210 conductometer). For each washing step, the same volume of solvent was used as was the volume of the DMF used for the reaction. Some dispersions were optionally further purified using dialysis by transferring the dispersion into the membrane and letting it stand in a beaker with 5 L of deionized water for three weeks with water being changed every workday. For some characterization techniques, the materials were lyophilized by freezing the sample to – 80 °C before placing it into the freeze drier and dried until the sample had a form of powder.

3.2.2 Synthesis of GOA materials

For the synthesis of GOA materials, 400 mg of relevant GF was mixed with 30 mL of DMF in a 100mL glass round-bottom flask with an attached three-way valve with a nitrogen-containing balloon. After the GF and DMF were mixed, the flask was filled with nitrogen by repeated evacuation (using a vacuum pump) and filling with nitrogen from the balloon. Then, the GF dispersion was stirred under a nitrogen atmosphere for 3 days with 4 hours of sonication (Sonorex Digitec) on the third day of stirring. Then, 5 mL of n-octylamine (n-OA) was added to the GF-DMF dispersion and the mixture was stirred at 500 rpm and heated to 130 °C under an inert atmosphere with reflux for 24 hours. Then, after the mixture cooled down to room temperature, it was transferred into a 50mL centrifuge tube. The solid product was precipitated from the liquid by centrifugation using Sigma 4-16K centrifuge at 13 000 rpm for 5 minutes and washed with DMF, acetone, EtOH, and deionized water. For each washing step, the material was dispersed in the relevant solvent by quick sonication and centrifuged using the same parameters as the initial centrifugation had. For washings, 2x hot and 2x room temperature

solvent was used, consecutively. Then the resulting GOA materials were three times washed using DCM and dispersed in a minimum amount of DCM.

3.3 Characterization methods of starting materials and products

3.3.1 Raman microscopy analysis

Principle: Raman spectroscopy (named after its Indian discoverer) uses the inelastic scattering of light (that must not be absorbed by any component of the studied system) on the studied species to study their structure by tracking the differences between energies of original and inelastically scattered light. Such differences correspond to vibration modes of bonds or structures that are associated with the change of polarizability of the bond or structure during the vibration. Except for the most intense elastic Rayleigh scattering producing light with the same energy as the incident light, two types of inelastic scattering may occur during the scattering, Stokes, and anti-Stokes. Stokes scattering causes light energy to be lower by the energy of the vibration. This is due to the structure of the species in the virtual excited state causing relaxation into a higher vibrational state than the vibrational state before the irradiation. The latter one, Anti-Stokes scattering is the opposite – a structure in a vibrationally excited state is irradiated forming the virtual excited state and which then relaxes into a lower vibrational state than the structure originally had. Since the probability of Stokes scattering is much higher, Stokes scattering is generally used for measuring Raman spectroscopy. Because the intensity of inelastic scattering is compared to Rayleigh scattering still very low, a very intense and monochromatic source of radiation is needed. Such criteria meet lasers. For the measurement, the sample can be irradiated directly by the laser beam and the light scattered 90 ° away from the incident illumination is analyzed by the spectrometer, or, the sample illumination and collection of the scattered light can be performed through a microscope objective. The latter method is called Raman microscopy and is very convenient in terms of sample size allowing measurements of objects of very small spatial dimensions thanks to the magnification.[86]

Measurement conditions. For the measurements of Raman spectra through Raman microscopy, DXR™3 Raman microscope (Thermo Scientific) with 532 nm laser was used. The studied sample in the form of acetone suspension was placed onto a gold substrate, dried, and placed into the instrument. The sample was magnified 50x using the microscope objective and measured with a resolution of 2 cm^{-1} by summing 32 exposures at a laser power of 2 mW. To spectra of graphite fluorides, second-order polynomial fluorescence corrections were applied using the OMNIC software.

3.3.2 FTIR analysis

Principle. Infrared spectroscopy (IR) is a technique of studying matter by absorbing electromagnetic radiation in the infrared region. The absorbed radiation has a distinct frequency corresponding to the energy difference between two energy states of normal vibration modes of bonds or molecules (collective vibration) associated with changes of the dipole moment of the species during the vibration. Fourier-transform infrared spectroscopy (FTIR) is a fast means of measurement of IR spectra. Instead of scanning through all wavenumbers of used radiation by dispersing it into monochromatic beams (dispersive spectroscopy), it uses radiation made by an interferometer that recombines several frequencies into a single beam. Many such beams are passed through the sample and intensities of the passed radiation are measured by a detector creating an interferogram (intensity of detected radiation dependent on the position of the mirror of the interferometer) that is then transformed by Fourier transformation into the spectrum. The most widely used technique of measurement is attenuated total reflectance (ATR) where instead of passing the radiation through the sample the technique uses an internal reflection of the radiation on the interface of a sample and a crystal of high refractive index.[86]

Measurement and data processing. FTIR spectra were recorded using an iS5 FTIR spectrometer (Thermo Nicolet) using the Smart Orbit ZnSe ATR accessory allowing nitrogen flow through the accessory to suppress gaseous H_2O and CO_2 absorption bands. Before measurement, the crystal was first cleaned with ethanol after which the background was scanned. Then, water-, EtOH- or DCM-based dispersion was deposited onto the crystal and allowed to dry. Optionally, powder of the relevant material was placed on the ZnSe crystal and pressed against the face of the crystal with the steel tip of the accessory. Spectra were then acquired with 1 cm^{-1} resolution by summing 32 scans. Baseline corrections were optionally applied to the collected spectra. Spectra heavily affected by noise were smoothed using Savitzky-Golay filter using 50 points of convolution.

3.3.3 XPS analysis

Principle. X-ray photoelectron spectroscopy (XPS) is an instrumental technique used for the determination of the elemental composition of material surfaces and even the oxidation or bonding state of individual observed elements. The principle of the technique is irradiating the studied sample with monochromatic X-ray radiation which causes the emission of core electrons from samples' atoms. The number of ejected photoelectrons is then detected with respect to their kinetic energy that is measured by a hemispherical analyzer, where electrons are separated depending on their kinetic energy by passing between two hemispheres of different potentials that create an electric field. In this environment, the electrons with higher kinetic energy have

trajectories with higher radius and vice versa. Thus, the kinetic energy E_k of the photoelectrons is measured, from which the binding energy E_B of the original electron can be determined according to the relation (eq 1):

$$E_k = h\nu - E_B - \phi \tag{1}$$

where $h\nu$ is the energy of the incident X-ray radiation and ϕ is the spectrometer work function. Therefore, the X-ray radiation needs to be strictly monochromatic. As a source of X-ray radiation, an Mg or Al anode bombarded with an electron gun is used. This emits characteristic X-ray radiation for the material of the anode, which is further monochromated and focused on the sample by reflecting it from the quartz monocrystal. The work function ϕ is dependent on the conditions of each measurement, therefore, all the spectra need to be shifted according to a certain characteristic line, mostly carbon 1s sp^2 line (284.8 eV). The binding energy of the original electron is the energy needed for that electron to leave the atom and depends on the effective charge of the nucleus, which depends on the element, on the electron energy level within the atom of the element, on the spin-orbit splitting, and the electron density around the atom of the observed element. The higher is the electron density around the atom, the lower the binding energy of the electron is since the charge of the nucleus is more shielded by higher electron density. This allows using XPS for determination of elemental composition and for observation in what binding or oxidation state each element is, which can be more evident by deconvolution of the spectra into mixed Gaussian-Lorentzian components. For the elemental composition determination, the number of atoms of one type of element per cm^3 of the sample (n) is given by (eq 2)

$$n = \frac{I}{S} \tag{2}$$

where I is the number of photoelectrons detected per second of the measurement and S is the atomic sensitivity factor, which is specific for each element spectral line and spectrometer itself. From this, the atomic concentration C_x of the element x can be determined according to equation 3.[87] This is done by using mathematical software.

$$C_x = \frac{n_x}{\sum_i n_i} = \frac{\frac{I_x}{S_x}}{\sum_i \frac{I_i}{S_i}} \tag{3}$$

Measurement and data processing. XPS measurements were performed by employing a PHI VersaProbe II (Physical Electronics) spectrometer using an Al $K\alpha$ source (15 kV, 50 W). Samples were deposited onto the silicon holder as water-, ethanol- or acetone-

based slurry that was let to dry prior to the measurement. The obtained spectra were evaluated and deconvoluted using the MultiPak (Ulvac - PHI, Inc.) software package. The spectral analysis included shifting the spectra by positioning the C 1s sp^2 lines at 284.8 eV, atomic composition determination with Shirley background subtraction (according to eq 3), and peak deconvolution employing mixed Gaussian–Lorentzian functions.

3.3.4 XRD analysis

Principle. X-Ray Powder Diffractometry (XRD) is a technique of studying crystallinity and composition of powdered crystalline samples. When the sample is irradiated by X-ray radiation, the beam is reflected by an angle specific to the spacing of all possible crystal planes of the crystal according to the Braggs law (eq 4) that formulates the condition of constructive interference of the waves reflected from two neighboring crystal planes with their characteristic spacing. The measurement is done by detector measuring the intensity of reflected radiation at all diffraction angles by rotating over the irradiated sample during the process.[86]

Measurement and data processing. X-ray diffraction (XRD) patterns were recorded on PANalytical X'Pert PRO diffractometer (iron-filtered Co Kα radiation: λ = 0.178901 nm, 40 kV, and 30 mA) in the Bragg–Brentano geometry, equipped with an X'Celerator detector, programmable divergence, and diffracted beam anti-scatter slits. Samples were placed on a zero-background Si slide, gently pressed with sheet glass to create a uniform surface layer, and scanned with a step size of 0.0334°, and 2θ scan range from 5° to 90°. Measured diffractograms were normalized to [0,1] with respect to the intensity of (001) diffraction line of graphite fluoride and plotted using OriginPro software. The desired parameters were spacings (d_{hkl}) of observable crystal planes (hkl) characteristic to graphite and full-width half-maximum (FWHM, β_{hkl}) of each reflection. The crystal plane spacings were calculated according to relation derived from Bragg's law (eq 4):

$$d = \frac{n\lambda}{2\sin\theta} \tag{4}$$

where d is the interplanar distance, n is an order of the diffraction ($n = 1$), λ is the wavelength of incident X-ray radiation in nm and θ is the diffraction angle that equals half of the 2θ position of the maximum reflection of the relevant plane. FWHM of the reflections was determined using a peak analyzer in OriginPro software. Acquired d_{hkl} and β_{hkl} values were used as variables for PCA analysis for summarizing such crystalline characteristics of scrutinized materials to principal components and thus sorting the materials according to their crystallinity.

3.3.5 NMR analysis

Principle. Nuclear magnetic resonance (NMR) is a spectroscopic method used for structure determination of the sample containing non-zero-spin nuclei (such as ^{1}H, ^{13}C, ^{15}N, ^{19}F, …). When such nuclei are placed into the strong magnetic field, their nuclear spins align with the vector of magnetic field intensity in either antiparallel or parallel alignment representing two energy states with higher and lower energy, respectively. The energy difference ΔE depends on the strength of the intensity of magnetic field B according to the equation (eq 5):

$$\Delta E = h\nu = \frac{h\gamma B}{2\pi} \tag{5}$$

where h is Planck constant ($h = 6.626 \cdot 10^{-34} m^2 \cdot kg \cdot s^{-1}$), γ is the gyromagnetic ratio of the nucleus and ν is Larmor frequency characteristic of precession motion of the nuclear spin. This precession generates an electric field that interacts with the radiation of the same frequency (resonance with radio-frequency radiation) by absorbing it which causes the lower-state parallel-oriented nuclear spins to flip. These spins then precede in the same phase; therefore, the magnetization of the sample may be recorded by the coil surrounding the sample. By the Fourier transforming this record, a Larmor frequency is obtained. The frequency is characteristic of not only the type of nuclei but also of electron density around it. The higher the electron density around the nucleus, the higher is the shielding of B_0 by the electrons, therefore, the effective B influencing the nucleus is lower, so the Larmor frequency is thus lower. For each nuclear domain, an internal standard is used to normalize the x-axis of the NMR spectra, since the differences in the Larmor frequencies are very low and depend on the used instrument (operating magnetic field intensity). This is done according to the equation (eq 6):

$$\delta = \frac{\nu - \nu_{sd}}{\nu_{sd}} \tag{6}$$

where δ is chemical shift with respect to the standard, ν is observed Larmor frequency and ν_{sd} is the Larmor frequency of the internal standard.[86]

In the solid state, the nuclear spins experience dipolar interactions, chemical shift anisotropy, and quadrupolar interactions leading to very broad and featureless lines. However, these are orientation-dependent and can be averaged using the NMR measurement technique of magic angle spinning (MAS). The dipole-dipole interactions between magnetic moments of nuclei average to zero only at the magic angle $\theta_m = 54.74°$ (angle between the space diagonal of a cube and its edge) with respect to the direction of the magnetic field. The chemical shift anisotropy, nuclear-electron interactions, and quadrupolar interactions are however only

partially averaged. Thus, when the sample is measured while rotating with high frequency (12 to 35 kHz) at the magic angle, the signal then appears as narrow bands for isotropic lines and as spinning sidebands for each isotropic line which can be used to determine the chemical shift anisotropy of the nuclei.[86] To better enhance the spectra, the technique of cross-polarization is used, during which the sample is irradiated with radiation pulses of energy corresponding to differences between precession frequencies of two different spins, such as ^{1}H-^{13}C.[88,89] If it is not desirable to observe the spinning sidebands, a technique called total sideband suppression (TOSS) can be used to completely suppress the sidebands. In this technique, a sequence of timed radio-wave excitation pulses synchronized with the MAS rotor is used for the measurement. By doing so for an isotropic sample, the sidebands from different orientations interfere destructively thus canceling each other.[90]

Measurement and data processing. The solid-state NMR measurements were performed using a JEOL spectrometer JNM-ECZ400R with a superconducting coil having a magnetic field of 9.4 T (working frequency: 399.8 MHz for ^{1}H, 376.3 MHz for ^{19}F, and 100.5 MHz for ^{13}C NMR) equipped with a 3.2 mm MAS probe. The ^{19}F-TOSS technique was used to suppress residual spinning sidebands. The ^{19}F-^{13}C cross-polarization magic angle spinning (CPMAS) NMR spectra were collected at ambient temperature at the spinning rate of 18 kHz, using contact time and relaxation delay 10 ms and 1 ms, respectively, for all measurements.

3.3.6 EPR analysis

Principle. Electron paramagnetic resonance (EPR) spectroscopy is a technique used for studying paramagnetic substances. Since the electrons in such samples are unpaired, their magnetic moment is non-zero and responds to a high external magnetic field by aligning in antiparallel or parallel way with the vector of magnetic field intensity thus creating two states with lower and higher energy, respectively. The energy difference between those states can be expressed by the following equation (eq 7)

$$\Delta E = h\nu = g\mu_B B_0 \tag{7}$$

where h is Planck constant, ν is Larmor frequency of the spin precession and, therefore, frequency of the absorbed radiation (the same principle as in NMR), μ_B is Bohr magneton ($\mu_B = 9.274 \cdot 10^{-24} J \cdot T^{-1}$), B_0 is the intensity of external magnetic field and g is Landé g-factor characterizing the environment of the unpaired electron since the external magnetic field is locally shielded by other electrons in its vicinity. The unpaired electron may also interact with magnetic moments of other unpaired electrons or nuclei with non-zero spin located in its

vicinity by exchange coupling and hyperfine coupling, respectively, causing several possible transitions manifested by splitting of the observed signal. The spectra are mostly measured by irradiating the sample with microwave radiation of fixed frequency while modulating the magnetic field applied to the measured sample.[86]

Measurement and data processing. Prior to the measurement, dispersions of graphite fluorides in 1,2-dichlorobenzene (oDCB) were prepared by dispersing 20 mg of relevant material in 500 μL of oDCB. Then, 100 mL of this dispersion was transferred into highly pure quartz tubes (Suprasil, Wilmad, ≤ 0.5 OD), cooled using liquid nitrogen, and then the spectra were collected at the temperature of 78 K on a JEOL JES-X-320 spectrometer operating at the X-band frequency (~9.14–9.17 GHz) equipped with variable temperature control ES 13060DVT5 apparatus. For all the measurements the microwave power was set to be 0.5 mW to minimize the power saturation effect and the modulation width of 0.7 mT and modulation frequency 100 Hz were used. To improve the signal-to-noise ratio, all spectra were recorded with a 30ms time constant and 2 minutes sweep time with 3 accumulations. Accuracy on g-values was obtained against a Mn2+/MgO standard (JEOL standard). For the determination of the value of the external magnetic field at which the maximum resonance occurred a linear baseline was subtracted from all the spectra. Some spectra with very low EPR intensity that were heavily distorted by noise had to be additionally smoothed by using Savitzky-Golay filter using 1000 points of convolution to help determine a position of maximum resonance. The g-values for each material was calculated according to the formula (eq 8)

$$g = \frac{h\nu}{\mu_B B_0} \tag{8}$$

where g is g-value, h is Planck constant, ν is the frequency of used microwave radiation, μ_B is Bohr magneton and B_0 is the intensity of the external magnetic field at the maximum resonance when the signal (absorption derivative) intersects the x-axis.

3.3.7 DRS analysis

Principle. Irradiation of dull surfaces, for example of powders and powder films, leads to radiation being reflected at angles independent of the angle of the incident beam, or in other words, scattered. This phenomenon is called diffuse reflection and is accompanied by many complex processes. The radiation might be specularly reflected from the surfaces of the individual particles, however, since the particle surfaces are randomly distributed, the incoming radiation also penetrates inside the particles via the refraction and exits the particles' surface other reflections and diffractions. During this process, the radiation may be partially absorbed

in energies characteristic of the material. For the measurement, the sample is irradiated while being placed at the bottom of the integrating sphere – a hollow enclosure diffusely reflecting all wavelengths of interest with no absorption and directing the radiation reflected by the sample into the detector.[91]

Measurement and data processing. Diffuse reflectance spectra (DRS) were recorded using ANALYTIK JENA - SPECORD 250 PLUS spectrophotometer using substitution method integrating sphere accessory in the wavelength range between 190 and 1100 nm with a resolution of 1 nm. The spectra were measured with respect to the Spectralon reference. Prior to the measurement, the powdered sample was placed into the holder and pressed with sheet glass to create a uniform surface layer. Then, the holder with the accordingly prepared sample was mounted onto the bottom of the DRS integrating sphere and the whole accessory was placed into the instrument for measurement.

The measured data were then processed using the Tauc method to estimate the electronic properties of inspected materials. For the determination of material's bandgap energy (E_g), the following equation (eq 9) was used:

$$(F(R_\infty) \cdot h\nu)^{1/\gamma} = B(h\nu - E_g) \tag{9}$$

where h is the Planc constant, ν is the frequency of the incident radiation, B is a constant and γ is the factor of the nature of the electron transition.[92] Since graphite fluorides with stoichiometries of C_2F and CF are regarded as semiconductors with a direct transition bandgap,[46] the γ factor is in this case equal to ½.[92] The $F(R_\infty)$ is the Kubelka-Munk function used for transformation of the reflectance spectra to absorption spectra according to equation (eq 10):

$$F(R_\infty) = \frac{K}{S} = \frac{(1 - R_\infty)^2}{2R_\infty} \tag{10}$$

where K and S are absorption and scattering coefficients, respectively, and R_∞ is reflectance of an infinitely thick layer of the sample, in practice corresponding to reflectance on layers thicker than 5 mm, which corresponds for used measurement conditions.[91]

By doing so, Tauc plots for each material were thus acquired. To determine the bandgap energy E_g of the material, the regions showing a linear increase of light absorption with increasing energy were fitted using a linear function. The x-axis intersection point of this linear fit gives an estimate of the bandgap energy E_g of the studied material. If the studied material exhibits non-zero absorption in the ranges of lower energies than absorption maximum, E_g in

such cases corresponds to the x-axis intersection point of the linear fit of that linear increase and baseline, a linear fit of the lowest energies of the spectrum exhibiting linear increase.[92]

3.3.8 Thermal analysis

Principle. Materials can be characterized by heating them and monitoring their thermal decomposition. The behavior and thermal stability of the material during the process can be monitored by thermogravimetric analysis (TGA) that records the change in its weight with respect to temperature. Regarding the measurement, two pans, one with a sample and one as a reference, are placed onto the high precision balances recording the weight of the sample heated by a high-temperature oven. The thermally induced processes of the material produce or drain the heat. The heat flow can be measured by differential scanning calorimetry (DSC) by measuring temperature differences between the sample and the empty reference pan and controlling the heating elements near each pan thus reporting the differential power required for heating the sample with respect to the reference. Both methods can be performed simultaneously during a single measurement called simultaneous thermal analysis (STA).[86]

Methods. Thermal analysis of graphite fluorides was performed using SDT650 instrument. First, approximately 7 mg of the relevant material was placed into the 90μL alumina pan and an empty crucible was used as a reference for heat flow measurement for differential scanning calorimetry (DSC). Each sample was tested by heating up to 800 °C with a temperature ramp of 5 °C/min and nitrogen gas passing through the instrument during the measurement. At the end of the analysis, the sample was heated for 1 minute at 800 °C. The thermal decomposition process was characterized by TGA and DSC.

4 Results and discussion

In the first part of this chapter, the characterization results of all the tested graphite fluorides are presented. To better highlight the main differences in the structure and properties of tested graphite fluorides, three GF and relevant GN3 materials were selected for more thorough analysis, while the characterization results of the rest of the GF and GN3 materials are briefly summarized. In addition, GOA materials synthesized using selected graphite fluorides are thoroughly characterized to further support the results obtained from the GN3 products.

4.1 Characterization of graphite fluorides

All graphite fluorides have been scrutinized using a broad array of experimental instrumental methods to link their appearances, structural properties, chemical composition as well as magnetic properties with their reactivity.

4.1.1 Optical images of graphite fluorides

Figure 12 shows the appearance of all the tested graphite fluorides. GFS, GFC2L, and GFC2B materials were off-white powders, which explains the transparency of the materials in the visible radiation and their high reflectivity. GFA2 and GFC3 materials appeared to be light-gray powders, GFA1 was significantly darker and GFC1 was black. The material with the most different appearance among all inspected graphite fluorides was GFA5, consisting of large crystals of dark-gray color.
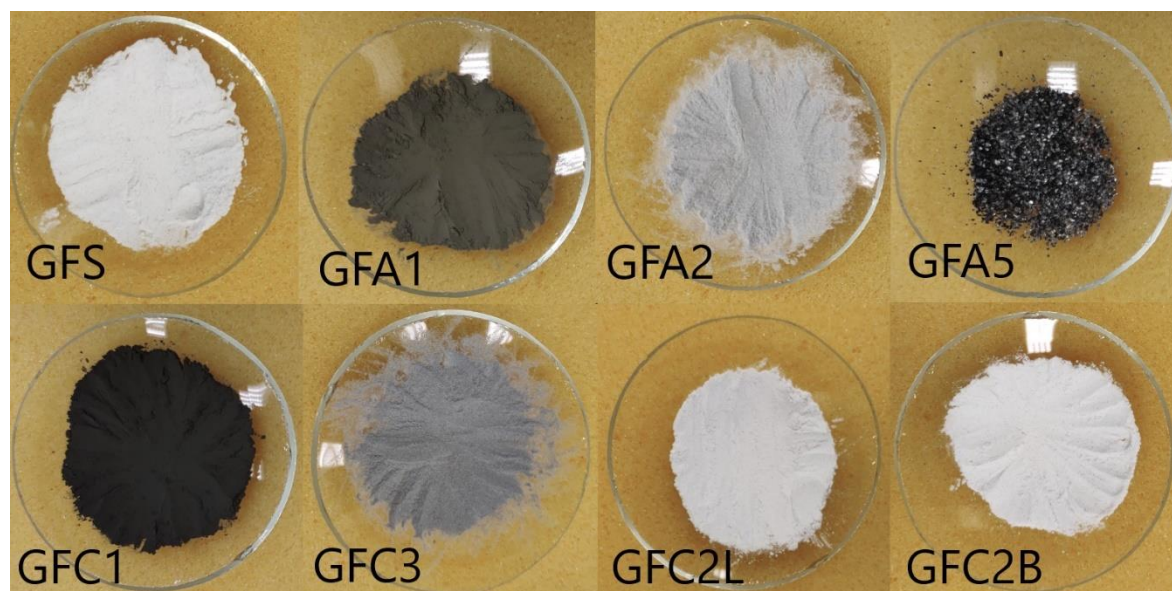

Figure 12: Optical images of all the tested graphite fluorides.

4.1.2 Raman microscopy analysis of graphite fluorides

The reason for the colors of the studied materials was more apparent when observed using a microscope at 10x magnification. The materials differed in particle sizes and numbers of partially fluorinated graphite crystals. The optical microscope images can be seen in Figure 13 depicting the area from where the spectra were collected (red spot in the center of each image). The corresponding Raman spectra of those areas of the samples are in Figure 14.
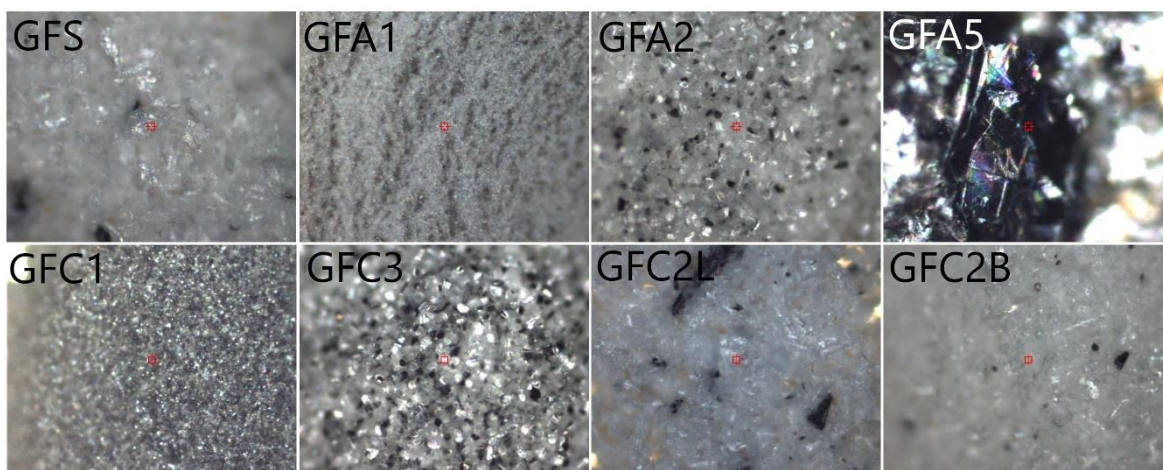

Figure 13: Optical microscope images of all the studied graphite fluorides with 10x magnification.

The off-white powders (GFS, GFC2L, and GFC2B) were composed of purely white crystals of graphite fluoride exhibiting no specific Raman signals and the spectrum was completely composed of the photoluminescence radiation of the material. These samples contained small numbers of crystals of darker color, connected to the minor presence of partially fluorinated graphite or residual graphite, as supported by the Raman spectra of the crystals differing in color (Figure 15). The spectra of the darker crystals exhibited the D and G bands characteristic of sp^2 carbon structure vibrations.[42] Light-gray powders (GFA2 and GFC3) contained a higher portion of these darker crystals but a majority of these samples were the white graphite fluoride crystals. The powders of darker color (GFA1 and GFC1) were uniform, therefore the signal from different areas of the sample was the same exhibiting presence of G and D bands representing the presence of sp^2 regions (i.e. nonfluorinated graphite). The last sample (GFA5) was composed of large crystals of almost black color (and a few with lighter-colored crystals) and its spectrum also exhibited D and G bands of graphite.
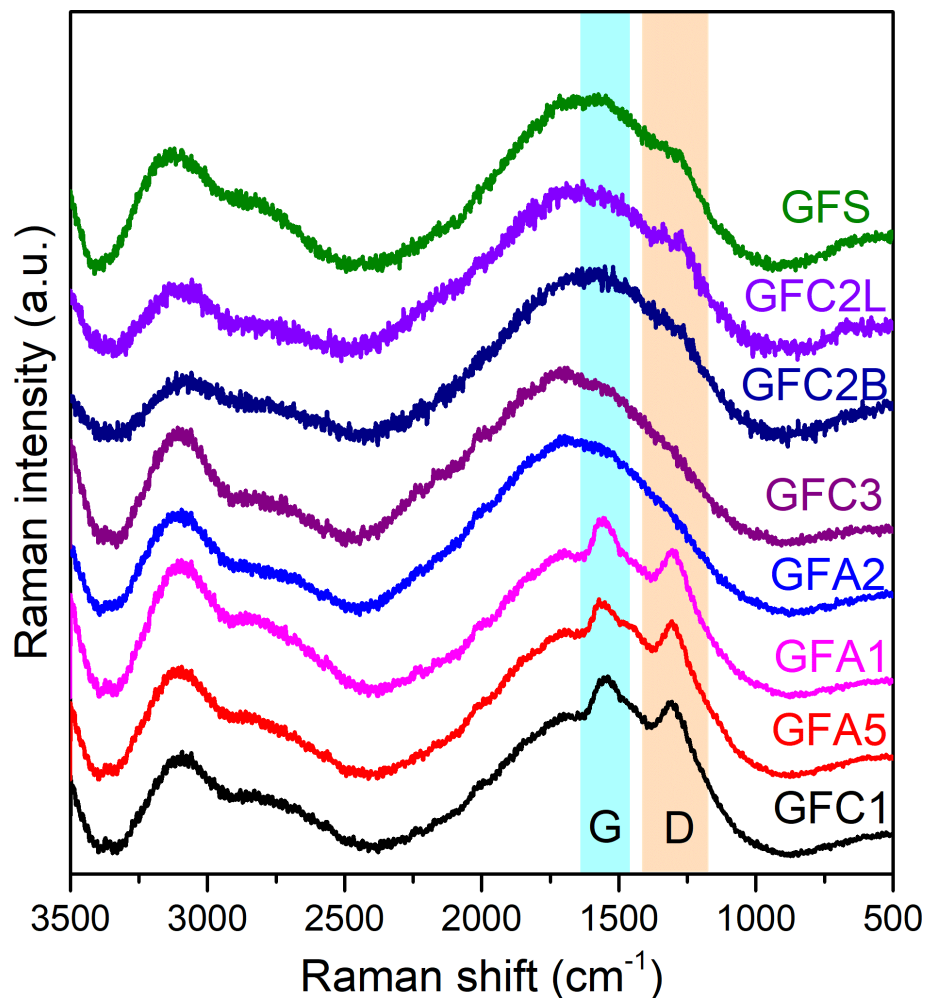
Figure 14: Raman spectra of all the studied graphite fluorides recorded on the crystals at the center of the images in Figure 13.

Figure 15: Raman spectra of GFC2L recorded on two crystals differing in color.

4.1.3 XRD of graphite fluorides

GF materials were subjected to powder X-ray diffraction (Figure 16) revealing broad reflections assigned to graphite fluorides' (001) and (100) planes at 2θ of 15°-17° and 48°, respectively. Some materials, namely GFC1, GFA1, GFA5, and, although with very low intensity, GFA2, also contained sharp feature at 31° signifying the presence of residual graphite in the material.
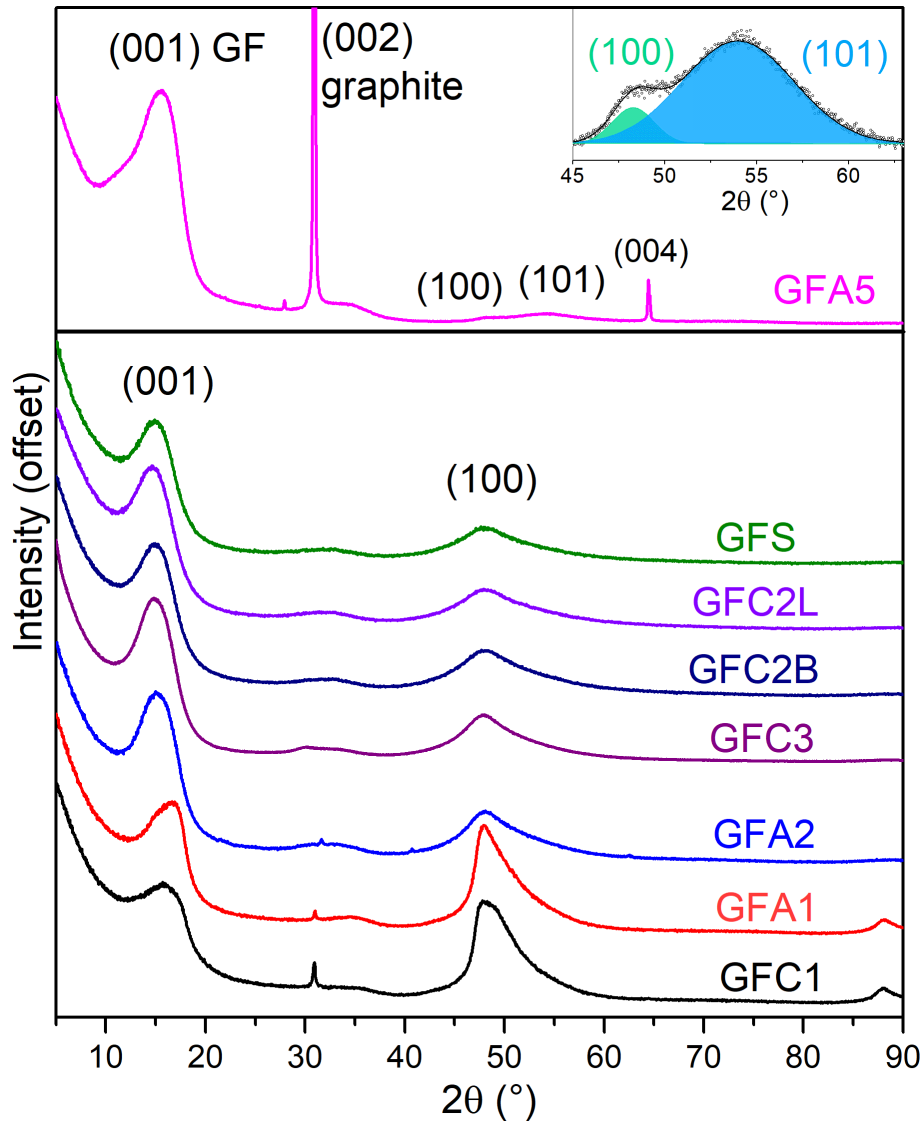
Figure 16: XRD patterns of all tested GFs with reflections assigned to GF characteristic planes. For its differences, GFA5 is plotted separately and the inset shows deconvolution of 45-65° region for determination of (100) reflection position and FWHM.

From the positions of the maxima of the (001) and (100) GF reflections, spacings (d_{hkl}) between crystal planes were calculated using Bragg's formula (Equation 4). The values of d_{001} represent average interlayer spacing between individual FG layers.[14] In GFA5 diffractogram, where the graphite reflections dominated, position and full-width half-maximum (FWHM) of (100) GF plane reflection could be only determined by deconvoluting the region between 2θ of 45° and 65°. These values, along with determined FWHM (β_{hkl}), which values are inversely proportional to the size of one crystallite coherent domain, are listed in Table 2 and were used as variables for statistical evaluation of these results using Principal Component Analysis (PCA) for sorting of the materials according to their crystallinity. A similar approach using PCA was used before for the classification of brucite nanoparticles.[93]

Table 2: Values of d_{001}, d_{100}, β_{001}, and β_{100} of each studied graphite fluoride characterizing its crystallinity and used as variables for principal component analysis.

GF	d_{001} (Å)	β_{001} (°)	d_{100} (Å)	β_{100} (°)
GFS	6.89	3.54	2.22	6.38
GFA1	6.18	3.52	2.20	4.13
GFA2	6.86	3.87	2.19	6.03
GFA5	6.61	4.43	2.13	2.67
GFC1	6.54	3.99	2.21	4.69
GFC3	6.78	3.76	2.20	6.26
GFC2L	7.03	3.65	2.20	6.89
GFC2B	6.88	3.52	2.21	6.94

The resulting PCA biplot can be seen in Figure 17. According to the depicted eigenvectors representing the crystallinity parameters, the principal component 1 is mainly defined by β_{001}, β_{100}, and d_{100} variables. Principal component 2 mainly reflects interlayer spacing of individual fluorographene lattice within graphite fluoride (d_{001}). As can be seen from the biplot, most of the materials clustered near the origin and are marked by the green circle. As it can be found later in the text of the next section, these materials were also found to be most reactive towards nucleophiles - defluorinating well and producing graphene derivatives with very high functionalization degree. Based on this analysis, two GFs, each representing the inside and outside of the cluster of the biplot, were selected for more detailed analysis and testing to prove that the reactivity of graphite fluoride can be deducted from its crystallinity. These materials and their derivatives will be compared with the results from GFS since this material proved itself to be a benchmark regarding the reactivity of graphite fluorides since it was used in many studies regarding graphene derivatives syntheses before. The selected GFs for more detailed analysis are therefore GFS, GFC2L, and GFA1.
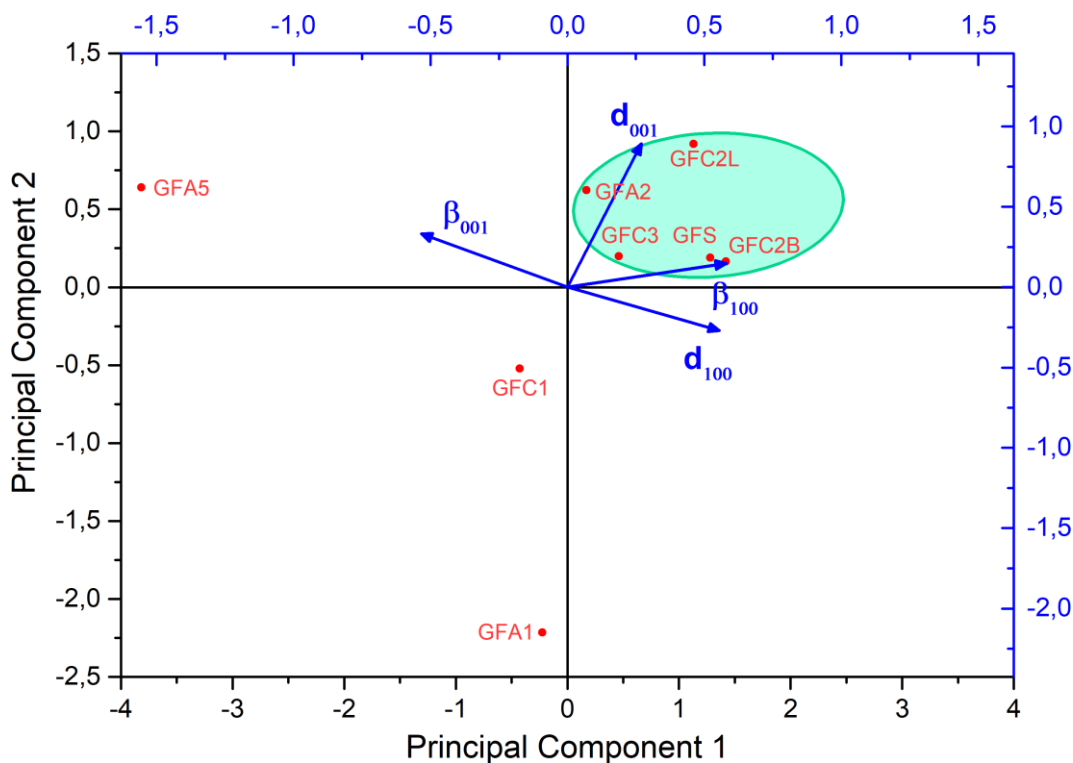
Figure 17: PCA biplot of graphite fluorides calculated from the crystallinity variables found from their XRD patterns. The green circle indicates the materials clustered near each other signifying their similar structural properties. Such materials were later found as more reactive.

4.1.4 DRS analysis and electric properties of studied graphite fluorides

Since the graphite fluorides differed in appearance, namely their colors, their diffuse reflectance (DR) spectra of the UV-VIS region were measured to specify the optical differences between them and to possibly determine their electrical properties by estimating their bandgap energies. The recorded DR spectra are in Figure 18. In the long-wave UV region, some materials reflected more radiation than the Spectralon plate which was used as a reference. Five materials (GFS, GFC2L, GFC2B, GFA2, and GFC3) exhibited a significant decrease of the reflectivity at around 217 nm (5.7 eV) due to the onset of the absorption of radiation of such energies. The rest of the materials, including GFA2 and GFC3, showed maximum absorption at around 370 nm (3.35 eV).
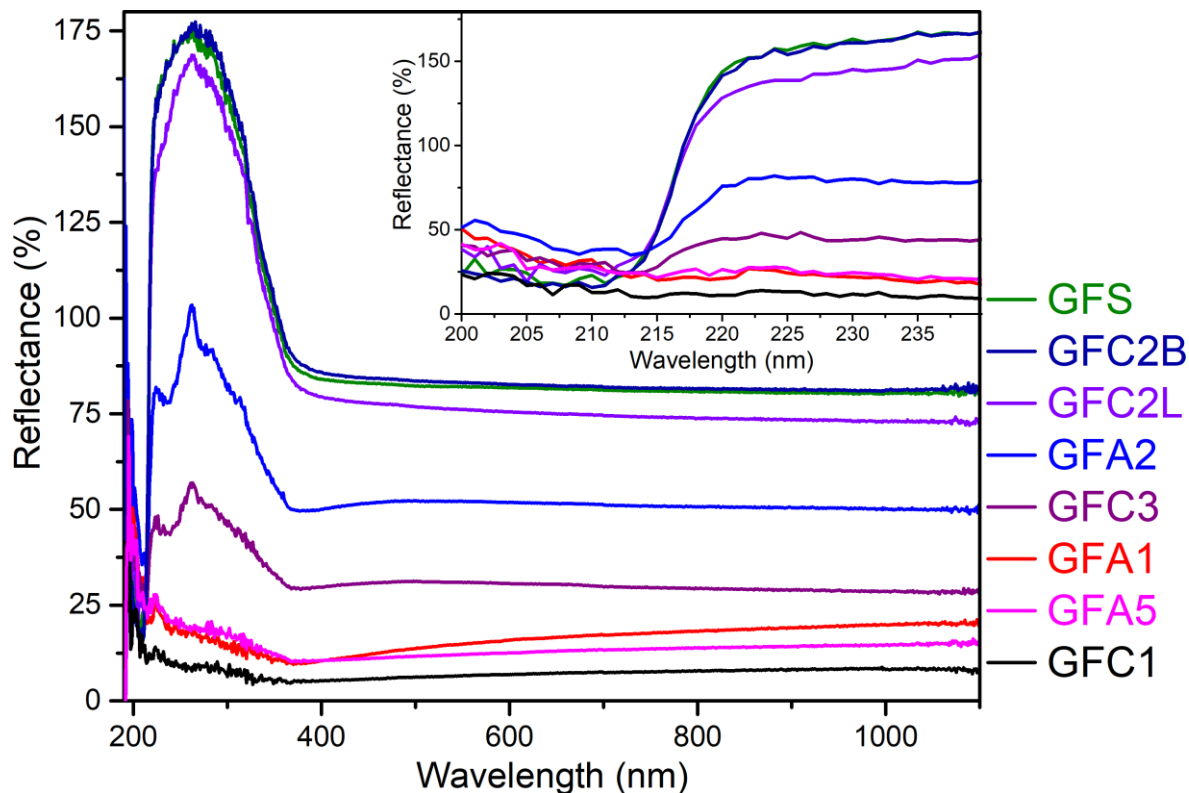
Figure 18: Diffuse reflectance spectra of all the graphite fluorides in the UV-VIS region. Inset shows a magnification of the spectra in the region between 200-240 nm.

The DR spectra were then transformed, according to the Tauc method (eq 9) and Kubelka-Munk function (eq 10), into the Tauc plots for every studied material shown in Figure 19. The bandgap (BG) energies of the materials that appeared off-white were estimated, based on the intercept of the x-axis and linear fit of the Tauc plot, to 5.79 eV, 5.76 eV, and 5.86 eV for GFS, GFC2L, and GFC2B, respectively. Along with this, a very weak band was identified in these materials in the region between 3.7 and 5.7 eV. This feature, however, originates from the region, where the reflectance of these materials was higher than that of the standard. Such data, therefore, give a false absorption when processed using the Kubelka-Munk function (eq 10). The materials that appeared light gray (GFA2 and GFC3) exhibited two absorption features. The first was the same as for the off-white-looking materials with estimated BG energy of 5.71 eV and 5.72 eV for GFA2 and GFC3, respectively. The second feature corresponded to estimated BG energies of 2.60 eV and 2.58 eV for GFA2 and GFC3, respectively. These materials, therefore, probably consisted of two distinct types of fluorographene structures differing in electronic and optical properties. Such phases, however, cannot be recognized by the XRD since the reflections of different structures may be found at very similar diffraction angles.[14,39] However, these may be distinguished by the optical microscopy images (Figure 13), the darker particles may reflect the portion of the material with a more narrow bandgap, and

47

the white particles the phase with a broad bandgap. The rest of the spectra consisted only of one absorption feature with corresponding BG energies estimated at 2.58 eV, 2.20 eV, and 2.26 eV for GFA1, GFA5, and GFC1, respectively.

To rationalize the presented results, the bandgap energy values of ~5.8 eV coincide with the first exciton peak of graphite fluoride that was estimated to 5.2 eV.[94] Although the discrepancy between the experimental and theoretical results is small, further study could lead towards its further clarification. The lower values of bandgap energy (~2.5 eV) coincided with those reported for partially fluorinated graphene.[52,61,95]

As found later from the reactivity testing of these materials, the materials with bandgap energies around 5.8 eV were found reactive, those with two band gap values were found slightly less reactive and those with bandgap determined to be around 2.5 eV exhibited very low reactivity. **This technique, since the measurement is very simple and quick, can be used for fast estimation of the reactivity of the inspected graphite fluoride and, therefore, sorting of the well-reactive materials from the less-reactive ones.**
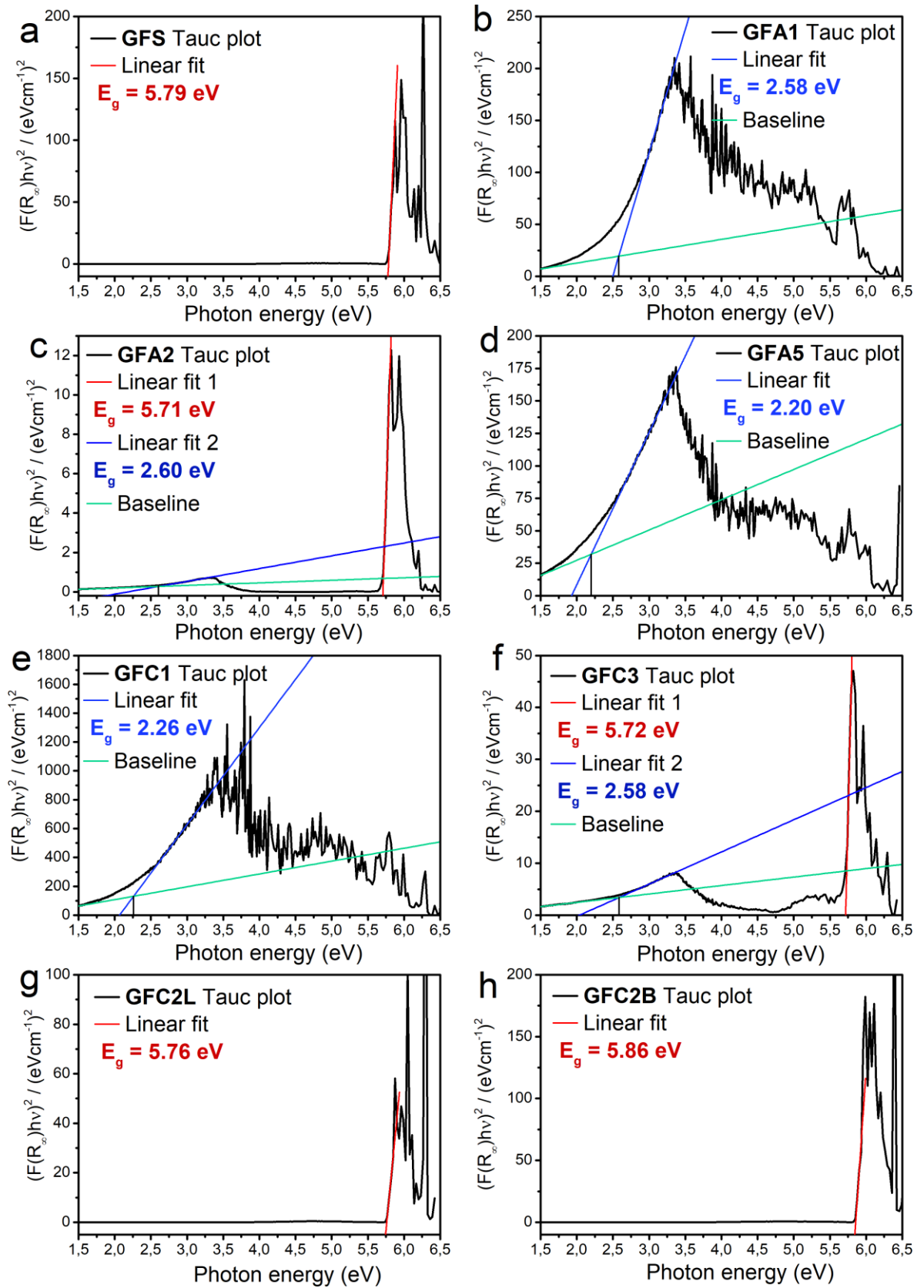
Figure 19: Tauc plots of all studied graphite fluorides: GFS (a), GFA1 (b), GFA2 (c), GFA5 (d), GFC1 (e), GFC3 (f), GFC2L (g) and GFC2B (h).

4.1.5 EPR characterization of all tested graphite fluorides

Since the reactivity of fluorographene and GFs is caused by the presence of unpaired electrons,[21] all GFs were inspected using electron paramagnetic resonance (EPR) spectroscopy (Figure 20). Spectra of GFA1, GFA5, GFC1, and GFS appeared very similar as sharp doublet features with little to no observable interactions with ^{19}F nuclei differing mainly in the intensity of the observed signal. Contrary to this, spectra of GFA2 and GFC3 were significantly different from other materials due to their broad signals signifying the presence of triplet states and hyperfine splitting of the signal due to ^{19}F nuclei adjacent to the unpaired electrons.[34] GFC3 material had also the highest EPR intensity of all scrutinized GFs. However, the spectra that differed the most from all other materials were those from GFC2B and GFC2L samples whereby the signals were much less intense (Figure 20, inset). Interestingly, when a different batch of GFS was measured (GFS2), the EPR spectrum was very similar to the GFC2L and GFC2B spectra, although, when analyzing using other techniques, the results were practically the same, therefore these are not included. All materials had similar g-value ranging from 1.9918 to 2.00324 for GFA2 and GFC2B, respectively (Table 3), values similar to that of free electron typical for lattice defects of graphite fluoride.[34,41]

Table 3: g-values of inspected graphite fluorides.

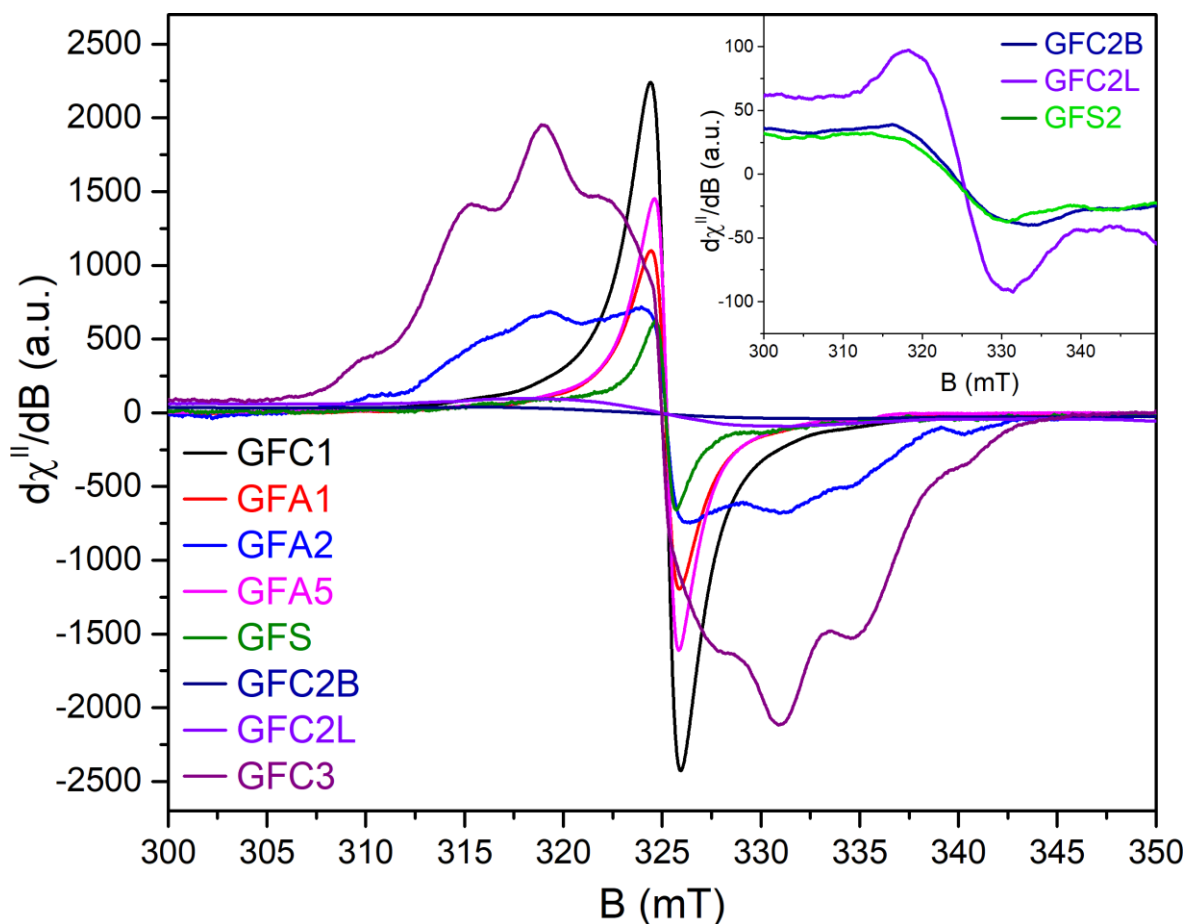|	GFS	GFA1	GFA2	GFA5	GFC1	GFC3	GFC2L	GFC2B
g-value	1.99357	1.99648	1.99182	1.99650	1.99638	1.99832	1.99572	2.00324

Figure 20: EPR spectra of studied graphite fluorides. The broad spectra of GFC3 and GFCA2 indicate triplet states Inset shows spectra of GFs with very low EPR intensity magnified along the y-axis are in the inset.

A possible explanation for the very low signal of GFC2B and GFC2L materials as well as of the second batch of GFS (GFS2) is, that most of their spins might be positioned in a way allowing through space superexchange interaction between two spin centers. If the transfer integral of this interaction would be strong enough, the two spins would then align in antiparallel arrangement (resulting in a signal loss) thus resembling through space covalent bond between the two radical centers, and, causing antiferromagnetic ordering.[96] Practically, this phenomenon might occur in one of the most stable divacancies in the fluorographene according to the theoretical calculations (Figure 21).[26] To prove this hypothesis, a temperature dependency of magnetic susceptibility of such materials would have to be done in order to determine Néel temperature above which the paramagnetic response could be observed.
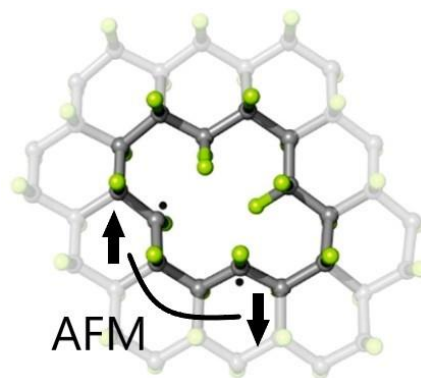
Figure 21: Depiction of hypothetical antiferromagnetic ordering in fluorographene divacancy.

Although the presence of spins has been found to cause the reactivity of graphite fluorides and fluorographene, single EPR measurements of the individual samples alone cannot provide proofs that can be linked to the reactivity of GFs and fluorographene. However, these findings may stimulate further research for a better understanding of the role of radical centers in the reactivity of GFs.

4.1.6   FTIR analysis of graphite fluorides

A comparison of FTIR spectra of all GFs (Figure 22) showed that there are two types of materials with underlying differences in the shapes of their absorption bands. One group exhibited a single broad absorption located at around 1200 cm^{-1} (GFS, GFA2, GFC2L, GFC2B, and GFC3 materials). This nicely coincides with the crystallinity PCA, since the same materials were forming the cluster in the biplot (Figure 17). The patterns of the C-F vibration bands of these GFs coincide with those of fluorinated petroleum coke.[14] On the other hand, the 1200 cm^{-1} band of the other materials was much steeper with additional bands around it. The differences can be observed more clearly by deconvoluting the fingerprint area of FTIR spectra into individual components representing different types of C-F bond vibrations.
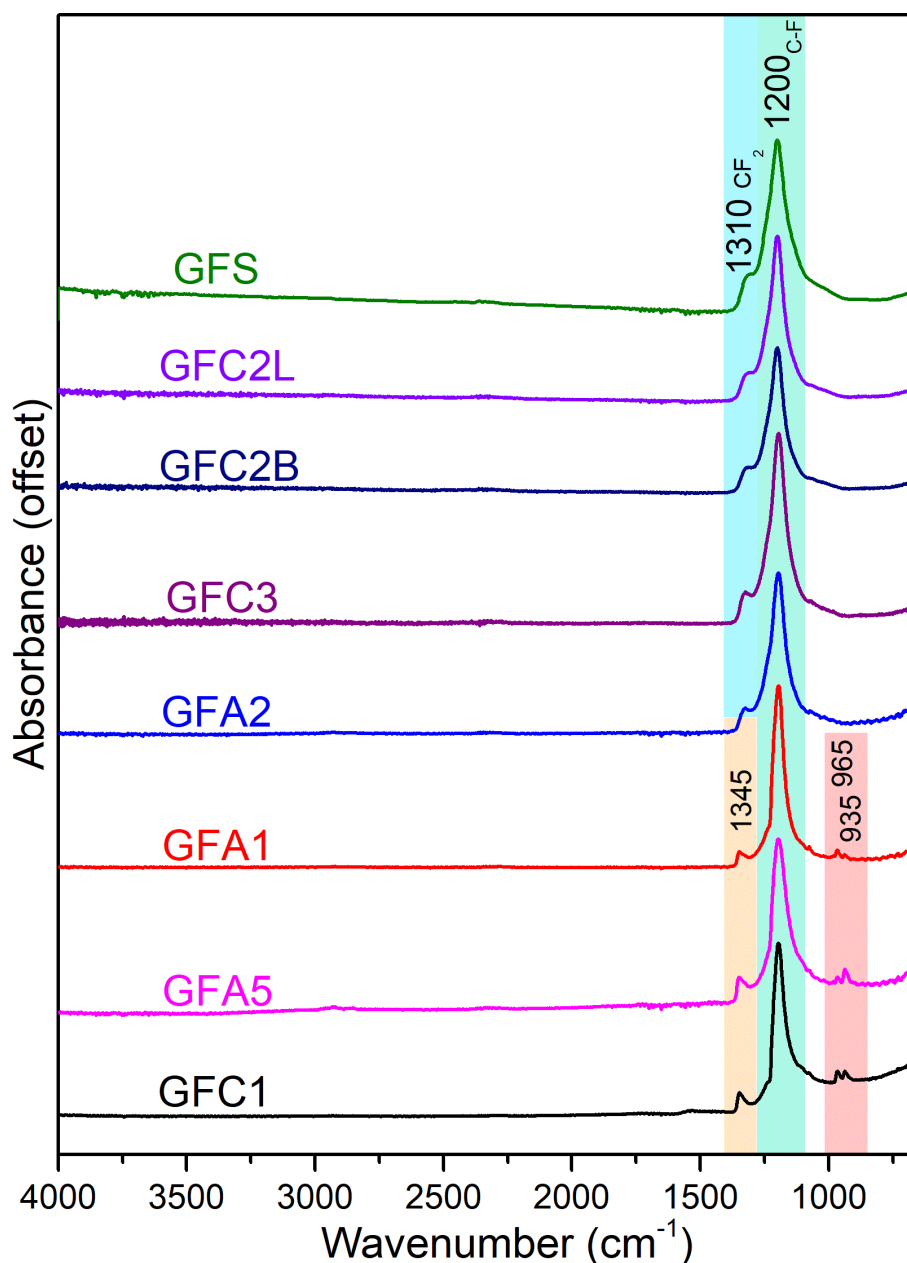
Figure 22: Full FTIR spectra of all inspected graphite fluorides.

From the deconvoluted spectra of selected GFs, the high similarity of GFS and GFC2L materials is evident (Figure 23ab). As for the origin of these individual components, the most intense band at 1200 cm^{-1} was assigned to C-F covalent bond vibration in accordance with the literature.[14,33,44,97–99] The second most prominent feature was the CF_2 moiety vibration at 1310 cm^{-1} signifying higher fluorine amounts.[14,98,99] The component located at 1150 cm^{-1} was ascribed to the C-C bond vibration with F_2 dimer bonded to these two carbon atoms, according to theoretical calculations[100] and polarization ATR-FTIR measurements[97] (Figure 23d). Such components could be found in the $(CF)_n$ sheets of boat conformation or C-F inversion defect. Further proofs for the presence of this conformation were observed in the NMR spectra of

GFs as described below. Nevertheless, this band is also often linked with semi-ionic C-F bond vibration (C-F$_i$)[98,99] that can be also ascribed to the broad component at 1080 cm^{-1}, which is in good agreement with a reported value of 1100 cm^{-1}.[33,44] The last component at 1250 cm^{-1} was also linked with the semi-ionic bond vibration since it was found to decrease concurrently with 1080 cm^{-1} when the GF materials' thermal stability was studied.[98,99] All of these vibrations were also observed in the GFA1 sample (Figure 23c), although in weaker intensities and at slightly different wavenumbers, probably due to structural differences. Moreover, three additional components at 1345, 965, and 935 cm^{-1} are observable. These have been ascribed to vibration modes characteristic of (C$_2$F)$_n$ found at 1350 and 940 cm^{-1} in literature,[14] which is in good agreement with the present results. The 965 and 935 cm^{-1} features might arise from the splitting of the 940 cm^{-1} band, possibly due to the two different stacking patterns of the sheets.
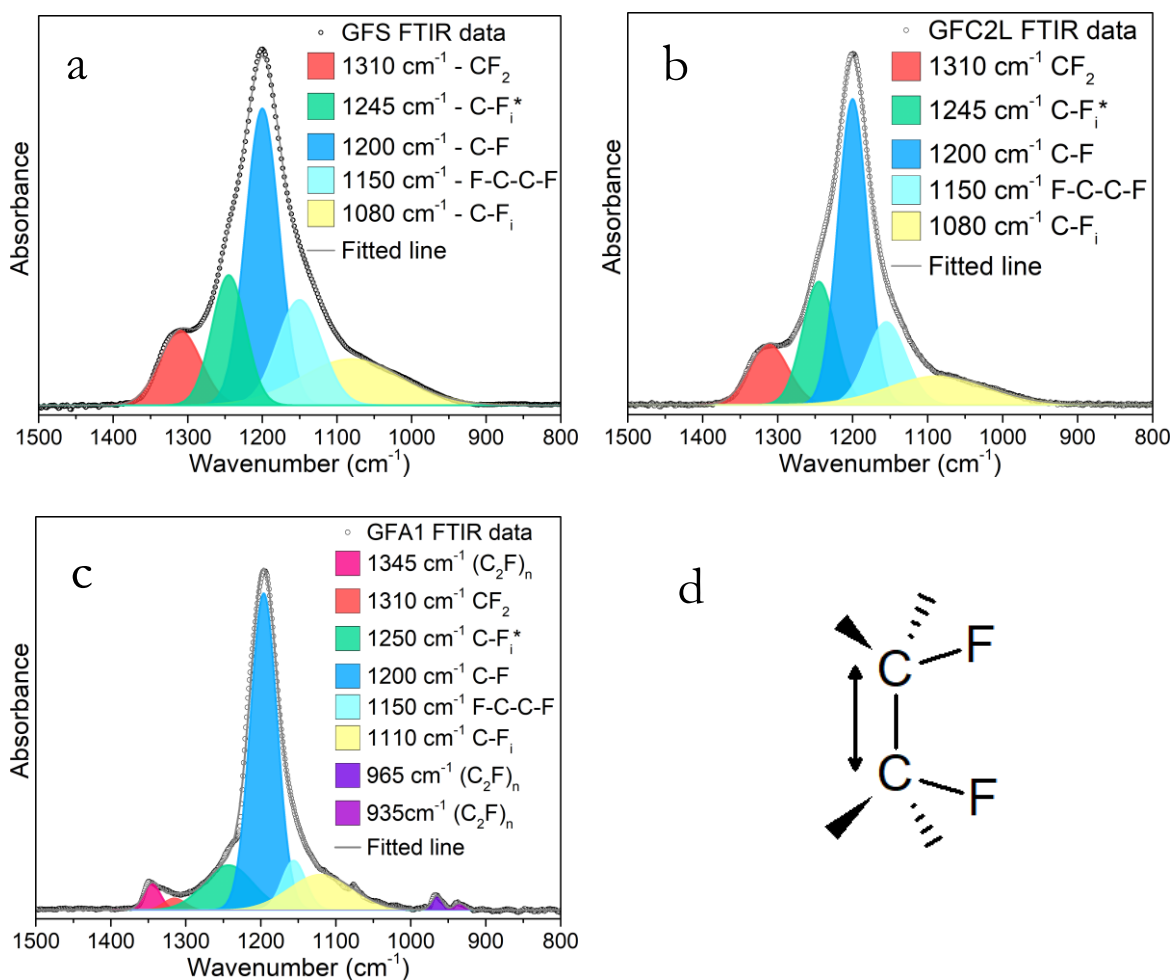
Figure 23: Deconvoluted FTIR spectra of selected graphite fluorides: of GFS (a), GFC2L (b). GFA1 (c). Part (d) shows a depiction of the 1150 cm^{-1} vibration mode of fluorine dimer bonded to graphene.

4.1.7   XPS analysis of graphite fluorides

All GFs were analyzed with XPS (Figure 24) to determine their elemental composition (Table 4) and to observe different bonding configurations of carbon atoms (Figure 25, Table 5). The materials with the highest fluorine contents (more than 53 at. %) were also found to be clustered in PCA biplot (Figure 17) classifying GFs according to their crystallinity determined by XRD.

Figure 24: Survey XPS spectra of all inspected graphite fluorides. Peaks are assigned to electrons of the described energy level of the relevant atom.

Table 4: Elemental compositions of all inspected graphite fluorides determined using XPS

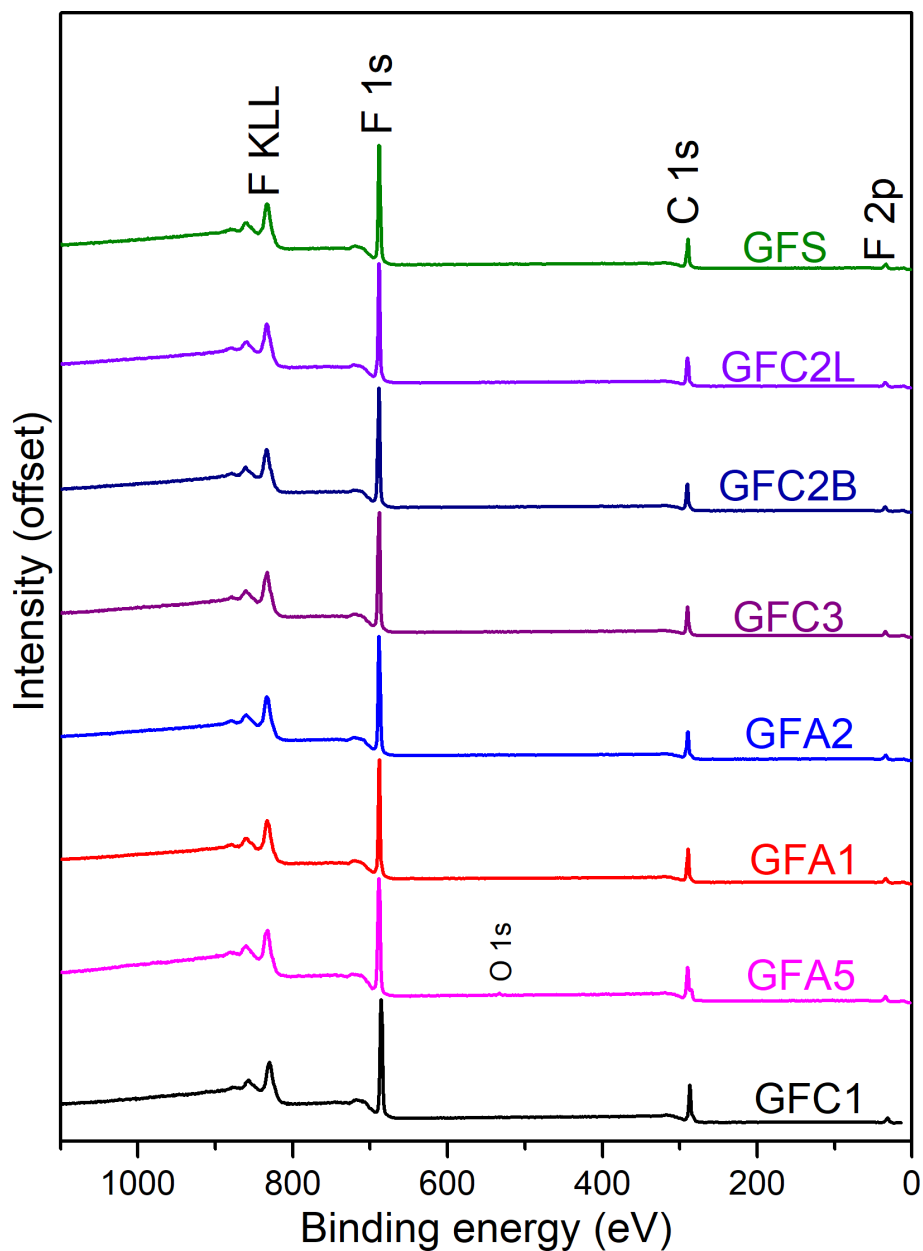|	XPS - Composition (at. %)			F/C ratio
	C	O	F	
GFS	45.6	-	54.4	1.19
GFA1	47.8	-	52.2	1.09
GFA2	47	-	53	1.13
GFA5	53.5	1.7	44.8	0.84
GFC1	49.7	-	50.3	1.01
GFC3	46.3	-	53.7	1.16
GFC2L	46.4	-	53.7	1.16
GFC2B	46.6	-	53.4	1.15

The C 1s core level high-resolution XPS spectra (Figure 25) demonstrated a very low content of sp^2 and sp^3 carbon components (located at 284.8, 285.8 eV, respectively),[14] suggesting high fluorination degrees in selected GFs (GFS, GFC2L, and GFA1). The component at 287.6 eV can be assigned to semi-ionic bonding (C-F$_i$)[30] and was slightly more apparent (>5% of the C 1s envelope, Table 5) in GFS and GFC2L. Components at 289.4 eV corresponding to covalent C-F bonds of $(CF)_n$ compound were the most prominent features in all the spectra. The spectra of graphite fluorides that were later found reactive (GFS and GFC2L) exhibited higher contents of CF_2 groups (found at 291.2 eV).[14] Except for the edges of the fluorographene sheets, CF_2 groups are also found in the vacancies, which are probably connected to the reactivity of the material due to the presence of unpaired electrons within them. **Therefore, the number of CF_2 groups can be another indicator of the reactivity of the graphite fluoride.**
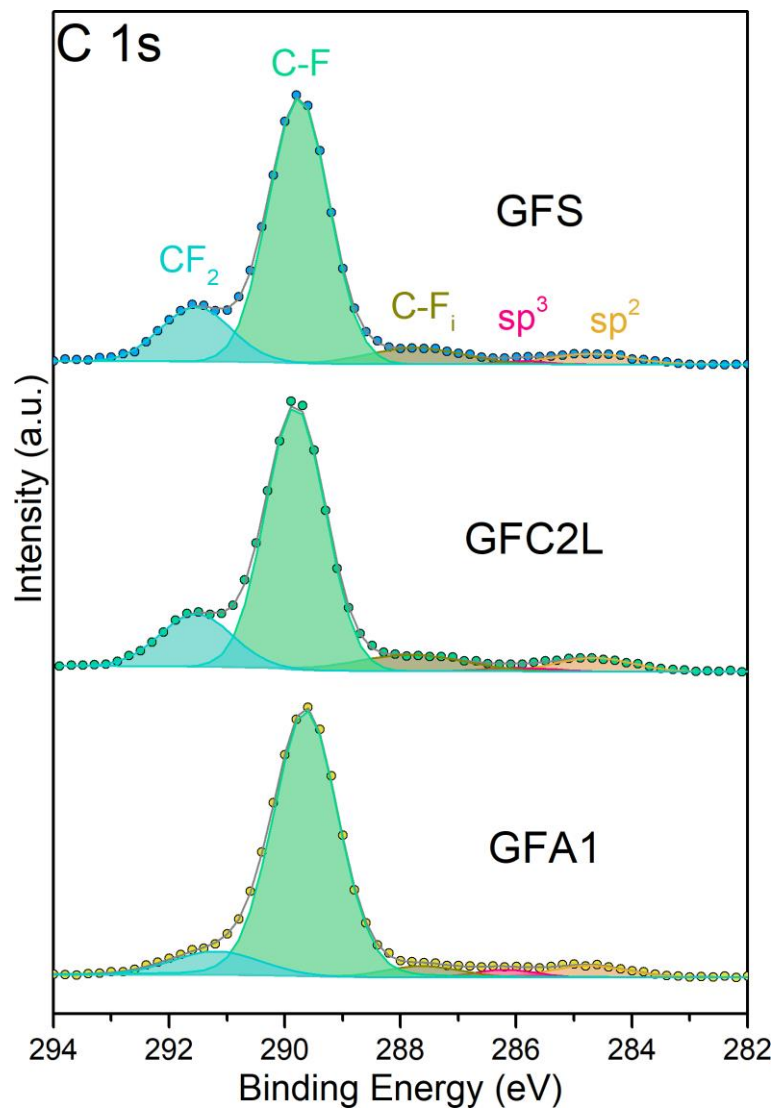
Figure 25: Deconvolution of HR-XPS of C 1s and F 1s envelopes of selected graphite fluorides.

Table 5: Results of C 1s deconvolution of selected graphite fluorides - percentiles of C1s components.

	Quantities of C 1s core-level spectra deconvolution components (%)				
	sp^2	sp^3	C-F$_i$	C-F	C-F$_2$
	284.8 eV	285.8 eV	287.6 eV	289.4 eV	291.2 eV
GFS	3.9	0.7	6.9	71.4	17.2
GFC2L	4.7	1.1	7.8	69.6	16.8
GFA1	4.4	2.2	4	80.3	9.3

4.1.8 NMR analysis of selected graphite fluorides

To substantiate further the previous findings regarding the high fluorination, wide bandgap, and high CF_2 contents with the reactivity of GFs, a solid-state NMR analysis was done since the technique can provide insight into the structure of graphite fluorides.[39] Since solid samples were measured, the MAS technique was employed with TOSS pulse sequence for the ^{19}F domain since without it these spectra would be heavily affected by spinning sidebands.

Both the ^{19}F-NMR and ^{13}C-NMR spectra (Figure 26ab) showed a clear distinction between the GFA1 material outside the crystallinity PCA cluster (Figure 17) and the GFS and GFC2L materials within it. All the spectra were dominated by very intense peaks at around -180 ppm in ^{19}F and ~90 ppm in ^{13}C spectra, which were broader in the case of GFS and GFC2L. Some studies ascribe this broadening in ^{19}F spectra to the presence of a spinning sideband of the CF_2 spectral line.[41,44] It is however impossible for presented data to contain such bands since these were suppressed by the TOSS measurement, and, concerning those studies as they showed,[41,44] it is impossible to have a single spinning sideband placed asymmetrically with respect to the original spectral line. Moreover, it is also impossible for the spinning sideband to have a higher intensity than the original spectral line. Therefore, the broad features, both in ^{19}F and ^{13}C, certainly consisted of several components reflecting different structural motifs. For better understanding, all the spectra were deconvoluted and the individual components assigned to characteristic groups and structural variations of FG sheets (Figure 26).

Generally, the ^{19}F spectra (Figure 26a) consisted of three main regions according to how many fluorine atoms were bonded to a carbon atom – C-F, CF_2, or CF_3 groups. These groups were further shifted to additional components, since the chemical shifts highly depend on more factors, such as type of conformation of the neighboring $(CF)_n$ structure, presence of vacancies in the structure,[39] and presence of unpaired electrons in the vicinity of the groups.[101] In general, the components at higher chemical shifts (from -25 to -90 ppm) can be assigned to CF_3 groups, because the more fluorine atoms are bonded to a single carbon atom, the lower electron density on each of the fluorine atoms is since they all pull out electrons from the same carbon atom. Also, other experimental works assigned those features to CF_3 groups.[39,102] It is however interesting, that the CF_3 groups could not be recognized by ^{13}C NMR (Figure 26b), including the previously reported results.[39]
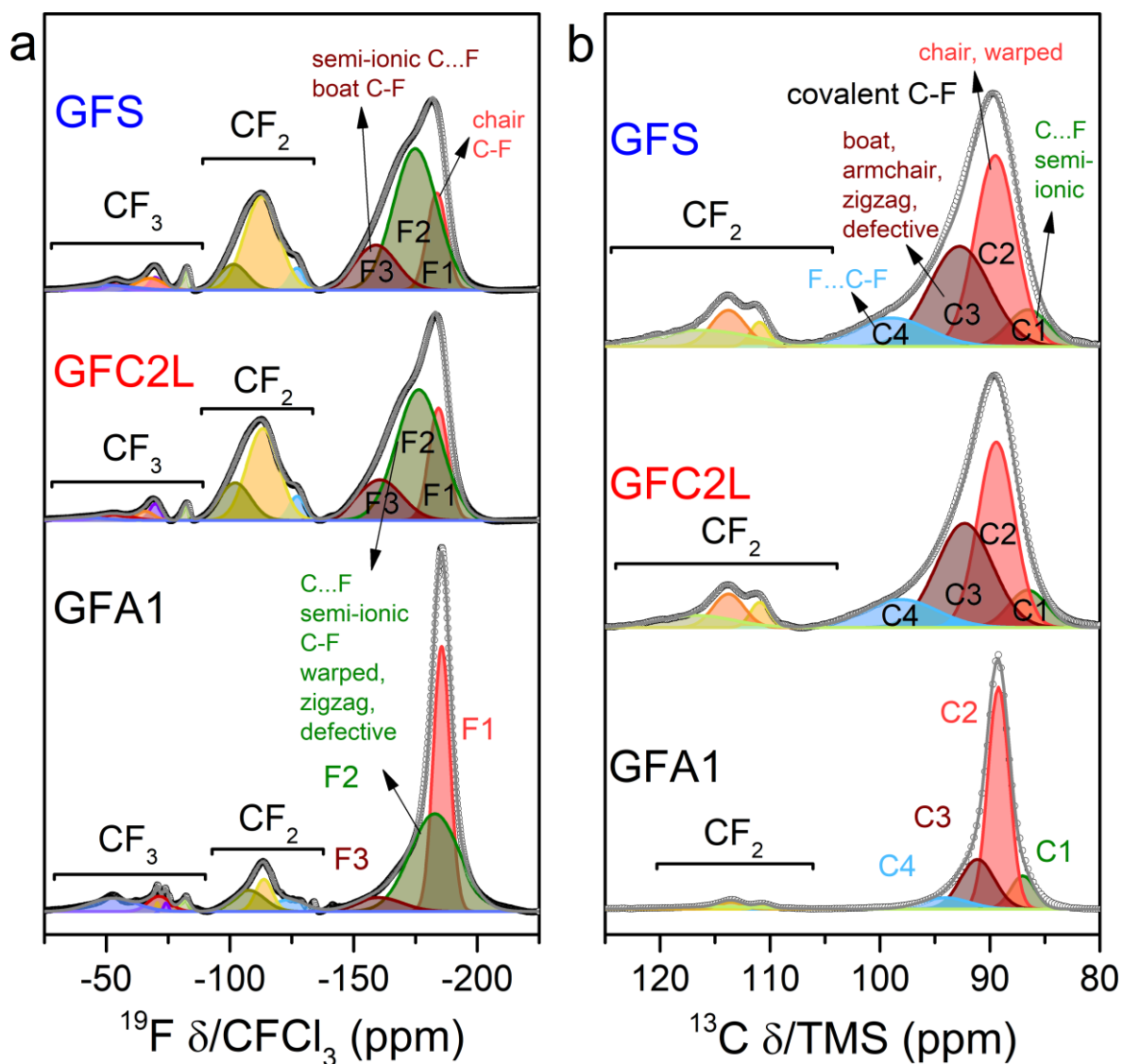
Figure 26: Deconvoluted ^{19}F (a) and ^{13}C (b) MAS NMR spectra of selected GFs with a description of the most important components.

In the case of CF_2 groups, these could be tracked by both ^{19}F and ^{13}C NMR spectroscopies and were represented by three components. In the ^{13}C spectra, two of these components were distinct even without deconvolution. These two main features could originate from two different regions where the CF_2 groups can reside – the vacancies and the edges of the fluorographene sheets. However, it is not certain which component corresponds to which environment. To answer this question, theoretical simulations would be needed. From all the spectra it is clear that the GFC2L and GFS samples contain significantly more CF_2 groups which could be linked to higher numbers of defects in their structures. This further substantiates the observations from FTIR and XPS results, and it appears to be the key structural feature connected to the higher reactivity of these materials.

The peak from the C-F groups was found between -183.5 and -185.5 ppm and at +89.5 ppm in ^{19}F and ^{13}C domain, respectively, represented by components marked as F1 and C2 in Figure 26ab. According to the simulations done by Rimsza et al.,[39] these components refer to the covalent C-F bond of $(CF)_n$ structures of chair conformation stacked in hexagonal symmetry that can be found at -182.5 ppm and +93.9 ppm in ^{19}F and ^{13}C domain spectra, respectively. This component was dominant in GFA1 material spectra and was much less prominent in the spectra of GFS and GFC2L since their spectra were highly influenced by broad components found at higher chemical shifts manifesting as a shoulder in the ^{19}F spectrum or as a broadening of the ^{13}C spectra.[39] The shoulder of C-F feature found at higher chemical shifts was assigned to C-F bond with lower covalence already once, however, the work lacked proper reasoning for this phenomenon.[102] The reason for that might arise from altering the structure of the $(CF)_n$ sheets which results in differences in the shielding of both fluorine and carbon nuclei. In some cases, the effect of shielding is the opposite for each of these nuclei. One of the different variations of the structure of $(CF)_n$ sheets may be the boat conformation. Such sheets would then be stacked in an orthorhombic structure. This can be observed in the spectra as a part of components marked as F3 and C2 since this conformation may be found, according to the simulations, at shift ranges between -146.3 and -157.8 ppm and between +98.7 and +96.9 ppm for ^{19}F and ^{13}C, respectively. There are other possible conformations of $(CF)_n$ structures, such as zigzag, twist-boat, armchair, and tricycle, that are variations of the boat conformation. These conformations are mainly represented by components F2 and C3 in Figure 26ab since these can be observed at ranges of chemical shifts between -136.8 and -168.3 ppm and between +94.1 and +99.5 ppm for ^{19}F and ^{13}C spectra, respectively. The presence of defects in the chair conformation of $(CF)_n$ sheets in the form of vacancies or C-F inversions may also cause higher shielding of both ^{19}F nuclei causing the presence of features between -140 and -180 ppm.[39] However, in the publication of Rimsza et al. the calculations did not count with the presence of unpaired electrons in these vacancies which can also significantly alter the shielding of the fluorine and carbon nuclei.[101] Hypothetically, unpaired electrons may intermix with the C-F bond orbitals causing a decrease in bond order thus weakening the covalent C-F bonds. As a result, the ^{19}F nuclei would be deshielded due to loss of electron density and therefore found at higher chemical shifts (part of F2 and F3 components). Such C-F bond of lower bond order could be also referred to as a semi-ionic bond, although until now it was proposed to be found in partially fluorinated graphenes or graphites originating from intermixing of C-F bonds and adjacent π-orbitals of sp^2 regions.[30,95] On the other hand, the ^{13}C nuclei are due to higher electron density caused by the unpaired electron shielded more and, therefore, found at lower chemical

shifts (as a component C1). For ^{13}C nuclei, this was also proven theoretically, when the ^{13}C nuclei adjacent to the spin-containing site were shielded more.[101] ^{13}C spectra show, that the number of these semi-ionic C-F bonds is similar in all three analyzed GFs. The carbon might be also bonded to two fluorine atoms by bonds differing in bond orders. To this possible configuration, the C4 component was assigned. It may be also represented by one of the CF_2 components of ^{19}F spectra. As a final note, the complete ^{13}C spectra show that GFA1 material contained sp^2 regions and $(C_2F)_n$ sp^3 C atoms (at 142[41,98,103] and 47.6 ppm,[41] respectively, (Figure 27), unlike the reactive GFs which did not contain such features, pointing out the lower fluorination degree of the GFA1 sample.
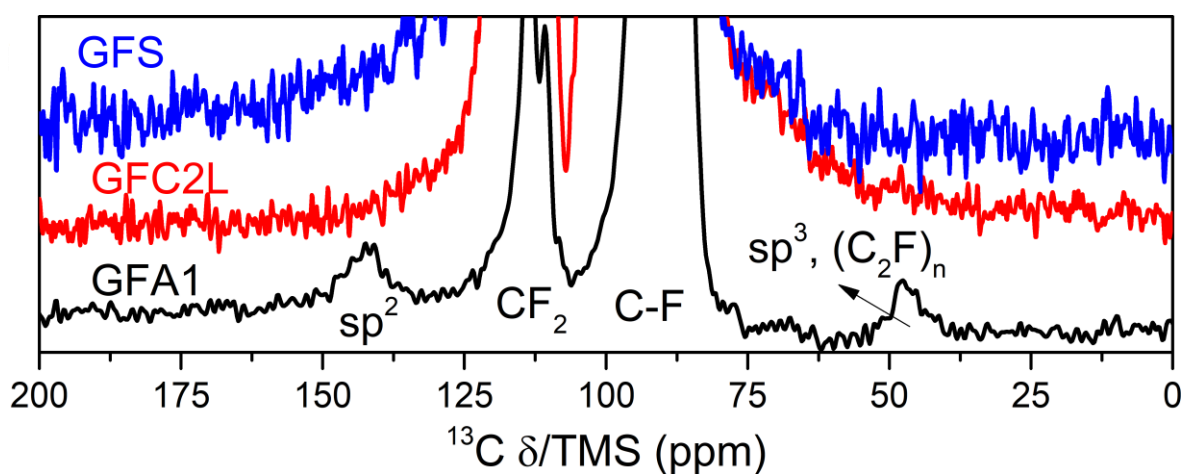

Figure 27: Comparison of ^{13}C NMR of selected graphite fluorides enlarged along the y-axis.

Based on the NMR observations it can be concluded that GFS and GFC2L graphite fluorides are highly disordered materials composed of various polymorph structures of $(CF)_n$ sheets with high numbers of vacancies, which are also manifested by higher numbers of CF_2 groups. These findings can be linked to the graphitic source material used for the synthesis of GFC2L by fluorination – petroleum coke, a highly disordered solid which might also be the cause of the highly disordered structure of the resulting graphite fluoride. On the other hand, GFA1 material is more ordered with the lower portion of the material being in different conformations and has lower amounts of CF_2 groups signifying lower numbers of vacancies causing its lower reactivity. This was observed by both ^{19}F and ^{13}C NMR further proving XPS and FTIR spectra and partially reflected by slightly lower fluorine content causing the presence of sp^2 and sp^3 regions observable by ^{13}C NMR representing unreacted graphite and $(C_2F)_n$ graphite fluoride, respectively.

4.1.9 Thermal analysis of the selected graphite fluorides

The structural differences between the scrutinized graphite fluorides inflict their differences in reactivity as shown further in the text. This should be also manifested in their thermal stabilities.[50] Simultaneous thermal analysis of selected GFs comprising thermogravimetric analysis (TGA) and differential scanning calorimetry (DSC) performed by heating each sample up to 800 °C with the temperature ramp of 5 °C/min (Figure 28) showed, that both the GFS and GFC2L materials start to decompose at lower temperatures around 400 °C with a very slow pace that was exponentially accelerating as the temperature increased, which coincides with previously reported behavior of fluorinated petroleum coke.[50] In the case of GFA1, however, the decomposition was more sudden starting at around 580 °C although the total decomposition of the GFS and GFC2L ended later than decomposition of GFA1. The residual mass of the GFA1 sample after the analysis was 20.1 % of the initial mass, 16.3 % for GFS, and 14.6 % for GFC2L (Figure 28, top). These findings may be again linked to a more ordered structure of GFA1 with lower numbers of defects making the material more thermal resistant and also, as found out further by two different reactions, much less reactive towards nucleophiles.
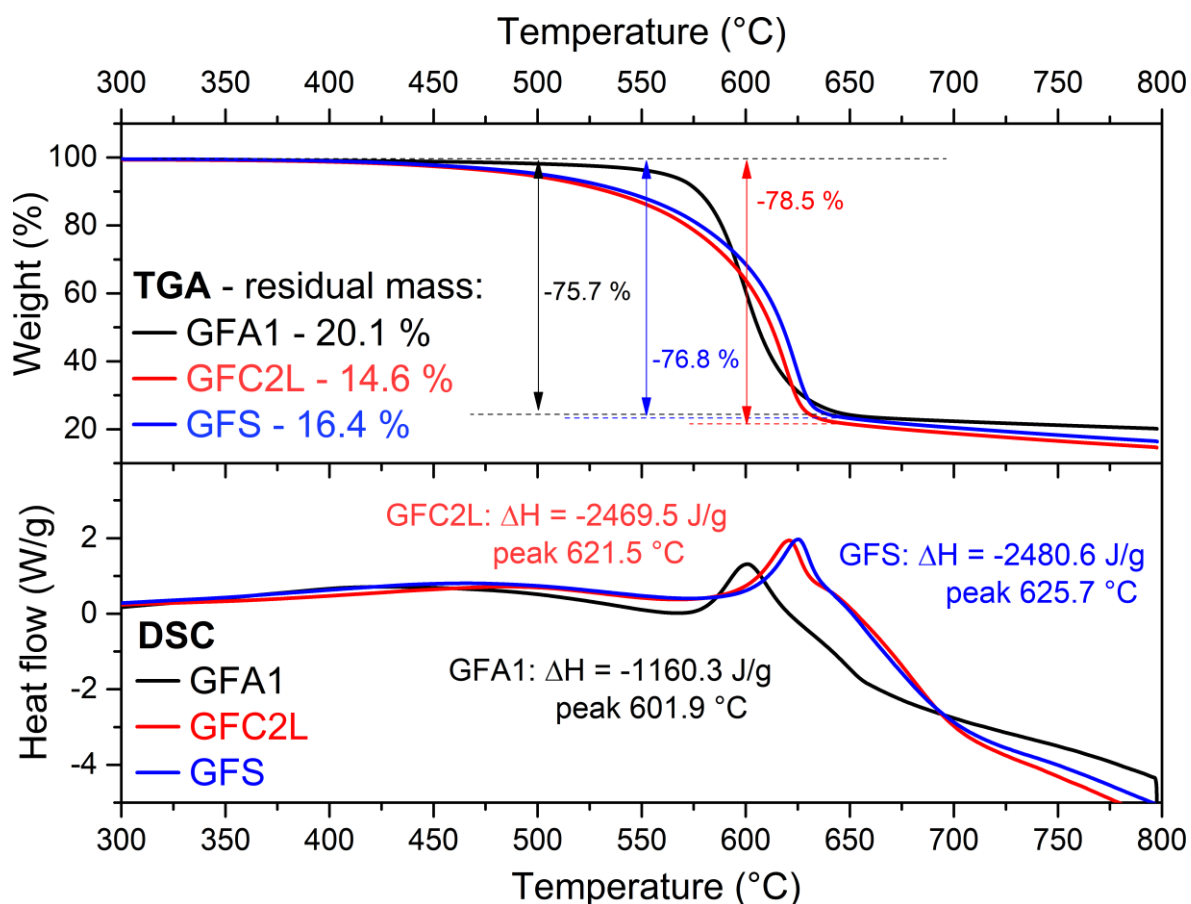

Figure 28: Results of TGA and DSC analysis of the selected graphite fluorides.

The DSC results (Figure 28, bottom) revealed that although the decomposition of more reactive materials (GFS and GFC2L) started sooner, the peak of the thermal decomposition process was at higher temperatures in contrast to GFA1 decomposition. The decomposition was exothermic in all cases, and the enthalpy of the process was approximately twice as high for GFS and GFC2L (-2481 and -2470 J/g, respectively) compared to GFA1 (-1160 J/g).

4.2 Characterization of GN3 materials derived from GFs

Reactivity of all scrutinized GFs was tested by reaction with sodium azide in DMF, which is producing nitrogen-doped graphene.[76] This was done by first preparing fluorographene by dispersing the GFs in DMF and sonicating the dispersion, to which sodium azide was added and the mixture was heated at 130 °C for 3 days while stirring (according to PCT/CZ2021/050016 and EP 20173178.3). For details see the Experimental section. Products were then characterized using Raman, FTIR, and X-ray photoelectron spectroscopies. All the samples were codenamed according to their parent graphite fluoride as is shown in Table 6.

Table 6: Codenames of GN3 derivatives according to the parent GFs.

GN3 derivative	parent GF
GN3S	GFS
GN3A1	GFA1
GN3A2	GFA2
GN3A5	GFA5
GN3C1	GFC1
GN3C3	GFC3
GN3C2L	GFC2L
GN3C2B	GFC2B

4.2.1 Raman spectra of synthesized GN3 derivatives

Raman spectroscopy is commonly used to estimate the functionalization degree of the graphene derivatives synthesized with covalent functionalization of graphene by calculating the I_D/I_G ratio. I_D represents the intensity of the D-band located at 1350 cm^{-1}, which corresponds to defect-induced vibrations of the sp^2 structure. Such defects can be either vacancies or groups grafted onto the graphene causing it to be in sp^3 hybridization. I_G ratio corresponds to the intensity of G-band located at 1590 cm^{-1} originating from vibrations of aromatic regions. In such cases, the higher the I_D/I_G ratio, the higher the functionalization degree.[104]

However, when using fluorographene as a starting material, the residual C-F bonds act as defects making the D-band more intense. Therefore, in the case of the synthesis of nitrogen-doped graphene from fluorographene, it can be assumed, that the lower is the I_D/I_G ratio the higher is the reaction degree. From the presented results (Figure 29) it can be already said that the reaction ran the best using GFS, GFC2L, and GFC2B materials since I_D/I_G ratios of their GN3 analogs with values around 1.05 were the lowest of all measured materials. All these materials were prepared by using the off-white-colored graphite fluorides as starting materials. Slightly higher I_D/I_G ratio values of 1.11 and 1.20 were observed in GN3A2 and GN3C3, respectively, prepared by using the graphite fluorides of light-gray color. The I_D/I_G ratio values of 1.55, 1.64, and 1.74 indicated the lowest reaction degree in the GN3A1, GN3C1, and GN3A5 products, respectively.
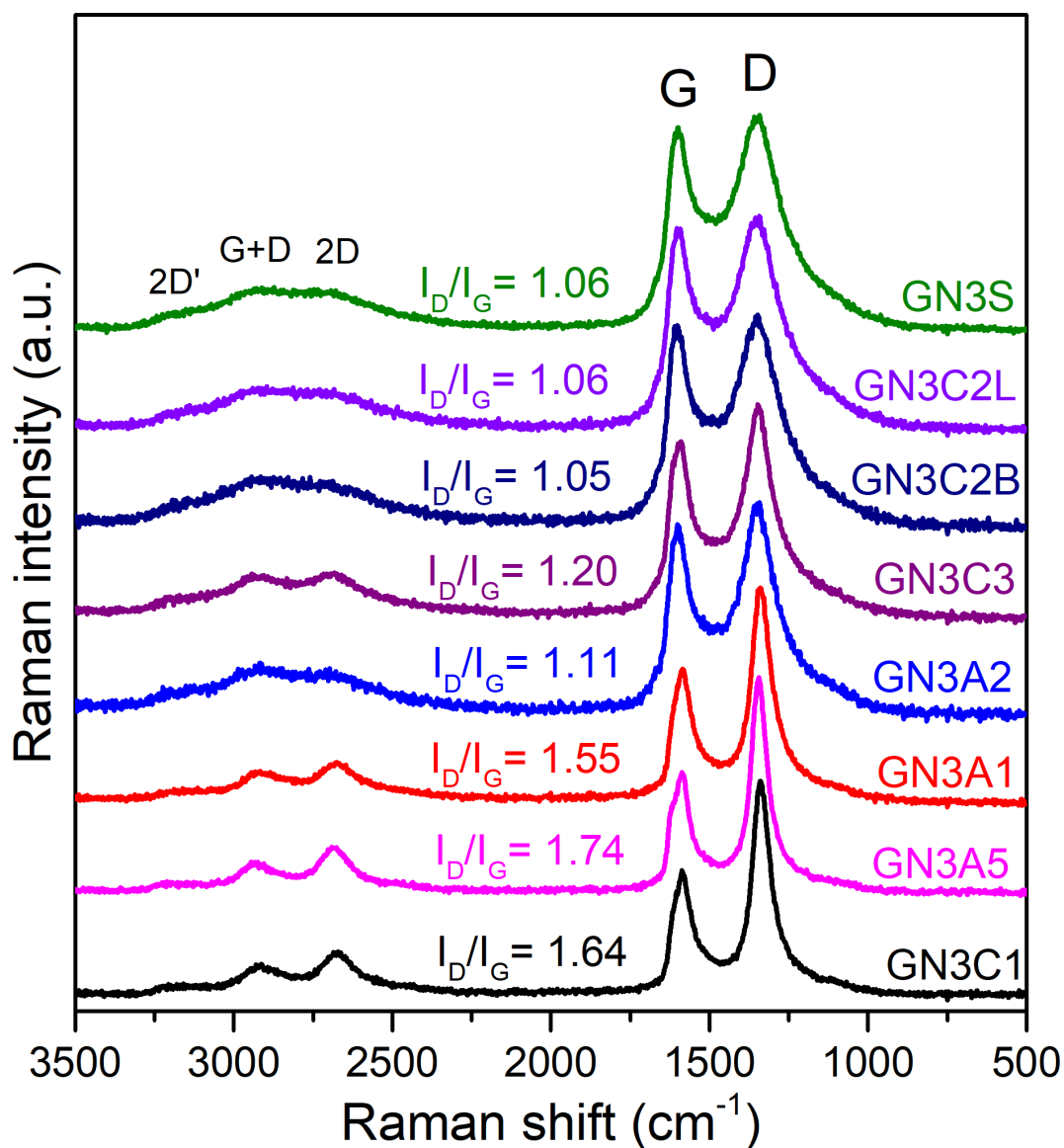

Figure 29: Raman spectra of GN3 products synthesized from all inspected graphite fluorides.

4.2.2 FTIR analysis of GN3 materials

FTIR spectra of all GN3 materials synthesized using different GFs are plotted in Figure 30. Although in the spectra of GN3A5, GN3A1 and GN3C1 samples a broad feature at 1550 cm^{-1} appeared signifying the presence of sp^2 regions, these materials still retained sharp feature at 1200 cm^{-1} corresponding to covalent C-F bond stretching due to the presence of residual fluorine. Moreover, the 1350 cm^{-1} feature of $(C_2F)_n$ was still distinguishable in the spectra of GN3C1 and GN3A5. These results coincide with Raman spectroscopy results pointing out a lower degree of the reaction when GFA5, GFA1, and GFC1 materials were used as the starting materials. In contrast, spectra of GN3S, GN3A2, GN3C2L, GN3C2B, and GN3C3 materials (synthesized from GFS, GFA2, GFC2L, GFC2B, and GFC3, respectively) contained little to no evidence of residual fluorine signifying higher reaction degree when these graphite fluorides were used as starting materials. Their spectra consisted of two main broad bands at 1205 and 1575 cm^{-1} that are typical for nitrogen-doped graphene with developed sp^2 region since these correspond to vibration modes of aromatic carbon rings and heterocyclic aromatic carbon rings. The less intense and narrower peak at 1400 cm^{-1} was assigned to vibrations linked with nitrogen substitution in pyridinic and pyrrolic configurations.[26] This feature was observed to be split into two bands in the spectrum of the GN3C2L sample.
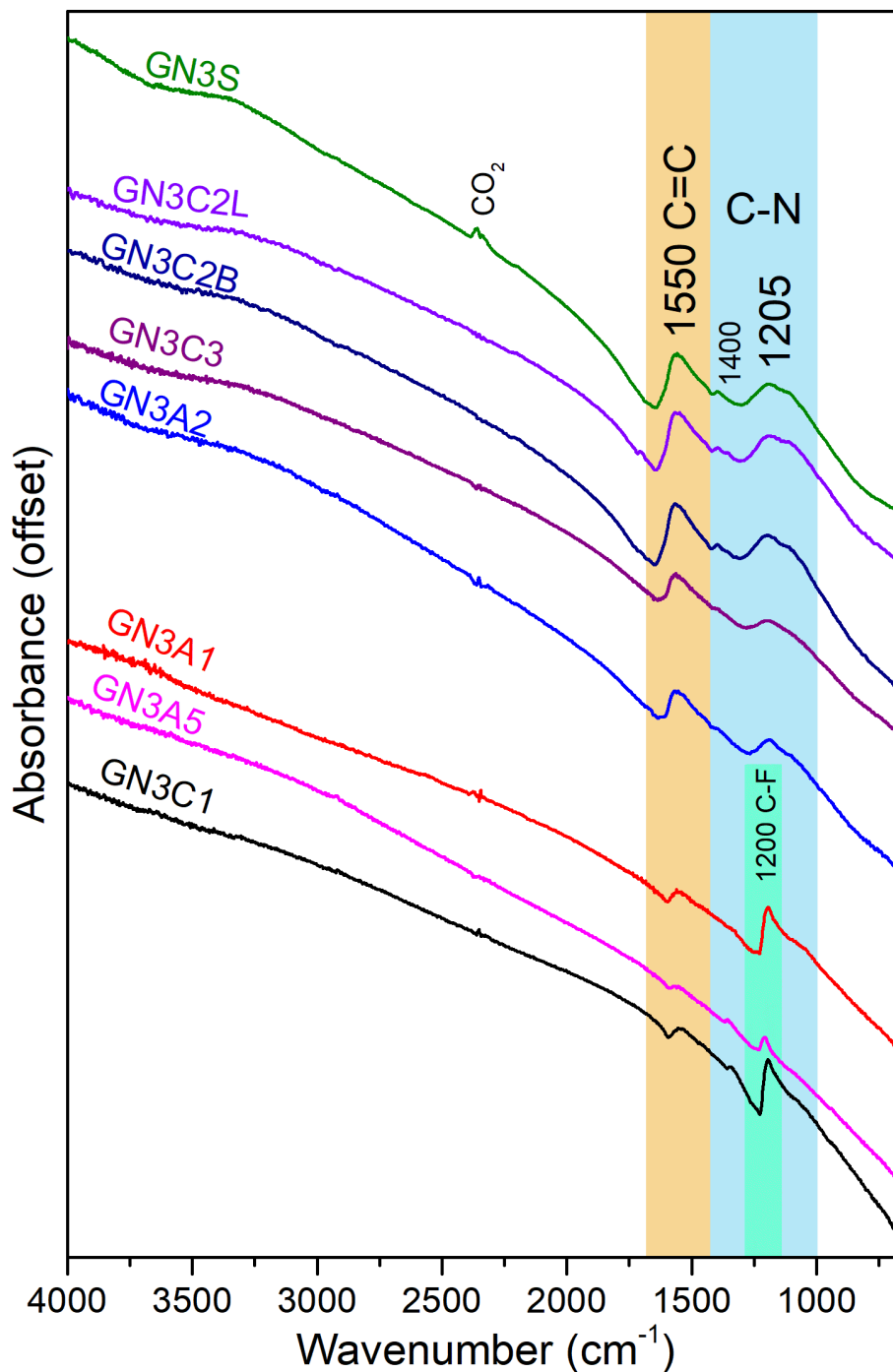
Figure 30: FTIR spectra of all GN3 materials synthesized using all inspected graphite fluorides.

4.2.3 XPS analysis of GN3 materials

Corroborating the Raman and FTIR spectra, XPS analysis showed notable differences between the GN3 materials and provided quantitative results regarding their composition. The survey spectra of all GN3 materials are in Figure 31 and the elemental compositions determined based on the measured spectra are in Table 7. The first category of materials whose starting GFs were outside the XRD PCA cluster (GN3A5, GN3A1, and GN3C1 samples) contained high amounts of residual fluorine (8.7, 16.5, and 16 at. %, respectively) and lower nitrogen contents (5.3, 4.6

and 4.3 at. %, respectively). These results confirm that the reaction degree was very low for GFA1, GFA5, and GFC1 materials, verifying their particularly poor reactivity under the conditions of liquid-phase reactions.

Table 7: Elemental compositions of GN3 materials determined using XPS.

| | Elemental composition (at. %) | | | |
	C	N	O	F
GN3S	78.5	15.8	2.7	3
GN3A1	77.7	4.6	1.2	16.5
GN3A2	81.1	12	2.4	4.5
GN3A5	84.4	5.3	1.6	8.7
GN3C1	78.8	4.3	1	16
GN3C3	79.6	14.1	3.3	3
GN3C2L	78.9	15.3	2.6	3.2
GN3C2B	78.7	14.6	3.3	3.4

Regarding the products that were synthesized using graphite fluorides from the XRD PCA cluster, these can be further divided into two groups, as already observed from the Raman spectroscopy results of the GN3 products and the optical appearance of the graphite fluorides – those of off-white color and those of light-gray color. The light-gray colored graphite fluorides (GFC3 and GFA2) produced GN3C3 and GN3A2 materials, whose composition resembled that of the GN3S (material synthesized from benchmark material GFS), however, the reaction degree was slightly lower since GN3S material contained 15.8 at. % of nitrogen and 3 at. % of residual fluorine and these materials 14.1 and 12 at. % of nitrogen, and 3 and 4.5 at. % of fluorine, respectively. The materials that resembled GN3S material the most were GN3C2L and GN3C2B synthesized from GFC2L and GFC2B, respectively, which had also the same off-white color and very similar DRS results. Their nitrogen contents were 15.3 at. % and 14.6 at. %, respectively, and fluorine contents 3.2 and 3.4 at. %, respectively. All inspected materials also contained low amounts of oxygen originating from adventitious contamination by air oxygen or moisture, or from DMF molecules reacting to the graphene surface.[21] The higher the reactivity of the GF was, the more nitrogen and less fluorine its GN3 derivative contained.
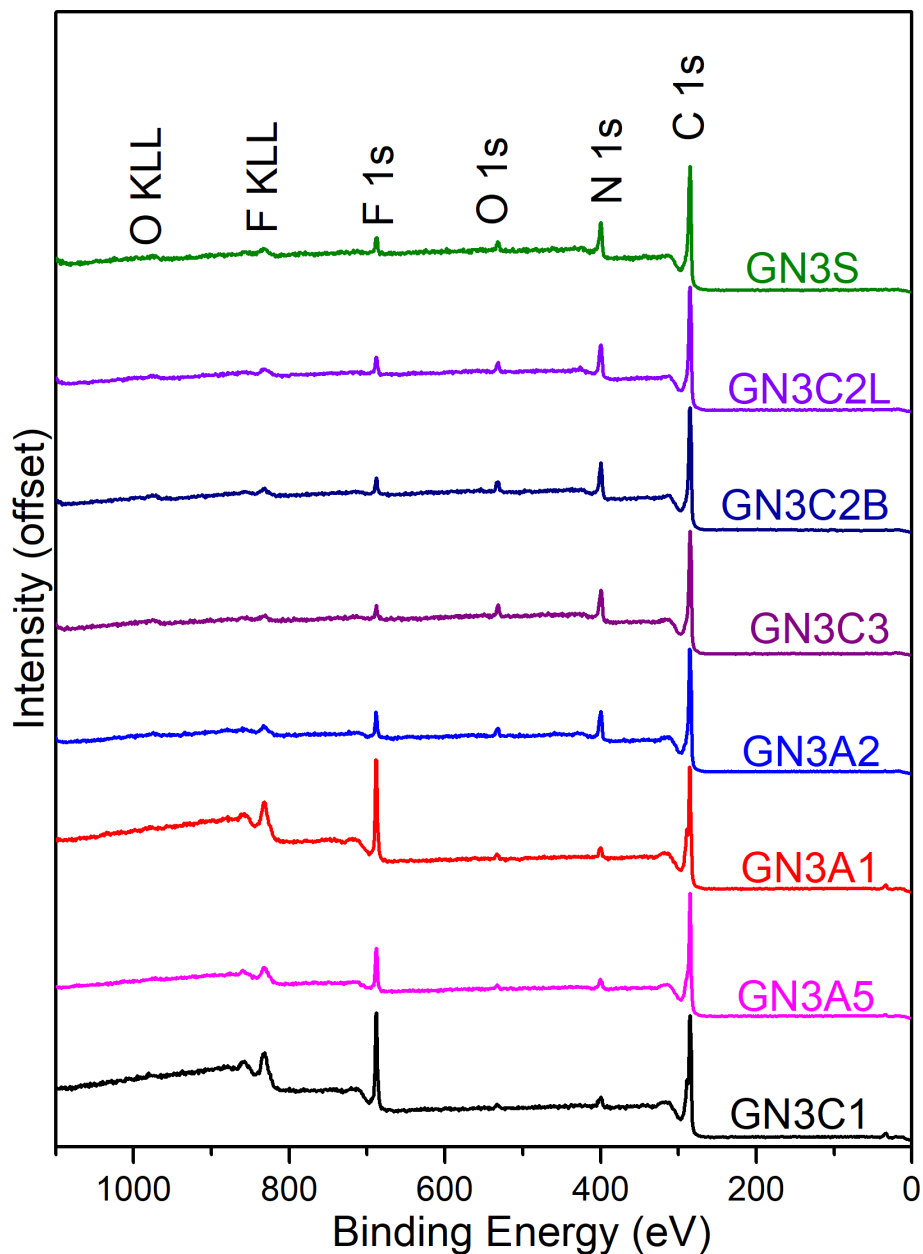
Figure 31: Survey XPS spectra of GN3 materials synthesized from all inspected graphite fluorides.

To gain better insight into the main structural differences between synthesized GN3 materials, deconvolution of HR-XPS data of 1s orbital electrons of nitrogen and carbon atoms was performed by using the data of GN3 materials derived from graphite fluorides selected according to the XRD PCA (Figure 17). As it can be seen from Figure 32a and Table 8, both GN3S and GN3C2L were very similar with well-developed sp^2 regions and high content of carbon atoms bonded to nitrogen. From the deconvolution of the C 1s envelope of the GN3A1 sample (the less reactive one), it is however evident, that it contains more C-F bonds due to the high intensity of component at 289.5 eV. Regarding the component at ~288.1 eV, since GN3S and GN3C2L materials were synthesized using more reactive GFs and thus have more oxygen

contamination, this component was in these samples assigned to carbon bonded to oxygen. In the GN3A1, since it contained much less oxygen and much more residual fluorine, the component represented rather fluorine atoms bonded to carbon atoms in semi-ionic nature (C-F$_i$). The component at 291.2 eV represents in the GN3A1 sample residual CF$_2$ moieties and in GN3C2L and GN3S, due to their low fluorine contents, corresponds to π-π* transition.

The shape of the N 1s envelope for all compared materials consisted of three similar components (Figure 32b, Table 9). These components correspond to pyridinic nitrogen configuration with a maximum at 398.5 eV, pyrrolic at 400 eV, and graphitic nitrogen at 401.5 eV.[105] The only notable difference was the fact that the content of graphitic nitrogen in GN3A1 material was slightly lower. This means that the starting GFA1 material had a lower number of monovacancies with respect to other types of vacancies in its structure than that is in the GFS and GFC2L.

Table 8: Contents of components from C 1s HR-XPS deconvolution of selected GN3 materials.

	Quantities of C 1s core-level spectra deconvolution components (%)					
	sp^2	sp^3	C-N	C-O/C-F$_i$	C-F	CF$_2$/π-π*
	284.8 eV	285.6 eV	286.7 eV	288.1 eV	289.5 eV	291.2 eV
GN3S	58.6	14.3	16.2	4.6	3.9	2.4
GN3C2L	61.1	14.4	14.2	4.3	3.7	2.3
GN3A1	47.9	17.4	8.5	4.2	18.6	3.5

Table 9: Contents of components from N 1s HR-XPS deconvolution of selected GN3 materials.

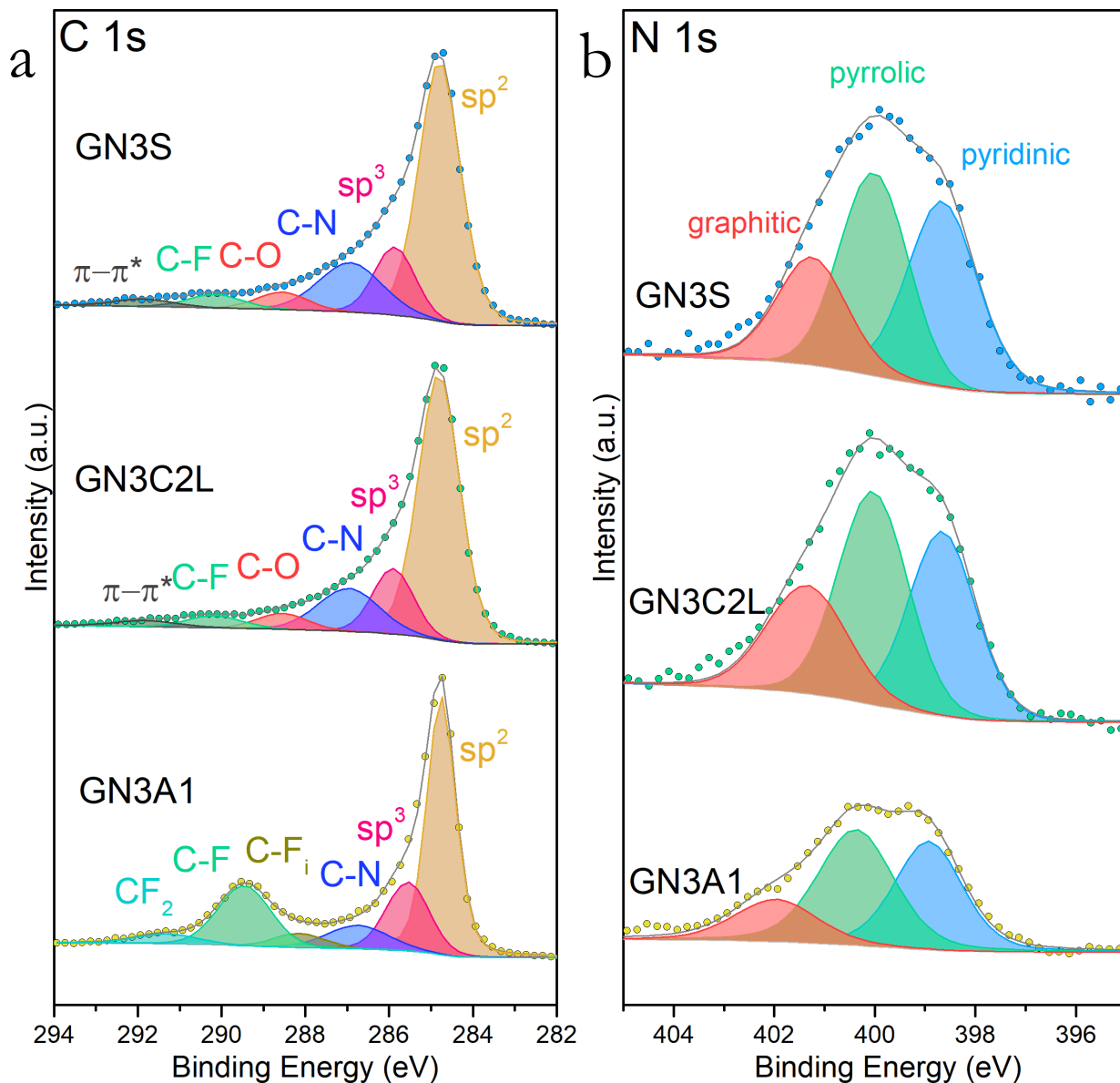|	Quantities of N 1s core-level spectra deconvolution components (%)		
	pyridinic N	pyrrolic N	graphitic N
	398.5 eV	400 eV	401.5 eV
GN3S	39.2	38.1	22.7
GN3C2L	34.5	41.3	24.2
GN3A1	37.5	44.7	17.8

Figure 32: Deconvolution of HR-XPS spectra of C 1s (a) and N 1s (b) envelopes of GN3 materials synthesized using selected GFs.

Based on the so far acquired results, the reactivity of graphite fluoride highly depends on its structure. Specifically, the more disordered the material is, the more reactive it is, reflected by the higher nitrogen contents in the GN3 products. The disorder may be manifested by different polymorphs of $(CF)_n$ structures present in the starting GFs, but, more importantly, by the high number of defects within the fluorographene sheets, mainly vacancies. **These vacancies are probably connected to the presence of unpaired electrons triggering the reactivity of fluorographene** as recently proved.[26] The number of defects may be simply indicated by the number of CF_2 groups, present either at the edges of the sheets or in the vacancies. Therefore, the more CF_2 groups the material contains the more defects its structure has, which is also reflected by the slightly higher fluorine contents of these materials. The

reactivity can be also linked to the appearance of the materials – the whiter materials are more reactive, as observed from optical and microscopy images of the graphite fluorides as well as from the DRS analysis. In turn, this is also connected to the wide bandgap of the whiter graphite fluorides.

4.3   Characterization of GOA materials

To further verify the previously observed reactivity trends and the generality of the conclusions, the reactivity of selected GFs was also tested using another reaction with n-octylamine (n-OA). In this reaction, the octylamine is bonded to the electrophilic site of fluorographene due to the nucleophilic nature of the amino group of octylamine. The synthesized GOA materials and the parent graphite fluorides are shown in Table 10.

Table 10: Codenaming of GOA samples according to the parent GFs used for its synthesis as a starting material.

GOA derivative	Parent GF
GOAS	GFS
GOAC2L	GFC2L
GOAA1	GFA1

According to FTIR spectra of GOA materials (Figure 33), GFS and GFC2L reacted with n-OA very well since GOAS and GOAC2L displayed intense C-H vibrations at 2900 cm^{-1}, whereas such bands were hardly observed in the case of GOAA1, confirming its poor reactivity. The GOAC2L spectrum also displayed lower intensity of the C-H band in comparison to the GOAS.
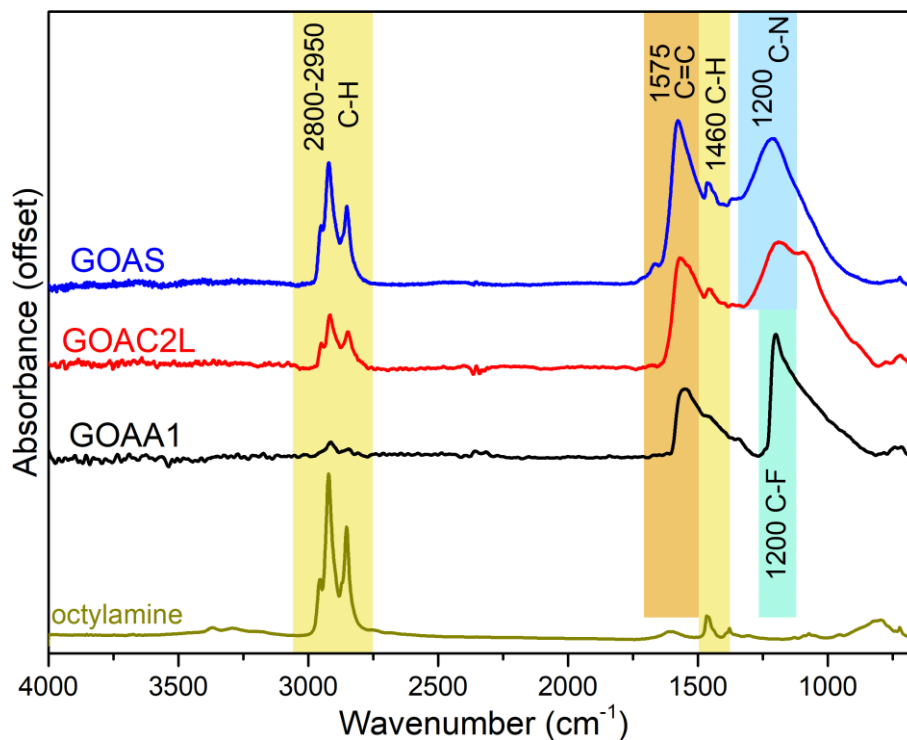
Figure 33: Comparison of FTIR spectra of GOA materials prepared using different GFs. The spectrum of octylamine is showed below the materials' spectra for clarity.

Elemental and structural analysis of these derivatives with XPS (Figure 34a) showed similar nitrogen and fluorine contents for both GFS and GFC2L, and higher oxygen contamination of GOAS product (Table 11). The GFA1 reacted again poorly (i.e. only slightly defluorinated) and the GOAA1 product contained low nitrogen levels. The deconvolution of C 1s HR-XPS spectra (Figure 34b, Table 12) were similar for the GOAS and GOAC2L samples. The GOAA1 spectrum showed intense C-F-related components proving its low reactivity.[22] Therefore, GFA1 and similar graphite fluorides structurally different from the clustered ones (Figure 17) have lower reactivity, and this statement may be generalized for any liquid-phase reaction using GF as a starting material used for the synthesis of graphene derivatives.

Table 11: Elemental compositions of GOA materials from different GFs.

| | Elemental composition (at. %) | | | |
	C	N	O	F
GOAS	80.1	8.5	9	2.5
GOAC2L	84.7	8.5	4.8	2
GOAA1	75.6	3.1	2.1	19.2
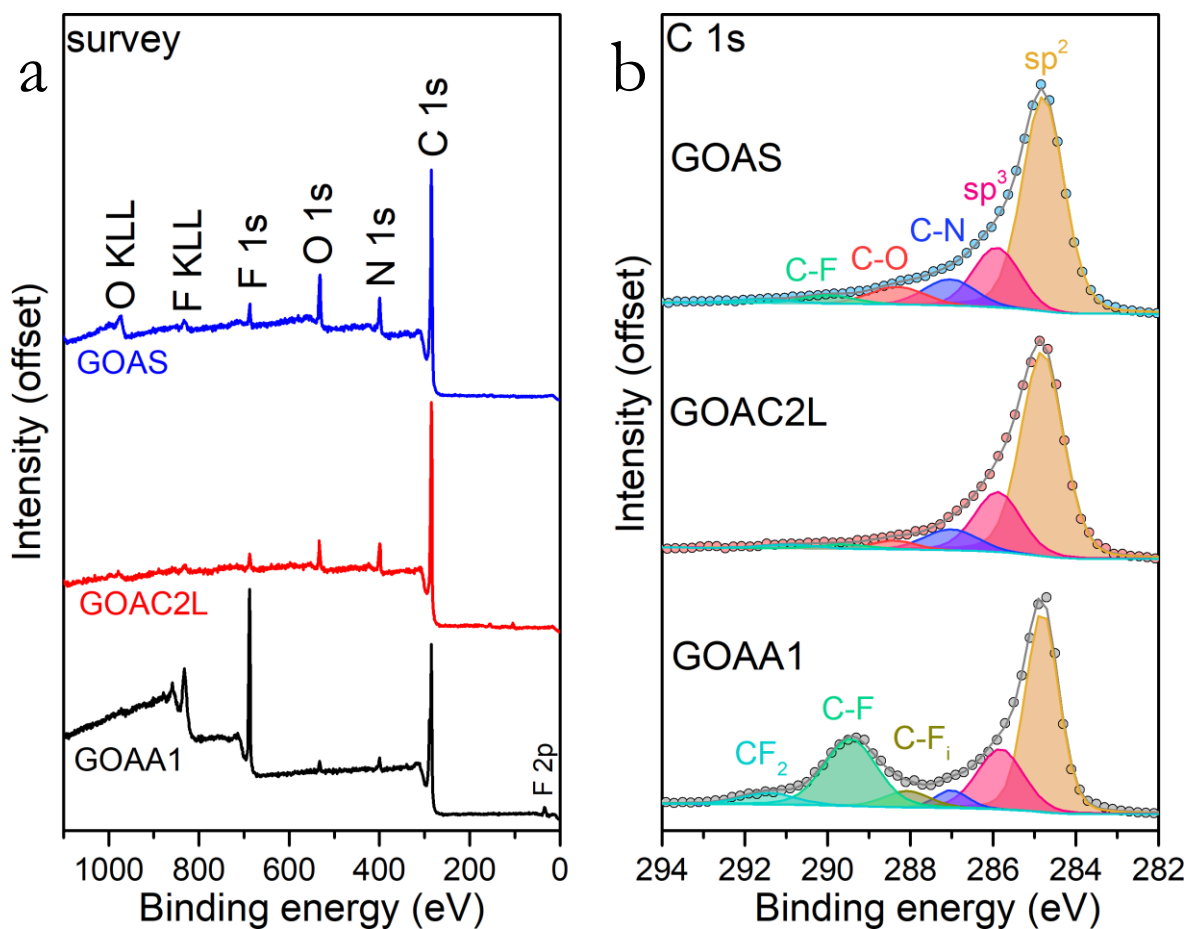
Figure 34: Survey XPS (a) and deconvoluted C 1s HR-XPS spectra (b) of GOA materials prepared by using different graphite fluorides as starting materials.

Table 12: Comparison of quantities of components of C 1s core-level spectra based on the deconvolution of the XPS spectra.

	Quantities of C 1s core-level spectra deconvolution components (%)					
	sp^2	sp^3	C-N	C-O/C-F$_i$	C-F	CF$_2$/
	284.8 eV	285.6 eV	286.7 eV	288.1 eV	289.5 eV	291.2 eV
GN3S	63.2	17.8	8.6	6.2	2.8	1.4
GN3C2L	65.6	21.3	7.7	2.6	1.5	1.3
GN3A1	44.7	18.7	3.9	5.7	23.5	4.2

5 Conclusion

Motivated by observations on the variable reactivities of graphite fluorides and fluorographenes derived thereof, we thoroughly studied the structural features of graphite fluorides obtained from different commercial suppliers, prepared by fluorination of different types of carbons. The studied graphite fluorides originated from the fluorination of natural graphite, petroleum coke, carbon fibers and charcoal, and other unspecified carbon sources. Thorough characterization with UV-VIS diffuse reflectance spectroscopy, X-ray diffraction, X-ray photoelectron spectroscopy, EPR, and NMR spectroscopies showed that their optical properties, bandgap, crystallinity, and fluorine and CF_2 groups content varied significantly, depending on the original carbon source.

In order to connect the identified structural differences to the chemical properties and reactivity in particular they were subjected to reactions with sodium azide or with octylamine in solvents under elevated temperature. These reactions afforded highly nitrogen-doped graphene derivatives for the sodium azide case, and alkyl derivatives for the octylamine case.

Infrared, Raman, and X-ray photoelectron spectroscopy studies of the products from both reactions reached the same conclusions; the graphite fluorides with higher reactivity consisted of white particles with large bandgap (~5.8 eV), they were structurally the most disordered, more thermally labile and contained the higher content of defects, specifically vacancies, indicated by the high content of CF_2 groups detected in starting fluorographites using infrared, X-ray photoelectron and nuclear magnetic resonance spectroscopies. These defects are radical rich triggering the reactivity of fluorographene, as it has been previously found.

It thus appears that the most reactive graphite fluorides are those prepared from the fluorination of petroleum coke or carbon fibers. These graphite fluorides, having a broad bandgap observable in the long-wave UV region, are whiter than the less fluorinated ones. Therefore, a facile method to distinguish the reactive and non-reactive graphite fluorides is visual observation (only the white materials are highly reactive), which can be substantiated by the UV-VIS diffuse reflectance spectra, whereby the materials with the onset of absorption at 5.7 eV are reactive.

6 Závěr

V této práci byly důkladně prostudovány strukturní znaky grafitfluoridů získaných od různých komerčních dodavatelů připravených fluorací různých forem uhlíku. Motivací pro tuto studii je pozorovaná rozdílná reaktivita grafitfluoridů a z nich připravených fluorografenů. Studované grafitfluoridy byly získány fluorací přírodního grafitu, ropného koksu, uhlíkových vláken, dřevěného uhlí a dalších blíže nespecifikovaných forem uhlíku. Důkladná charakterizace pomocí UV-VIS difúzní reflektanční spektroskopie, rentgenové difrakce, rentgenové fotoelektronové spektroskopie a spektroskopií elektronové paramagnetické rezonance a nukleární magnetické rezonance ukázala, že jejich optické vlastnosti, a tedy zakázaný pás, krystalinita, a obsah fluoru a CF_2 skupin se významně lišily v závislosti na formě zdroje uhlíku.

Pro spojení těchto strukturních rozdílů s jejich chemickými vlastnostmi a zejména reaktivitou byly tyto materiály vystaveny reakcím s azidem sodným a oktylaminem prováděných v rozpouštědlech za zvýšené teploty. V případě azidu sodného tyto reakce produkují dusíkem vysoce dopované grafenové deriváty a alkylované deriváty pro případ oktylaminu.

Studie produktů obou těchto reakcí pomocí infračervené, Ramanovy a rentgenové fotoelektronové spektroskopie došly ke stejným závěrům; grafitfluoridy vyšší reaktivity jsou složeny z částic bílé barvy s širokým zakázaným pásem (kolem 5,8 eV), jsou strukturně nejvíce neuspořádané, teplotně méně stálé a obsahují vyšší množství defektů, konkrétně vakancí, což je indikováno vyšším množstvím CF_2 skupin, které byly v původních grafitfluoridech pozorovány pomocí infračervené spektroskopie, rentgenové fotoelektronové spektroskopie a spektroskopie nukleární magnetické rezonance. Tyto defekty jsou bohaté na radikály, jenž jsou, dle zjištění předchozích studií, spouštěčem reaktivity fluorografenu.

Z prezentovaných výsledků navíc také vyplývá, že nejvíce reaktivní grafitfluoridy jsou ty připravované fluorací ropného koksu nebo uhlíkových vláken. Tyto grafitfluoridy tím, že mají široký zakázaný pás pozorovatelný až v krátkovlnné oblasti UV záření, jsou bělejší než ty méně fluorované. Jako snadná metoda pro rychlé rozpoznání reaktivních materiálů se tedy nabízí být pouhé pozorování vzhledu materiálů (pouze bílé jsou dobře reaktivní), které může být podpořeno měřením UV-VIS difúzních reflektančních spekter, z nichž je patrné, že materiály s počátkem absorpce kolem 5,7 eV jsou reaktivní.

7 Literature

(1)   Georgakilas, V.; Perman, J. A.; Tucek, J.; Zboril, R. Broad Family of Carbon Nanoallotropes: Classification, Chemistry, and Applications of Fullerenes, Carbon Dots, Nanotubes, Graphene, Nanodiamonds, and Combined Superstructures. *Chem. Rev.* **2015**, *115* (11), 4744–4822. https://doi.org/10.1021/cr500304f.

(2)   Novoselov, K. S. Electric Field Effect in Atomically Thin Carbon Films. *Science (80-.).* **2004**, *306* (5696), 666–669. https://doi.org/10.1126/science.1102896.

(3)   Novoselov, K. S.; Fal'ko, V. I.; Colombo, L.; Gellert, P. R.; Schwab, M. G.; Kim, K. A Roadmap for Graphene. *Nature* **2012**, *490* (7419), 192–200. https://doi.org/10.1038/nature11458.

(4)   Sturala, J.; Luxa, J.; Pumera, M.; Sofer, Z. Chemistry of Graphene Derivatives: Synthesis, Applications, and Perspectives. *Chem. - A Eur. J.* **2018**, *24* (23), 5992–6006. https://doi.org/10.1002/chem.201704192.

(5)   Monkul, B. Ö. Graphite Intercalation with Fluoroanions by Chemical and Electrochemical Methods, Oregon State University, 2010.

(6)   Emery, N.; Hérold, C.; Marêché, J.-F.; Lagrange, P. Synthesis and Superconducting Properties of CaC 6. *Sci. Technol. Adv. Mater.* **2008**, *9* (4), 044102. https://doi.org/10.1088/1468-6996/9/4/044102.

(7)   Brodie, B. C. XIII. On the Atomic Weight of Graphite. *Philos. Trans. R. Soc. London* **1859**, *149*, 249–259. https://doi.org/10.1098/rstl.1859.0013.

(8)   Kovtyukhova, N. I. Layer-by-Layer Assembly of Ultrathin Composite Films from Micron-Sized Graphite Oxide Sheets and Polycations. *Chem. Mater.* **1999**, *11* (3), 771–778. https://doi.org/10.1021/cm981085u.

(9)   Stankovich, S.; Dikin, D. A.; Piner, R. D.; Kohlhaas, K. A.; Kleinhammes, A.; Jia, Y.; Wu, Y.; Nguyen, S. T.; Ruoff, R. S. Synthesis of Graphene-Based Nanosheets via Chemical Reduction of Exfoliated Graphite Oxide. *Carbon N. Y.* **2007**, *45* (7), 1558–1565. https://doi.org/10.1016/j.carbon.2007.02.034.

(10)   Singh, R. K.; Kumar, R.; Singh, D. P. Graphene Oxide: Strategies for Synthesis, Reduction and Frontier Applications. *RSC Adv.* **2016**, *6* (69), 64993–65011. https://doi.org/10.1039/C6RA07626B.

(11)   Feicht, P.; Siegel, R.; Thurn, H.; Neubauer, J. W.; Seuss, M.; Szabó, T.; Talyzin, A. V.; Halbig, C. E.; Eigler, S.; Kunz, D. A.; Fery, A.; Papastavrou, G.; Senker, J.; Breu, J. Systematic Evaluation of Different Types of Graphene Oxide in Respect to Variations in Their In-Plane Modulus. *Carbon N. Y.* **2017**, *114*, 700–705. https://doi.org/10.1016/j.carbon.2016.12.065.

(12)   Erickson, K.; Erni, R.; Lee, Z.; Alem, N.; Gannett, W.; Zettl, A. Determination of the Local Chemical Structure of Graphene Oxide and Reduced Graphene Oxide. *Adv. Mater.* **2010**, *22* (40), 4467–4472. https://doi.org/10.1002/adma.201000732.

(13)   Ruff, O.; Bretschneider, O. Die Reaktionsprodukte Der Verschiedenen Kohlenstoffformen Mit Fluor II (Kohlenstoff-Monofluorid). *Zeitschrift für Anorg. und Allg. Chemie* **1934**, *217* (1), 1–18. https://doi.org/10.1002/zaac.19342170102.

(14)   Watanabe, N.; Nakajima, T.; Touhara, H. Preparation, Stoichiometry and Structure of Graphite Fluoride. In *Graphite Fluorides*; Elsevier Science Publishers B.V., 1988; pp 23–89. https://doi.org/10.1016/B978-0-444-42885-1.50007-5.

(15)   Cadman, P.; Gossedge, G. M. The Chemical Reactivity of Graphite Fluoride in Conjunction with Its Use as a Solid Lubricant. *J. Mater. Sci.* **1979**, *14* (6), 1465–1472. https://doi.org/10.1007/BF00549323.

(16)   Nakajima, T. Lithium–Graphite Fluoride Battery—History and Fundamentals. In *New Fluorinated Carbons: Fundamentals and Applications*; Elsevier, 2017; pp 305–323. https://doi.org/10.1016/B978-0-12-803479-8.00013-9.

(17)   Watanabe, N. Characteristics and Applications of Graphite Fluoride. *Phys. B+C* **1981**, *105* (1–3), 17–21. https://doi.org/10.1016/0378-4363(81)90207-2.

(18)   Zbořil, R.; Karlický, F.; Bourlinos, A. B.; Steriotis, T. A.; Stubos, A. K.; Georgakilas, V.; Šafářová, K.; Jančík, D.; Trapalis, C.; Otyepka, M. Graphene Fluoride: A Stable Stoichiometric Graphene Derivative and Its Chemical Conversion to Graphene. *Small* **2010**, *6* (24), 2885–2891. https://doi.org/10.1002/smll.201001401.

(19)   Karlický, F.; Kumara Ramanatha Datta, K.; Otyepka, M.; Zbořil, R. Halogenated Graphenes: Rapidly Growing Family of Graphene Derivatives. *ACS Nano* **2013**, *7* (8), 6434–6464. https://doi.org/10.1021/nn4024027.

(20)   Dubecký, M.; Otyepková, E.; Lazar, P.; Karlický, F.; Petr, M.; Čépe, K.; Banáš, P.; Zbořil, R.; Otyepka, M. Reactivity of Fluorographene: A Facile Way toward Graphene Derivatives. *J. Phys. Chem. Lett.* **2015**, *6* (8), 1430–1434. https://doi.org/10.1021/acs.jpclett.5b00565.

(21)   Medveď, M.; Zoppellaro, G.; Ugolotti, J.; Matochová, D.; Lazar, P.; Pospíšil, T.; Bakandritsos, A.; Tuček, J.; Zbořil, R.; Otyepka, M. Reactivity of Fluorographene Is Triggered by Point Defects: Beyond the Perfect 2D World. *Nanoscale* **2018**, *10* (10), 4696–4707. https://doi.org/10.1039/c7nr09426d.

(22)   Matochová, D.; Medved, M.; Bakandritsos, A.; Steklý, T.; Zbořil, R.; Otyepka, M. 2D Chemistry: Chemical Control of Graphene Derivatization. *J. Phys. Chem. Lett.* **2018**, *9* (13), 3580–3585. https://doi.org/10.1021/acs.jpclett.8b01596.

(23)   Bakandritsos, A.; Pykal, M.; Błoński, P.; Jakubec, P.; Chronopoulos, D. D.; Poláková, K.; Georgakilas, V.; Čépe, K.; Tomanec, O.; Ranc, V.; Bourlinos, A. B.; Zbořil, R.; Otyepka, M. Cyanographene and Graphene Acid: Emerging Derivatives Enabling High-Yield and Selective Functionalization of Graphene. *ACS Nano* **2017**, *11* (3), 2982–2991. https://doi.org/10.1021/acsnano.6b08449.

(24)   Chronopoulos, D. D.; Bakandritsos, A.; Lazar, P.; Pykal, M.; Čépe, K.; Zbořil, R.; Otyepka, M. High-Yield Alkylation and Arylation of Graphene via Grignard Reaction with Fluorographene. *Chem. Mater.* **2017**, *29* (3), 926–930. https://doi.org/10.1021/acs.chemmater.6b05040.

(25)   Chronopoulos, D. D.; Medveď', M.; Błoński, P.; Nováček, Z.; Jakubec, P.; Tomanec, O.; Bakandritsos, A.; Novotná, V.; Zbořil, R.; Otyepka, M. Alkynylation of Graphene via the Sonogashira C–C Cross-Coupling Reaction on Fluorographene. *Chem. Commun.* **2019**, *55* (8), 1088–1091. https://doi.org/10.1039/C8CC08492K.

(26)   Zaoralová, D.; Hrubý, V.; Šedajová, V.; Mach, R.; Kupka, V.; Ugolotti, J.; Bakandritsos, A.; Medved', M.; Otyepka, M. Tunable Synthesis of Nitrogen Doped Graphene from Fluorographene under Mild Conditions. *ACS Sustain. Chem. Eng.* **2020**, *8* (12), 4764–4772. https://doi.org/10.1021/acssuschemeng.9b07161.

(27)   Williams, B. A.; Dobulis, M. A.; Losovyj, Y.; Werner-Zwanziger, U.; Siedle, A. R.; Jarrold, C. C. Synthesis and Laser Ablation Mass Spectrometry of Nitrogen-Doped Carbon Materials. *J. Phys. Chem. C* **2021**. https://doi.org/10.1021/acs.jpcc.0c10322.

(28)   Watanabe, N.; Kumon, K. A Reaction of Graphite and Fluorine. *Denki-Kagaku* **1967**, *35* (19).

(29)   Watanabe, N.; Nakajima, T.; Touhara, H. Graphite Intercalation Compound of Fluorine. In *Graphite Fluorides*; Elsevier Science Publishers B.V., 1988; pp 240–261. https://doi.org/10.1016/B978-0-444-42885-1.50013-0.

(30)   Sato, Y.; Itoh, K.; Hagiwara, R.; Fukunaga, T.; Ito, Y. On the So-Called "Semi-Ionic" C–F Bond Character in Fluorine–GIC. *Carbon N. Y.* **2004**, *42* (15), 3243–3249. https://doi.org/10.1016/j.carbon.2004.08.012.

(31)   TAKASHIMA, M.; WATANABE, N. Effect of Hydrogen Fluoride on the Formation of Graphite Fluoride. *Nippon KAGAKU KAISHI* **1976**, No. 8, 1222–1227. https://doi.org/10.1246/nikkashi.1976.1222.

(32)   Meshri, D. T.; White, W. E.; Sowell, C. L. Synthesis of Fluorographite. U.S. Patent 3,929,918,

1975.

(33) Delabarre, C.; Guérin, K.; Dubois, M.; Giraudet, J.; Fawal, Z.; Hamwi, A. Highly Fluorinated Graphite Prepared from Graphite Fluoride Formed Using BF 3 Catalyst. *J. Fluor. Chem.* **2005**, *126* (7), 1078–1087. https://doi.org/10.1016/j.jfluchem.2005.03.019.

(34) Panich, M.; Shames, A. I.; Nakajima, T. On Paramagnetism in Fluorinated Graphite: EPR and Solid State NMR Study. *J. Phys. Chem. Solids* **2001**, *62* (5), 959–964. https://doi.org/10.1016/S0022-3697(00)00264-X.

(35) Watanabe, N. Two Types of Graphite Fluorides, (CF)n and (C2F)n, and Discharge Characteristics and Mechanisms of Electrodes of (CF)n and (C2F)n in Lithium Batteries. *Solid State Ionics* **1980**, *1* (1–2), 87–110. https://doi.org/10.1016/0167-2738(80)90025-9.

(36) Sato, Y.; Itoh, K.; Hagiwara, R.; Fukunaga, T.; Ito, Y. Short-Range Structures of Poly(Dicarbon Monofluoride) (C2F)n and Poly(Carbon Monofluoride) (CF)N. *Carbon N. Y.* **2004**, *42* (14), 2897–2903. https://doi.org/10.1016/j.carbon.2004.06.042.

(37) Charlier, J. C.; Gonze, X.; Michenaud, J. P. First-Principles Study of Graphite Monofluoride (CF)„. *Phys. Rev. B* **1993**, *47* (24), 162–168. https://doi.org/10.1103/PhysRevB.47.16162.

(38) Ebert, L. B.; Brauman, J. I.; Huggins, R. A. Carbon Monofluoride. Evidence for a Structure Containing an Infinite Array of Cyclohexane Boats. *J. Am. Chem. Soc.* **1974**, *96* (25), 7841–7842. https://doi.org/10.1021/ja00832a054.

(39) Rimsza, J. M.; Walder, B. J.; Alam, T. M. Influence of Polymorphs and Local Defect Structures on NMR Parameters of Graphite Fluorides. *J. Phys. Chem. C* **2021**, *125* (4), 2699–2712. https://doi.org/10.1021/acs.jpcc.0c09957.

(40) Touhara, H.; Kadono, K.; Fujii, Y.; Watanabe, N. On the Structure of Graphite Fluoride. *ZAAC - J. Inorg. Gen. Chem.* **1987**, *544* (1), 7–20. https://doi.org/10.1002/zaac.19875440102.

(41) Giraudet, J.; Dubois, M.; Guérin, K.; Hamwi, A.; Masin, F. Solid State NMR Studies of Covalent Graphite Fluorides (CF)n and (C2F)N. *J. Phys. Chem. Solids* **2006**, *67* (5–6), 1100–1105. https://doi.org/10.1016/j.jpcs.2006.01.030.

(42) Gupta, V.; Nakajima, T.; Ohzawa, Y.; Žemva, B. A Study on the Formation Mechanism of Graphite Fluorides by Raman Spectroscopy. *J. Fluor. Chem.* **2003**, *120* (2), 143–150. https://doi.org/10.1016/S0022-1139(02)00323-8.

(43) Wang, B.; Sparks, J. R.; Gutierrez, H. R.; Okino, F.; Hao, Q.; Tang, Y.; Crespi, V. H.; Sofo, J. O.; Zhu, J. Photoluminescence from Nanocrystalline Graphite Monofluoride. *Appl. Phys. Lett.* **2010**, *97* (14), 1–4. https://doi.org/10.1063/1.3491265.

(44) Ahmad, Y.; Dubois, M.; Guérin, K.; Hamwi, A.; Fawal, Z.; Kharitonov, A. P.; Generalov, A. V.; Klyushin, A. Y.; Simonov, K. A.; Vinogradov, N. A.; Zhdanov, I. A.; Preobrajenski, A. B.; Vinogradov, A. S. NMR and NEXAFS Study of Various Graphite Fluorides. *J. Phys. Chem. C* **2013**, *117* (26), 13564–13572. https://doi.org/10.1021/jp401579u.

(45) Palchan, I.; Crespin, M.; Estrade-Szwarckopf, H.; Rousseau, B. Graphite Fluorides: An XPS Study of a New Type of C-F Bonding. *Chem. Phys. Lett.* **1989**, *157* (4), 321–327. https://doi.org/10.1016/0009-2614(89)87255-0.

(46) Takagi, Y.; Kusakabe, K. Transition from Direct Band Gap to Indirect Band Gap in Fluorinated Carbon. *Phys. Rev. B* **2002**, *65* (12), 121103. https://doi.org/10.1103/PhysRevB.65.121103.

(47) Parry, D. E. Self Consistent Semi-Empirical Calculation of the Electronic Band Structures of Crystalline Solids. Application to Graphite Monofluoride. *J. Chem. Soc. Faraday Trans. 2* **1977**, *73* (6), 774. https://doi.org/10.1039/f29777300774.

(48) Nair, R. R.; Ren, W.; Jalil, R.; Riaz, I.; Kravets, V. G.; Britnell, L.; Blake, P.; Schedin, F.; Mayorov, A. S.; Yuan, S.; Katsnelson, M. I.; Cheng, H.; Strupinski, W.; Bulusheva, L. G.; Okotrub, A. V; Grigorieva, I. V; Grigorenko, A. N.; Novoselov, K. S.; Geim, A. K. Fluorographene: A Two-Dimensional Counterpart of Teflon. *Small* **2010**, *6* (24), 2877–2884.

https://doi.org/10.1002/smll.201001555.

(49) Karlický, F.; Otyepka, M. Band Gaps and Optical Spectra of Chlorographene, Fluorographene and Graphane from G 0 W 0 , GW 0 and GW Calculations on Top of PBE and HSE06 Orbitals. *J. Chem. Theory Comput.* **2013**, *9* (9), 4155–4164. https://doi.org/10.1021/ct400476r.

(50) Watanabe, N.; Nakajima, T.; Touhara, H. Chemical Properties of Graphite Fluorides. In *Graphite Fluorides*; Elsevier Science Publishers B.V., 1988; pp 102–147. https://doi.org/10.1016/B978-0-444-42885-1.50009-9.

(51) Jeon, K.; Lee, Z.; Pollak, E.; Moreschini, L.; Bostwick, A.; Park, C.; Mendelsberg, R.; Radmilovic, V.; Kostecki, R.; Richardson, T. J.; Rotenberg, E. Fluorographene : A Wide Bandgap Semiconductor with Ultraviolet Luminescence. **2011**, No. 2, 1042–1046. https://doi.org/10.1021/nn1025274.

(52) Chang, H.; Cheng, J.; Liu, X.; Gao, J.; Li, M.; Li, J.; Tao, X.; Ding, F.; Zheng, Z. Facile Synthesis of Wide-Bandgap Fluorinated Graphene Semiconductors. *Chem. - A Eur. J.* **2011**, *17* (32), 8896–8903. https://doi.org/10.1002/chem.201100699.

(53) Meľnikov, V. P.; Shashkin, D. P.; Shchegolikhin, A. N. Defluorination of Fluorinated Coke by Triethylamine. *Dokl. Chem.* **2008**, *421* (2), 182–185. https://doi.org/10.1134/S0012500808080041.

(54) Worsley, K. A.; Ramesh, P.; Mandal, S. K.; Niyogi, S.; Itkis, M. E.; Haddon, R. C. Soluble Graphene Derived from Graphite Fluoride. *Chem. Phys. Lett.* **2007**, *445* (1–3), 51–56. https://doi.org/10.1016/j.cplett.2007.07.059.

(55) Bourlinos, A. B.; Georgakilas, V.; Zboril, R.; Jancik, D.; Karakassides, M. A.; Stassinopoulos, A.; Anglos, D.; Giannelis, E. P. Reaction of Graphite Fluoride with NaOH-KOH Eutectic. *J. Fluor. Chem.* **2008**, *129* (8), 720–724. https://doi.org/10.1016/j.jfluchem.2008.05.020.

(56) Chronopoulos, D. D.; Bakandritsos, A.; Pykal, M.; Zbořil, R.; Otyepka, M. Chemistry, Properties, and Applications of Fluorographene. *Appl. Mater. Today* **2017**, *9* (May), 60–70. https://doi.org/10.1016/j.apmt.2017.05.004.

(57) Zhang, M.; Liu, L.; He, T.; Wu, G.; Chen, P. Melamine Assisted Solid Exfoliation Approach for the Synthesis of Few-Layered Fluorinated Graphene Nanosheets. *Mater. Lett.* **2016**, *171*, 191–194. https://doi.org/10.1016/j.matlet.2016.02.042.

(58) Jankovský, O.; Mazánek, V.; Klímová, K.; Sedmidubský, D.; Kosina, J.; Pumera, M.; Sofer, Z. Simple Synthesis of Fluorinated Graphene: Thermal Exfoliation of Fluorographite. *Chem. - A Eur. J.* **2016**, *22* (49), 17696–17703. https://doi.org/10.1002/chem.201604078.

(59) Bordes, É.; Szala-Bilnik, J.; Pádua, A. A. H. Exfoliation of Graphene and Fluorographene in Molecular and Ionic Liquids. *Faraday Discuss.* **2018**, *206*, 61–75. https://doi.org/10.1039/C7FD00169J.

(60) Bourlinos, A. B.; Safarova, K.; Siskova, K.; Zbořil, R. The Production of Chemically Converted Graphenes from Graphite Fluoride. *Carbon N. Y.* **2012**, *50* (3), 1425–1428. https://doi.org/10.1016/j.carbon.2011.10.012.

(61) Gong, P.; Wang, Z.; Wang, J.; Wang, H.; Li, Z.; Fan, Z.; Xu, Y.; Han, X.; Yang, S. One-Pot Sonochemical Preparation of Fluorographene and Selective Tuning of Its Fluorine Coverage. *J. Mater. Chem.* **2012**, *22* (33), 16950. https://doi.org/10.1039/c2jm32294c.

(62) Robinson, J. T.; Burgess, J. S.; Junkermeier, C. E.; Badescu, S. C.; Reinecke, T. L.; Perkins, F. K.; Zalalutdniov, M. K.; Baldwin, J. W.; Culbertson, J. C.; Sheehan, P. E.; Snow, E. S. Properties of Fluorinated Graphene Films. *Nano Lett.* **2010**, *10* (8), 3001–3005. https://doi.org/10.1021/nl101437p.

(63) Tahara, K.; Iwasaki, T.; Furuyama, S.; Matsutani, A.; Hatano, M. Asymmetric Transport Property of Fluorinated Graphene. *Appl. Phys. Lett.* **2013**, *103* (14), 143106. https://doi.org/10.1063/1.4823798.

(64)   Ho, K. I.; Liao, J. H.; Huang, C. H.; Hsu, C. L.; Zhang, W.; Lu, A. Y.; Li, L. J.; Lai, C. S.; Su, C. Y. One-Step Formation of a Single Atomic-Layer Transistor by the Selective Fluorination of a Graphene Film. *Small* **2014**, *10* (5), 989–997. https://doi.org/10.1002/smll.201301366.

(65)   Chen, M.; Zhou, H.; Qiu, C.; Yang, H.; Yu, F.; Sun, L. Layer-Dependent Fluorination and Doping of Graphene via Plasma Treatment. *Nanotechnology* **2012**, *23* (11), 115706. https://doi.org/10.1088/0957-4484/23/11/115706.

(66)   Yang, H.; Chen, M.; Zhou, H.; Qiu, C.; Hu, L.; Yu, F.; Chu, W.; Sun, S.; Sun, L. Preferential and Reversible Fluorination of Monolayer Graphene. *J. Phys. Chem. C* **2011**, *115* (34), 16844–16848. https://doi.org/10.1021/jp204573z.

(67)   Lee, W. H.; Suk, J. W.; Chou, H.; Lee, J.; Hao, Y.; Wu, Y.; Piner, R.; Akinwande, D.; Kim, K. S.; Ruoff, R. S. Selective-Area Fluorination of Graphene with Fluoropolymer and Laser Irradiation. *Nano Lett.* **2012**, *12* (5), 2374–2378. https://doi.org/10.1021/nl300346j.

(68)   Nair, R. R.; Sepioni, M.; Tsai, I. L.; Lehtinen, O.; Keinonen, J.; Krasheninnikov, A. V.; Thomson, T.; Geim, A. K.; Grigorieva, I. V. Spin-Half Paramagnetism in Graphene Induced by Point Defects. *Nat. Phys.* **2012**, *8* (3), 199–202. https://doi.org/10.1038/nphys2183.

(69)   Wang, X.; Wang, W.; Liu, Y.; Ren, M.; Xiao, H.; Liu, X. Controllable Defluorination of Fluorinated Graphene and Weakening of C–F Bonding under the Action of Nucleophilic Dipolar Solvent. *Phys. Chem. Chem. Phys.* **2016**, *18* (4), 3285–3293. https://doi.org/10.1039/C5CP06914A.

(70)   Whitener, K. E.; Stine, R.; Robinson, J. T.; Sheehan, P. E. Graphene as Electrophile: Reactions of Graphene Fluoride. *J. Phys. Chem. C* **2015**, *119* (19), 10507–10512. https://doi.org/10.1021/acs.jpcc.5b02730.

(71)   Huang, F.; Li, Y.; Liu, X.; Lai, W.; Fan, K.; Liu, X.; Wang, X. Suzuki–Miyaura Reaction of C–F Bonds in Fluorographene. *Chem. Commun.* **2021**, *57* (3), 351–354. https://doi.org/10.1039/D0CC07651A.

(72)   Barès, H.; Bakandritsos, A.; Medveď, M.; Ugolotti, J.; Jakubec, P.; Tomanec, O.; Kalytchuk, S.; Zbořil, R.; Otyepka, M. Bimodal Role of Fluorine Atoms in Fluorographene Chemistry Opens a Simple Way toward Double Functionalization of Graphene. *Carbon N. Y.* **2019**, *145*, 251–258. https://doi.org/10.1016/j.carbon.2019.01.059.

(73)   Bosch-navarro, C.; Walker, M.; Wilson, N. R.; Rourke, J. P. Covalent Modification of Exfoliated Fluorographite with Nitrogen Functionalities. **2015**.

(74)   Li, Y.; Wang, X.; Wang, W.; Qin, R.; Lai, W.; Ou, A.; Liu, Y.; Liu, X. Nitrogen-Doping Chemical Behavior of Graphene Materials with Assistance of Defluorination. *J. Phys. Chem. C* **2019**, *123* (1), 584–592. https://doi.org/10.1021/acs.jpcc.8b10276.

(75)   Zoppellaro, G.; Bakandritsos, A.; Tuček, J.; Błoński, P.; Susi, T.; Lazar, P.; Bad'ura, Z.; Steklý, T.; Opletalová, A.; Otyepka, M.; Zbořil, R. Microwave Energy Drives "On–Off–On" Spin-Switch Behavior in Nitrogen-Doped Graphene. *Adv. Mater.* **2019**, 1902587. https://doi.org/10.1002/adma.201902587.

(76)   Šedajová, V. Synthesis and Characterization of Graphene Derivatives from Graphite Fluoride, Palacký University Olomouc, 2018.

(77)   Tuček, J.; Holá, K.; Bourlinos, A. B.; Błoński, P.; Bakandritsos, A.; Ugolotti, J.; Dubecký, M.; Karlický, F.; Ranc, V.; Čépe, K.; Otyepka, M.; Zbořil, R. Room Temperature Organic Magnets Derived from Sp3 Functionalized Graphene. *Nat. Commun.* **2017**, *8*, 14525. https://doi.org/10.1038/ncomms14525.

(78)   Langer, R.; Fako, E.; Błoński, P.; Vavrečka, M.; Bakandritsos, A.; Otyepka, M.; López, N. Anchoring of Single-Platinum-Adatoms on Cyanographene: Experiment and Theory. *Appl. Mater. Today* **2019**, *1* (1), 100462. https://doi.org/10.1016/j.apmt.2019.100462.

(79)   Bakandritsos, A.; Kadam, R. G.; Kumar, P.; Zoppellaro, G.; Medveď, M.; Tuček, J.; Montini, T.; Tomanec, O.; Andrýsková, P.; Drahoš, B.; Varma, R. S.; Otyepka, M.; Gawande, M. B.;

Fornasiero, P.; Zbořil, R. Mixed-Valence Single-Atom Catalyst Derived from Functionalized Graphene. *Adv. Mater.* **2019**, *31* (17), 1900323. https://doi.org/10.1002/adma.201900323.

(80)   Panáček, D.; Hochvaldová, L.; Bakandritsos, A.; Malina, T.; Langer, M.; Belza, J.; Martincová, J.; Večeřová, R.; Lazar, P.; Poláková, K.; Kolařík, J.; Válková, L.; Kolář, M.; Otyepka, M.; Panáček, A.; Zbořil, R. Silver Covalently Bound to Cyanographene Overcomes Bacterial Resistance to Silver Nanoparticles and Antibiotics. *Adv. Sci.* **2021**, *2003090*, 2003090. https://doi.org/10.1002/advs.202003090.

(81)   Šedajová, V.; Jakubec, P.; Bakandritsos, A.; Ranc, V.; Otyepka, M. New Limits for Stability of Supercapacitor Electrode Material Based on Graphene Derivative. *Nanomaterials* **2020**, *10* (9), 1731. https://doi.org/10.3390/nano10091731.

(82)   Seelajaroen, H.; Bakandritsos, A.; Otyepka, M.; Zbořil, R.; Sariciftci, N. S. Immobilized Enzymes on Graphene as Nanobiocatalyst. *ACS Appl. Mater. Interfaces* **2020**, *12* (1), 250–259. https://doi.org/10.1021/acsami.9b17777.

(83)   Bakandritsos, A.; Jakubec, P.; Pykal, M.; Otyepka, M. Covalently Functionalized Graphene as a Supercapacitor Electrode Material. *FlatChem* **2019**, *13* (November 2018), 25–33. https://doi.org/10.1016/j.flatc.2018.12.004.

(84)   Tantis, I.; Bakandritsos, A.; Zaoralová, D.; Medveď, M.; Jakubec, P.; Havláková, J.; Zbořil, R.; Otyepka, M. Covalently Interlinked Graphene Sheets with Sulfur-Chains Enable Superior Lithium–Sulfur Battery Cathodes at Full-Mass Level. *Adv. Funct. Mater.* **2021**, *2101326*, 2101326. https://doi.org/10.1002/adfm.202101326.

(85)   Stathis, A.; Stavrou, M.; Papadakis, I.; Bakandritsos, A.; Steklý, T.; Otyepka, M.; Couris, S. Octylamine-Modified Fluorographenes as a Versatile Platform for the Efficient Engineering of the Nonlinear Optical Properties of Fluorinated Graphenes. *Adv. Photonics Res.* **2020**, *1* (2), 2000014. https://doi.org/10.1002/adpr.202000014.

(86)   Raja, P. M. V; Barron, A. R. *Physical Methods in Chemistry and Nano Science*; OpenStax CNX. 20. 1. 2019 http://cnx.org/contents/ba27839d-5042-4a40-afcf-c0e6e39fb454@25.2.

(87)   Moulder, J. F.; Stickle, W. F.; Sobol, P. E.; Bomben, K. D. *Handbook of X-Ray Photoelectron Spectroscopy: A Reference Book of Standard Spectra for Identification and Interpretation of XPS Data*, Second edi.; Chastain, J., Ed.; Perkin-Elmer Corporation: Minnesota, 1992.

(88)   Pines, A.; Gibby, M. G.; Waugh, J. S. Proton-Enhanced Nuclear Induction Spectroscopy 13C Chemical Shielding Anisotropy in Some Organic Solids. *Chem. Phys. Lett.* **1972**, *15* (3), 373–376. https://doi.org/10.1016/0009-2614(72)80191-X.

(89)   Schaefer, J.; Stejskal, E. O. Carbon-13 Nuclear Magnetic Resonance of Polymers Spinning at the Magic Angle. *J. Am. Chem. Soc.* **1976**, *98* (4), 1031–1032. https://doi.org/10.1021/ja00420a036.

(90)   Geen, H.; Bodenhausen, G. Complete Sideband Suppression in Magic Angle Spinning Solid-State Nuclear Magnetic Resonance for Arbitrary Chemical Shift Anisotropies. *J. Am. Chem. Soc.* **1993**, *115* (4), 1579–1580. https://doi.org/10.1021/ja00057a055.

(91)   Blitz, J. P. Diffuse Reflectance Spectroscopy. In *Modern Techniques in Applied Molecular Spectroscopy*; Mirabella, F. M., Ed.; John Wiley & Sons, Inc., 1998; pp 185–219.

(92)   Makuła, P.; Pacia, M.; Macyk, W. How To Correctly Determine the Band Gap Energy of Modified Semiconductor Photocatalysts Based on UV–Vis Spectra. *J. Phys. Chem. Lett.* **2018**, *9* (23), 6814–6817. https://doi.org/10.1021/acs.jpclett.8b02892.

(93)   Matos, C. R. S.; Xavier, M. J.; Barreto, L. S.; Costa, N. B.; Gimenez, I. F. Principal Component Analysis of X-Ray Diffraction Patterns To Yield Morphological Classification of Brucite Particles. *Anal. Chem.* **2007**, *79* (5), 2091–2095. https://doi.org/10.1021/ac061991n.

(94)   Karlický, F.; Otyepka, M. Band Gaps and Optical Spectra from Single- and Double-Layer Fluorographene to Graphite Fluoride: Many-Body Effects and Excitonic States. *Ann. Phys.* **2014**, *526* (9–10), 408–414. https://doi.org/10.1002/andp.201400095.

(95) Langer, R.; Zaoralová, D.; Medved', M.; Banáš, P.; Błoński, P.; Otyepka, M. Variability of C–F Bonds Governs the Formation of Specific Structural Motifs in Fluorinated Graphenes. *J. Phys. Chem. C* **2019**, *123* (45), 27896–27903. https://doi.org/10.1021/acs.jpcc.9b07552.

(96) Anderson, P. W. Antiferromagnetism. Theory of Superexchange Interaction. *Phys. Rev.* **1950**, *79* (2), 350–356. https://doi.org/10.1103/PhysRev.79.350.

(97) Wang, X.; Wang, W.; Liu, Y.; Ren, M.; Xiao, H.; Liu, X. Characterization of Conformation and Locations of C − F Bonds in Graphene Derivative by Polarized ATR-FTIR. **2016**. https://doi.org/10.1021/acs.analchem.6b00115.

(98) Dubois, M.; Guérin, K.; Pinheiro, J. P.; Fawal, Z.; Masin, F.; Hamwi, A. NMR and EPR Studies of Room Temperature Highly Fluorinated Graphite Heat-Treated under Fluorine Atmosphere. *Carbon N. Y.* **2004**, *42* (10), 1931–1940. https://doi.org/10.1016/j.carbon.2004.03.025.

(99) Guérin, K.; Pinheiro, J. P.; Dubois, M.; Fawal, Z.; Masin, F.; Yazami, R.; Hamwi, A. Synthesis and Characterization of Highly Fluorinated Graphite Containing Sp 2 and Sp 3 Carbon. *Chem. Mater.* **2004**, *16* (9), 1786–1792. https://doi.org/10.1021/cm034974c.

(100) Ueta, A.; Tanimura, Y.; Prezhdo, O. V. Infrared Spectral Signatures of Surface-Fluorinated Graphene: A Molecular Dynamics Study. *J. Phys. Chem. Lett.* **2012**, *3* (2), 246–250. https://doi.org/10.1021/jz201496q.

(101) Vähäkangas, J.; Lantto, P.; Mareš, J.; Vaara, J. Spin Doublet Point Defects in Graphenes: Predictions for ESR and NMR Spectral Parameters. *J. Chem. Theory Comput.* **2015**, *11* (8), 3746–3754. https://doi.org/10.1021/acs.jctc.5b00402.

(102) Mar, M.; Ahmad, Y.; Dubois, M.; Guérin, K.; Batisse, N.; Hamwi, A. Dual C-F Bonding in Fluorinated Exfoliated Graphite. *J. Fluor. Chem.* **2015**, *174*, 36–41. https://doi.org/10.1016/j.jfluchem.2014.07.026.

(103) Murakami, M.; Matsumoto, K.; Hagiwara, R.; Matsuo, Y. 13C/19F High-Resolution Solid-State NMR Studies on Layered Carbon-Fluorine Compounds. *Carbon N. Y.* **2018**, *138*, 179–187. https://doi.org/10.1016/j.carbon.2018.06.004.

(104) Englert, J. M.; Dotzer, C.; Yang, G.; Schmid, M.; Papp, C.; Gottfried, J. M.; Steinrück, H.-P.; Spiecker, E.; Hauke, F.; Hirsch, A. Covalent Bulk Functionalization of Graphene. *Nat. Chem.* **2011**, *3* (4), 279–286. https://doi.org/10.1038/nchem.1010.

(105) Lazar, P.; Mach, R.; Otyepka, M. Spectroscopic Fingerprints of Graphitic, Pyrrolic, Pyridinic, and Chemisorbed Nitrogen in N-Doped Graphene. *J. Phys. Chem. C* **2019**, *123* (16), 10695–10702. https://doi.org/10.1021/acs.jpcc.9b02163.